THREE DIMENSIONAL DYNAMIC RESPONSE OF A CONCRETE GRAVITY DAM

A THESIS SUBMITTED TO
THE GRADUATE SCHOOL OF NATURAL AND APPLIED SCIENCES
OF
MIDDLE EAST TECHNICAL UNIVERSITY

BY

SEMA MELEK YILMAZTÜRK

IN PARTIAL FULFILLMENT OF THE REQUIREMENTS
FOR
THE DEGREE OF MASTER OF SCIENCE
IN
CIVIL ENGINEERING

JANUARY 2013

Approval of the thesis:

THREE DIMENSIONAL DYNAMIC RESPONSE OF A CONCRETE GRAVITY DAM

submitted by **SEMA MELEK YILMAZTÜRK** in partial fulfillment of the requirements for the degree of **Master of Science in Civil Engineering Department, Middle East Technical University** by,

Prof. Dr. Canan Özgen _____
Dean, Graduate School of **Natural and Applied Sciences**

Prof. Dr. Ahmet Cevdet Yalçıner _____
Head of Department, **Civil Engineering**

Prof. Dr. Barış Binici _____
Supervisor, **Civil Engineering Dept., METU**

Assoc.Prof. Dr. Yalın Arıcı _____
Co-Supervisor, **Civil Engineering Dept., METU**

Examining Committee Members:

Prof. Dr. Mehmet Utku _____
Civil Engineering Dept., METU

Prof. Dr. Barış Binici _____
Civil Engineering Dept., METU

Assoc. Prof. Dr. Yalın Arıcı _____
Civil Engineering Dept., METU

Assoc. Prof. Dr. Özgür Kurç _____
Civil Engineering Dept., METU

M.Sc Altuğ Akman _____
ES Project Engineering and Consultancy

Date: 29.01.2013

I hereby declare that all information in this document has been obtained and presented in accordance with academic rules and ethical conduct. I also declare that, as required by these rules and conduct, I have fully cited and referenced all material and results that are not original to this work.

Name, Surname : SEMA MELEK YILMAZTÜRK

Signature:

ABSTRACT

THREE DIMENSIONAL DYNAMIC RESPONSE OF A CONCRETE GRAVITY DAM

Yılmaztürk, Sema Melek

M.Sc., Department of Civil Engineering

Supervisor: Prof. Dr. Barış Binici

Co-Supervisor: Assoc.Prof. Dr. Yalın Arıcı

January 2013, 90 pages

Hydroelectric power is a commonly used alternative source of energy in developing countries. In this regard, concrete gravity dams are the most preferred dam type especially with the developments in the engineering industry. Roller compacted concrete became more popular in dam construction due to its advantages of speed and economy. Several methods are used for the design of concrete gravity dams by analyzing the dam response under static and dynamic loads. This study provides three dimensional linear dynamic analysis of roller compacted concrete gravity dam with a complete dam-foundation-water interaction by using EACD-3D-08 program. Foundation flexibility was included with damping and mass using boundary elements. Three dimensional solid elements were used for the idealization of the dam and water with using finite element methods. Compressibility of water with reservoir absorption was studied. In the light of USACE, performance criteria of linear analyses were assessed. Parametric study was conducted to determine the most influential parameters on the dam response. The importance and necessity of three dimensional analyses were investigated by comparing with linear two dimensional analyses. Linear analyses were then compared with three dimensional nonlinear analyses. In conclusion, the realistic dam seismic response can only be obtained by using three dimensional linear analyses with full interaction of dam-foundation-water.

Keywords: concrete gravity dam, three dimensional dynamic analysis, roller compacted concrete, dam-foundation-water interaction.

ÖZ

BETON AĞIRLIK BARAJIN ÜÇ BOYUTLU DİNAMİK DAVRANIŞLARININ İRDELENMESİ

Yılmaztürk, Sema Melek

Yüksek lisans, İnşaat Mühendisliği Bölümü

Tez Yöneticisi: Prof. Dr. Barış Binici

Ortak Tez Yöneticisi: Doç. Dr. Yalın Arıcı

Ocak 2013, 90 sayfa

Hidroelektrik enerji gelişmekte olan ülkelerde genel olarak diğer enerji kaynaklarına alternatif olarak kullanılmaktadır. Beton ağırlık barajlar, mühendislik alanlarındaki gelişmeler sayesinde oldukça tercih edilen baraj tipleri arasındadır. Ayrıca, silindirle sıkıştırılmış beton, ekonomik olması ve hızlı inşaa edilmesi gibi avantajlarından dolayı baraj yapımında popüler bir şekilde kullanılmaktadır. Beton ağırlık baraj tasarımlarında farklı yöntemler kullanılarak statik ve dinamik yükler altında baraj davranışı incelenmektedir. Bu tez çalışmasında EACD-3D-08 programı kullanılarak silindirle sıkıştırılmış beton ağırlık barajın üç boyutlu lineer dinamik analiz yöntemiyle gerçekçi su-zemin kaya-rezervuar ilişkisi sağlanarak sismik davranışı çalışılmıştır. Zemin kaya esnekliği kütle ve sönümleme özelliklerini içererek sınırlı elemanlarla modelleme yapılmıştır. Rezervuardaki su ve baraj, üç boyutlu sonlu elemanlar kullanılarak modellenmiştir. Suyun sıkıştırılabilir özelliği ve rezervuar emilimi soğurma katsayısı ile yansıtılmıştır. USACE prensipleri ışığında lineer analiz performans kriteri değerlendirilmiştir. Parametrik çalışma yapılarak baraj davranışını en çok etkileyen faktörler belirlenmiştir. Üç boyutlu analizin önemini ve gereksinimini daha iyi anlayabilmek için iki boyutlu lineer analiz ile karşılaştırılmıştır. Daha sonra, lineer analiz üç boyutlu lineer olmayan analizle karşılaştırılmıştır. Sonuç olarak, gerçekçi baraj davranışını elde edebilmek için üç boyutlu baraj-zemin- rezervuar etkileşiminin kullanılması gerektiği belirlenmiştir.

Anahtar Kelimeler: beton ağırlık baraj, üç boyutlu dinamik analiz, silindirle sıkıştırılmış beton, baraj-zemin kaya-rezervuar ilişkisi

ACKNOWLEDGEMENTS

I would like to express my special thanks to my thesis supervisor Prof. Dr. Barış Binici and co-advisor Assoc. Prof. Dr. Yalın Arıcı for their invaluable guidance, encouragement and assistance throughout the research. I was glad to work with them.

I would like to thank Alper Aldemir and Ali Rıza Yücel for their help and guidance whenever I asked for it.

I would like to express my sincere gratitude to my mother Gülhun and my father Neşet Yılmaztürk for their immeasurable love and support. I would like to thank my brother Mehmet Yılmaztürk for his endless encouragement. I would like to thank my cousin Aslı Halıcı for her support and friendship.

I am grateful to my friend Burhan Aleessa Alam for his great support and encouragement in the Materials of Construction Laboratory.

I would like express my gratitude to my sincere friends Açelya Ecem Yıldız, Melis Yıldız, Başak Bingöl, Fatoş İlbi and Seçil Üstünkol for sharing my feelings.

I am thankful to Tümay Çelikkol Koçak, Merve Zorlu Silay and Derya Över Kaman for their friendship.

Finally, I would like to express special thanks to Kıvanç Kasapgil who has always been there for me, for his love, support and encouragement.

To My Dear Family...

TABLE OF CONTENTS

ABSTRACT iv
ÖZ v
ACKNOWLEDGEMENTS vi
TABLE OF CONTENTS viii
LIST OF TABLES ix
LIST OF FIGURES x

CHAPTERS

1 INTRODUCTION 1

1.1 General 1
1.2 Literature Survey 3
1.3 EACD-3D-08 9

1.3.1 General 9
1.3.2 Finite Elements 10
1.3.3 Foundation 11
1.3.4 Impounded Water 12
1.3.5 Materials Models 13
1.3.6 Frequency Domain Equations 14

1.4 Scope and Objective 18

2 SEISMIC ASSESSMENT STUDY OF ANDIRAZ DAM 19

2.1 General 19
2.2 Seismic Safety Assessment Methodology 20
2.3 Finite Element Mesh 21
2.4 Material Properties 25
2.5 Ground Motion Characteristics 26
2.6 Modal Properties 31
2.7 Analysis Results 35

2.7.1 Stress Plots 35
2.7.2 Displacements 43
2.7.3 Assessment Results 45
2.7.4 Effect of Peak Ground Accelerations (PGA) on Stress and Displacement 49

2.8 Parametric Studies 50

2.8.1 Effect of Foundation Flexibility 50
2.8.2 Bottom Absorption of Reservoir 51
2.8.3 Effect of Slope of Cross-Section on the Behavior 53

2.9 Tornado Diagrams 59

2.9.1 OBE Analyses 60
2.9.2 SEE1 Analyses 63
2.9.3 SEE2 Analyses 66

2.10 Comparison of 3D Analysis Results with 2D Analysis Results 69
2.11 Comparison of Nonlinear Results with Linear Analyses 79

3 CONCLUSION 81

3.1 General 81

REFERENCES 83
APPENDIX A 86

LIST OF TABLES

TABLES

Table 1.1 Earthquake response of concrete dams (PGA>0.3g).....3
Table 2.1 Modal analysis comparison of meshes on ANSYS and EACD 24
Table 2.2 Maximum displacement comparison of meshes on ANSYS and EACD.....25
Table 2.3 Maximum principles stresses comparison of meshes on ANSYS.....25
Table 2.4 Determination of risk score by considering four risk factors 27
Table 2.5 Classification of risk groups according to total risk scores.....27
Table 2.6 Earthquake data characteristics.....28
Table 2.7 Earthquake Combinations.....31
Table 2.8 Natural Frequencies and Periods of the dam-foundation system 34
Table 2.9 Maximum Principle Stresses for three dimensional analyses 42
Table 2.10 Summary Table of maximum cumulative inelastic duration 45
Table 2.11 Parameter values used for compressible and incompressible analyses 50
Table 2.12 Ec/Ef ratios and their corresponding values.....50
Table 2.13 Results table of α effect on maximum stress and maximum displacement 52
Table 2.14 Effect of Slope of cross-section for SEE1-2 compressible analyses 54
Table 2.15 Effect of Slope of cross-section for SEE1-2 incompressible analyses.....55
Table 2.16 Downstream slope effect on volume of the dam.....56
Table 2.17 Effect of Slope of cross-section for SEE2- 2 compressible analyses 57
Table 2.18 Effect of Slope of cross-section for SEE2-2 incompressible analyses.....58
Table 2.19 Input Parameters table for OBE analyses.....60
Table 2.20 Median model results for OBE analyses.....60
Table 2.21 Maximum Principle stress results for OBE analyses 61
Table 2.22 Maximum top displacement results for OBE analyses 61
Table 2.23 Maximum duration of assessment results for OBE analyses 62
Table 2.24 Input Parameters table for SEE1 analyses.....63
Table 2.25 Median model results for SEE1 analyses.....63
Table 2.26 Maximum Principle stress results for SEE1 analyses 64
Table 2.27 Maximum top displacement results for SEE1 analyses 64
Table 2.28 Maximum duration of assessment results for SEE1 analyses 65
Table 2.29 Input Parameters table for SEE2 analyses.....66
Table 2.30 Median model results for SEE2 analyses.....66
Table 2.31 Maximum Principle stress results for SEE2 analyses 67
Table 2.32 Maximum top displacement results for SEE2 analyses 67
Table 2.33 Maximum duration of assessment results for SEE2 analyses 67
Table 2.34 Spectral acceleration values obtained from the response spectra of ground motions ..72
Table 2.35 Maximum principle stress results for 2D and 3D analyses.....76
Table 2.36 Crest displacement time histories of 3D and 2D analyses 78

LIST OF FIGURES

FIGURES

Figure 1.1 Electricity productions in terms of hydraulic distribution in Turkey 2
Figure 1.2 Westergaard's system of added-mass concept (Kuo, 1982) 4
Figure 1.3 Two dimensional dam system with infinite fluid (Hall, Chopra ,1980)..... 5
Figure 1.4 Three dimensional arch dam system with infinite fluid (Hall, Chopra ,1980)..... 6
Figure 1.5 Arch dam model in ADAP88 with nonlinear joint elements (Fenves et. al. 1989)..... 8
Figure 1.6 System of dam-foundation-water (Fok, Hall, Chopra, 86) 10
Figure 1.7 Element alternatives for modeling dam (Wang, Chopra, 2008) 11
Figure 1.8 Node numbering of solid dam elements (Wang, Chopra, 2008)..... 11
Figure 1.9 Surface boundary elements for foundation rock (Wang, Chopra, 2008) 12
Figure 1.10 Meshes used for modeling the irregular fluid region (Wang, Chopra, 2008) 13
Figure 1.11 Analysis Procedure 17
Figure 2.1 Earthquake zones of Kastamonu..... 20
Figure 2.2 Andıraz Dam..... 20
Figure 2.3 Andıraz Dam Sectional Properties a) downstream view b) cross sectional view 20
Figure 2.4 Calculation of time exceeding DCR 21
Figure 2.5 Performance criterion graph (USACE, 2003)..... 21
Figure 2.6 Dam cross section and valley from upstream views of coarse (Mesh1) and medium mesh (Mesh 2)..... 22
Figure 2.7 Mesh differences on the components of the coarse (Mesh 1) and medium (Mesh 2) models..... 23
Figure 2.8 Different meshes for ANSYS (Mesh 2, 3 and 4 respectively)..... 24
Figure 2.9 Ground motion time histories 29
Figure 2.10 Response spectra graphs of earthquakes..... 30
Figure 2.11 Mode shapes of the dam for first and second modes 32
Figure 2.12 Mode shapes of the dam for third and fourth modes 33
Figure 2.13 Frequencies of the dam with full reservoir 34
Figure 2.14 Maximum vertical stresses of OBE Analysis 36
Figure 2.15 Maximum vertical stresses of SEE1 Analysis 37
Figure 2.16 Maximum vertical stresses of SEE2 Analysis 38
Figure 2.17 Maximum of maximum principle stresses of OBE Analysis..... 39
Figure 2.18 Maximum of maximum principle stresses of SEE1 Analysis..... 40
Figure 2.19 Maximum of maximum principle stresses of SEE2 Analysis..... 41
Figure 2.20 Stress Locations exceeding tensile capacity for SEE1-3 combination 11..... 42
Figure 2.21 Stress Locations exceeding tensile capacity for SEE2-3 combination 11..... 43
Figure 2.22 Location of Dam Node 194..... 43
Figure 2.23 Displacement time history of node 194-x direction for each ground motion..... 44
Figure 2.24 Performance criterion graph and critical locations of OBE 46
Figure 2.25 Performance criterion graph and critical locations of SEE1 Analysis 47
Figure 2.26 Performance criterion graph and critical locations of SEE2 Analysis 48
Figure 2.27 PGA effect on a) maximum tensile stress b) maximum displacement at dam node 194 for compressible and incompressible cases..... 49
Figure 2.28 Ec/Ef effect on maximum tensile stress for compressible and incompressible cases 51
Figure 2.29 Ec/Ef effect on maximum displacement for compressible and incompressible cases 51
Figure 2.30 α Effect on max stress..... 52
Figure 2.31 α Effect on max displacement..... 52
Figure 2.32 Various downstream slopes 53
Figure 2.33 Performance criterion curves of downstream slope effect of SEE1-2 with compressible 54
Figure 2.34 Performance criterion curves of downstream slope effect of SEE1-2 with incompressible 55
Figure 2.35 Performance criterion curves of downstream slope effect of SEE2-2 with compressible 57
Figure 2.36 Performance criterion curves of downstream slope effect of SEE2-2 with incompressible 58
Figure 2.37 Tornado diagram preparation (Binici and Mosalam, 2006)..... 59
Figure 2.38 Tornado graphs of OBE analyses results 62
Figure 2.39 Tornado graphs of SEE1 analyses results 65

Figure 2.40 Tornado graphs of SEE2 analyses results 68
Figure 2.41 Different cross sections on the Andıraz Dam 70
Figure 2.42 Dam element mesh on EAGD-84 (2D).....70
Figure 2.43 Comparisons of 2D (EAGD-84) and 3D (EACD-3D-08).....71
Figure 2.44 Spectral acceleration values for 2D and 3D analyses for OBE1 ground motion 71
Figure 2.45 Maximum principle stress plots of SEE1-1 ground motion for deepest cross section (h=138m) a) 3D EACD-3D-08 b) 3D ANSYS c) 2D plane stress d) 2D plane strain respectively 73
Figure 2.46 Maximum principle stress plot of SEE1-1 ground motion for y=69 m 2D plane stress for sections A and F 73
Figure 2.47 Maximum principle stress plots of SEE1-2 ground motion for deepest cross section (h=138m) a) 3D EACD-3D-08 b) 3D ANSYS c) 2D plane stress d) 2D plane strain respectively 74
Figure 2.48 Maximum principle stress plot of SEE1-2 ground motion for y=69 m 2D plane stress for sections A and F 74
Figure 2.49 Maximum principle stress plots of SEE1-3 ground motion for deepest cross section (h=138m) a) 3D EACD-3D-08 b) 3D ANSYS c) 2D plane stress d) 2D plane strain respectively 75
Figure 2.50 Maximum principle stress plot of SEE1-3 ground motion for y=69 m 2D plane stress for sections A and F 75
Figure 2.51 Crest displacement time histories for SEE1-1, SEE1-2 and SEE1-3 ground motions respectively 77
Figure 2.52 Performance criterion graph of SEE1 in combination 1 (3D).....79
Figure 2.53 Sandwich model sketch 80
Figure 2.54 Differences of sandwich and classical model on crack pattern.....80

CHAPTER 1

INTRODUCTION

1.1 General

Industrial and technological developments in Turkey increase the energy demand which should be supplemented by proper sustainable energy resources. Hydroelectric power is one of the essential clean and renewable energy sources similar to solar and wind energy. Turkey utilized only about 35 % of its potential by 2009. The electricity produced in Turkey between 1970 and 2008 is listed on the bar chart shown in Figure1.1 considering thermic and hydraulic resources. It is observed that demand of energy increased tremendously. Unfortunately, percentage of hydroelectric energy production is decreasing. Turkey has sustainable hydropower potential of about 20000 MW with additional benefits of realization speed and use of water for irrigation purposes.

Most of the developed countries had already utilized their hydropower potential by the end of 1980s. For example, the utilization of hydroelectric power potential for energy production in France, Spain and Italy were about 70-80 %. In order to increase the utilization of hydroelectric power, Turkish government authorized the private entrepreneurs to be involved in the investments since 2006. Seismic analysis and design principles for concrete dams are recommended for the first time in Turkey in 2012 BK guidelines. This study follows the procedures recommended in the BK guidelines for a case study of a roller compacted concrete (RCC) dam.

More than 500 dams have been constructed in Turkey since the proclamation of the republic until 2006. Since then, 400 or more dams are being built or in the planning and construction stages. Most of the dams were earth-fill dams before 2000's, but this custom has changed and concrete dams became more popular due to the use of roller compacted concrete (RCC). The first concrete dam built in Turkey was Çubuk 1 Dam in 1936. Some of the other older concrete dams are the Porsuk Dam (1948), the Elmalı 2 Dam (1955), the Sarıyar Dam (1956), and the Kemer Dam (1958) (Öziş, 1990).

Roller compacted concrete is a good alternative to conventionally vibrated concrete for mass concrete. Use of roller compacted concrete started in Europe after the second world war and the use of roller compacted concrete in dam construction was reported first in Italy in 1960s (Öztürk, 1998) . This new material attracted the attention of dam engineers in USA, Japan, China and Spain due to the benefits of ease and speed of construction and economy. However, the knowledge about the behavior of roller compacted dams under strong earthquakes is rather limited. The strength of the horizontal joints in roller compacted dams is usually smaller than the strength of the parent concrete. Therefore, cracks may propagate along the lift joints in most cases similar to that observed in the Sefid Rud buttress dam in 1990 Manjil earthquake (Wieland, 2004).

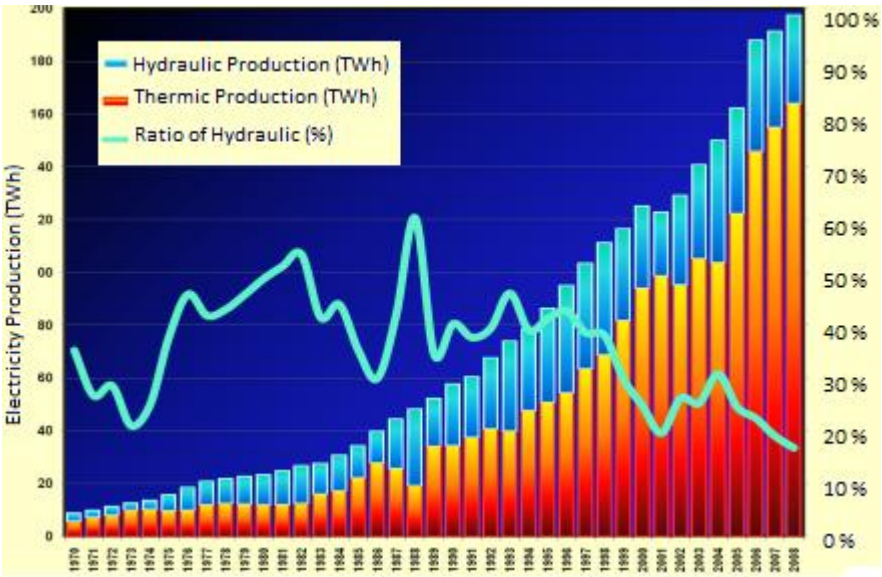

Figure 1.1 Electricity productions in terms of hydraulic distribution in Turkey

The use of roller compacted concrete for dam construction in our country started in the 1980's with the construction of Karakaya Dam, followed in 1990's with concrete arch Sır Dam in Kahramanmaraş and in 1999 with Berke Dam in Osmaniye. Since 2005, a significant number of dams is built or designed to be built with roller compacted concrete (RCC).

Seismic performance of concrete dams is generally deemed acceptable for the peak horizontal ground acceleration values in excess of 0.3g. Case histories of concrete dams (gravity, arch and buttress dams) were compiled by the United States Society on Dams (USSD) in order to understand the performance of concrete dams subjected to strong earthquakes. Dams with heights between 20-185 meters, exposed to 6.1-9.0 magnitude earthquakes and 0.3-0.7 PGA (peak ground acceleration) were considered (Table 1.1). In the Table 1.1 dams written in italic are the names of arch dams and the others are concrete gravity dams. Koyna, Rapel, Pacoima, Techi and Shapai dams were some of dams with heights greater than 60 meters. Failure of a concrete dam due to earthquakes was reported in Taiwan, Shih Kang Dam in Chi-Chi earthquake with magnitude of 7.6 (Nuss, 2012). Most of the dams proved to be invariably stronger than the designed performance under ground motion. These results may be due to the massive character of the dams with firm contact with valley sides and bottom, having some capacity of redistribution of stress transfer and possible material overstrength. It was observed that 0.3-0.7 PGA ground motions may result in moderate to extensive damage for dams greater than 60 meters height. Therefore, ground motion is one of the most essential parameter other than the design properties of the dam like geometry especially for regions with serious earthquake potential.

Turkey, being sectioned by two major and numerous minor seismic faults, is under great earthquake risk. Therefore, more attention should be given to the determination of the seismic parameters of design, for essential structures such as dams. According to studies in the USA, under the leadership of the Federal Energy Regulatory Commission (FERC) and United States Army Corps of Engineers (USACE) the basics of regulations for the seismic analyses of construction of hydropower systems have been developed since 1990s. Such regulations were missing in Turkey until the recent conference BK (Dams Congress) 2012.

Table 1.1 Earthquake response of concrete dams (PGA>0.3g)

Dam Name	Earthquake, Year, Magnitude	Height (m)	PGA	Damage
Williams	Loma Prieta, 1989, (7.1)	21	0.6	not damaged
Shih Kang	**Chi Chi, 1999 (7.6)**	**21.4**	**0.51**	**failure**
Bear Valley	Big Bear, 1992 (6.6)	28	0.57	not damaged
Gohonmatsu	Kobe, 1995 (7.2)	33	0.83	not damaged
Kasho	Western Tottori, 2000 (7.3)	46.4	0.54	low
Lower Crystal Springs	San Francisco, 1906 (8.3)	47	0.6	not damaged
Miyatoko	Tohoku, 2011 (9.0)	48	0.32	not damaged
Gibraltar	*Santa Barbara, 1925 (6.3)*	*52*	*0.3*	*not damaged*
Ambiesta	*Gemona-Friuili, 1976 (6.5)*	*59*	*0.36*	*not damaged*
Takou	Tohoku, 2011 (9.0)	77	0.38	moderate
Mingtan	Chi Chi, 1999 (7.6)	82	0.4	not damaged
Koyna	Koyna, 1967 (6.5)	103	0.6	moderate
Hsinfengkiang	Reservoir, 1962 (6.1)	105	0.5	high
Sefid Rud	Manjil, 1990 (7.7)	106	0.7	high
Rapel	*Santiago, 1985 (7.8)*	*111*	*0.31*	*low*
Pacoima	*Northridge, 1994 (6.8)*	*113*	*0.53*	*moderate*
Shapai	*Wenchuan, 2008 (8.0)*	*132*	*0.38*	*not damaged*
Techi	*Chi Chi, 1999 (7.6)*	*185*	*0.5*	*moderate*

1.2 Literature Survey

Various studies on the modeling the seismic response of arch dams and concrete gravity dams are available in the literature. Most of them have different assumptions in order to simplify the design; however these assumptions affect the results and cause the results to deviate from the real behavior of the dam under strong ground motion.

While analyzing the seismic response of a dam, the system consists of the dam body, foundation rock and reservoir of water. First static analysis is conducted including the construction stage, and dynamic analyses can be conducted for the given site specific ground motion data for under construction, operation and maximum earthquake conditions. Important considerations in the dam-reservoir- foundation interactions problem presented in the literature, are

1) Hydrodynamic effects,
2) Sub-structuring techniques,
3) Compressibility of impounded water,
4) Absorptive reservoir boundary,
5) Flexible foundation including inertial and damping effects,
6) Spatially uniform ground motion and spatially varying ground motion.

The milestone on the hydrodynamic effects on dams was the study of Westergaard in 1933. Rigid dams were modeled with vertical upstream face and the hydrodynamic forces were treated with an added-mass concept simplifying the incompressible water effects. The system is shown in Figure 1.2 and the added mass pressure is calculated in Equation 1.1 where "a" stands for horizontal ground acceleration in units of gravitational acceleration, "w" is the unit weight of water, "H" is the depth of reservoir and "z" is the distance from the base of the reservoir. Infinite reservoir condition was enforced where surface waves were ignored. Small displacements of the fluid particles were assumed. For the ground motion, only horizontal component in the upstream-

downstream direction was considered. This method was later generalized for any upstream geometry without any restrictions, since the added-mass was related with only on the total normal acceleration locally (Kuo, 1982). The hydrodynamic force consideration results in about 1.67 times the hydrostatic force acting on the dam. This result was an important contribution while considering the loads in the seismic design of dams.

$$P_z = \frac{7}{8} a w \sqrt{H(H - z)} \tag{1.1}$$

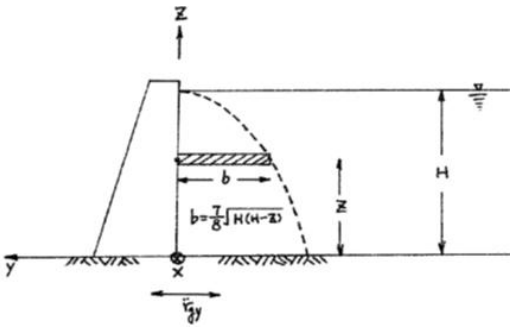

Figure 1.2 Westergaard's system of added-mass concept (Kuo, 1982)

The next essential development was the consideration of the water compressibility as introduced by Chopra in 1966. Rigid dam body was considered similar to Westergaard's approach. An analytical-numerical technique was developed to calculate the response history by considering the compressibility of water and both horizontal and vertical ground motions.

After these initial developments, with the rapid emergence of finite element method, different programs were developed in order to calculate the seismic response of dams. One of the first attempts was ADAP (Arch Dam Analysis Program) developed by Clough et al in 1973 which was capable of conducting three dimensional analyses of an arch dam including the static foundation flexibility. ADAP was generated from the computer program SAP. Finite element techniques were used in the program. Arch dam body could be modeled by using thick shell elements whereas three dimensional solid elements were employed for the foundation rock. For thick arch dams, dam body could also be modeled by three dimensional solid elements with eight nodes. Isoparametric hexahedron element with eight-nodes, first developed by Irons and Zienkiewicz (date), was used for the three dimensional dam elements in ADAP (1967). In the program ADAP, no special treatment was available for the fluid-structure and structure-foundation interactions besides the added mass concept. The program included a finite element mesh generator for the dam to ease the input preparation. The foundation mesh considered the deformability effect of foundation. However, it was massless to exclude foundation-structure interaction. Vogt flexibility coefficient concept was also included for foundation modeling. (Holand, 1968). The ADAP program could be used for static and dynamic analyses. For the static analysis of arch dams, three main loads were gravity, water and temperature loads. A constant temperature change was assumed at any elevation on each face of the dam. Natural frequencies and mode shapes of the system could also be calculated by using the subspace iteration methods.

Morrow Point dam was analyzed using ADAP program and results of dynamic analyses showed that due to ground motion arch dams were exposed to significant stresses and displacements. Fundamental period of the Morrow Point dam was calculated as 0.3 sec excluding the foundation flexibility.

Gutierrez and Chopra introduced the method of substructure to be used in the earthquake analyses of multi-component structures in 1976. The substructure method included the structure-foundation interaction, flexibility of the foundation, spatially varying free field ground motion

and interaction between two or more structures. In this method, the system was composed of different substructures. Linear elastic behavior was considered for the structure foundation system. It was proved that use of substructure finite elements provided almost identical results with the direct methods. As a result, due to the reduction in computational effort in substructure method, proposed method was found viable.

Dasgupta and Chopra presented a method for frequency dependent flexibility matrix computation for viscoelastic half space in generalized plane stress and strain in 1977. Dynamic stiffness matrices were determined from the results of boundary value problems related with harmonically time-varying stresses that were distributed uniformly. The stiffness matrix governs the steady-state response of the dam to harmonic seismic excitation, (Dasgupta and Chopra, 1977). Two dimensional generalized plane stresses were used in the idealization of the system of dam-foundation interaction with homogeneous, isotropic and linearly viscoelastic half space. The dynamic stiffness matrix from the work of Dasgupta and Chopra (1977) was later used by Fenves and Chopra (1985) in two dimensional dynamic analyses of gravity dams. The focus of the present study is three dimensional responses of gravity dams, therefore further discussions of two dimensional analysis methods are not given herein.

Hydrodynamic effects were investigated by Hall and Chopra starting from 1980 for the two and three dimensional channels extending to infinity. The aim of this study was to provide analyses tools to handle pressure calculations in arbitrary fluid domains with finite or infinite regions in both two and three dimensions. In the frequency domain, analysis including hydrodynamic interaction and water compressibility was performed using the substructure approach. Finite element method was used for dam and water elements in the model. A uniform cross-section beyond some point in the upstream was maintained for the infinite water domain which was the only restriction in terms of geometry (Hall, 1980). Rigid foundation was considered. The water compressibility effects resulted in frequency dependent pressure acting on the upstream face. Two dimensional concrete gravity and three dimensional arch dams could be analyzed. Consideration of water compressibility was found to be essential for arch dam analyses. It was proposed that concrete or earth gravity dams could be idealized by two dimensional models, whereas three dimensional models were necessary for arch dams.

Cross stream component of the ground motion cannot be included in the analysis for the two dimensional idealization. General system of two dimensional analyses is shown in Figure 1.3. Foundation was assumed rigid in this situation where there was no interaction between dam and foundation.

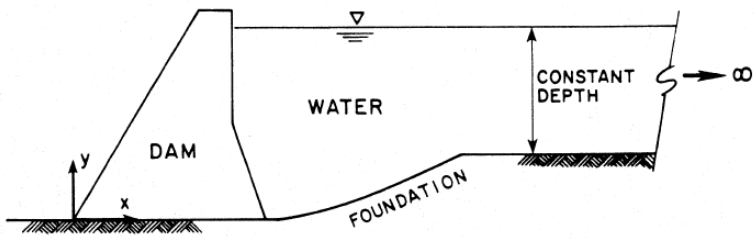

Figure 1.3 Two dimensional dam system with infinite fluid (Hall, Chopra ,1980)

Hydrodynamic effects on the response of concrete gravity dams were investigated with three different shapes of the reservoir. First one was a reservoir with constant depth infinite fluid domain, then infinite reservoir with variable depth and finally finite reservoir with variable depth (Figure 1.3). If the water compressibility was included, the frequency variation of hydrodynamic

force on the dam was mostly affected by the shape of the reservoir. For the first model which was with infinite water on constant depth, hydrodynamic forces due to horizontal (x) and vertical (y) components of ground motion were unbounded at the excitation frequencies same with the eigen-frequencies w_n^i.

Figure 1.4 shows the general view of a three dimensional arch dam analysis with infinite fluid domain. Cross section of the fluid domain was taken uniform beyond some point in the upstream direction. Linear behavior of dam and water was considered and rigid foundation was assumed. Morrow Point Dam (142 meter high single center arch dam) was selected as a case study in order to observe the hydrodynamic effects during the seismic response. It was observed that when empty reservoir or incompressible water was considered, the results of radial components of dam crest acceleration were independent of the modulus of elasticity of concrete. Hydrodynamic effect was also studied by Hall, Chopra in detail for rigid foundation in 1980. Foundation-dam interaction was the next important step to be considered for realistic seismic simulations of dams.

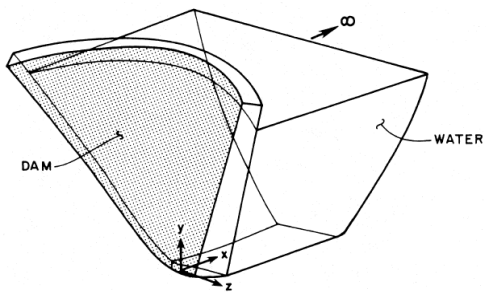

Figure 1.4 Three dimensional arch dam system with infinite fluid (Hall, Chopra ,1980)

Incompressible water consideration for dam-water interaction effects was studied by Kuo in 1982. Two basic procedures namely, Generalized Westergaard Formula and Galerkin Finite Element Method were used for the representation of hydrodynamic effect in calculations of the added-mass matrix. A case study of Techi Dam safety evaluation was performed under static loads and dynamic earthquake loads. It was observed that there was no major damage expected on the dam subjected to earthquake loads. However, joint opening and nonlinear response should be investigated independently due to the minor damages near the crest spillway.

A computationally efficient analytical program, called as EACD was developed by Fok and Chopra (1985) for the ground motion response of arch dams which was capable of handling dam-water interaction, foundation flexibility and effects of sediments at the boundary. Foundation flexibility was introduced by using massless finite element model of the foundation and damping effects were ignored similar to ADAP. Three dimensional solid elements were used for modeling the portion of foundation-rock region at the interface. Moreover, absorptiveness of the reservoir boundary was idealized with one dimensional damper, normal to the boundary. A wave reflection coefficient was defined as the ratio of the reflected hydrodynamic pressure waves to the amplitude of perpendicular pressure wave on the reservoir which is calculated from the Equation 1.2

$$\alpha = \frac{1-q}{1+q} \tag{1.2}$$

Where q is obtained from Equation 1.3

$$q = \frac{\rho C}{\rho_r C_r} \tag{1.3}$$

Here, $C_r = \sqrt{\frac{E_r}{\rho_r}}$ is the wave speed of the material on the reservoir bottom and sides and ρ_r is the unit mass of the foundation rock, ρ is the unit mass of water and C is the wave speed of water.

It was observed that dam-water interaction increased the earthquake response especially for the vertical component of ground motion for arch dams. Moreover, wave absorption of water resulted in a decrease in the dam response. Fok et al. (1985) stated that flexible foundation affects dam-water interaction and absorption capacity of reservoir not significantly, but may increase slightly the response of the dam. Water compressibility should definitely be included for the arch dam earthquake response analyses according to Fok et al. (1985).

Computer program EACD-3D was developed for three dimensional earthquake response of concrete dams (Fok, Hall, Chopra, 1986). It considered the dam-water interaction, sediments effect on the reservoir bottom and flexibility of foundation ignoring the inertia and damping. The concrete dam, foundation and reservoir were assumed to behave linearly. Foundation rock was idealized with the same procedure followed in ADAP program. A prismatic dam canyon in the upstream direction was assumed and a size parameter was used to define the foundation volume. The ratio of modulus of elasticity of foundation to concrete dam set the size parameter to be used in the analysis. Three dimensional solid elements were used to idealize the foundation. The program consisted of seven subsections. First subsection was the foundation mesh where impedance matrix was prepared and condensed to DOFs along the interface of the dam foundation. In Subprogram 2, dam mesh was assembled; mass, element stiffness and stress computation matrices were calculated. Then, in subprogram 3, dam stiffness and mass matrices were computed. Subprograms 4 and 5 were related to the impounded water. Frequency responses of dam and water were calculated in subprogram 6. Static analysis was computed in subprogram 6 in case of static option was selected. Final subprogram computed the time history response of the dam.

It was demonstrated with the parametric studies and the previous models that the water compressibility and reflection of pressure waves affect the response of the system (Chopra, 1988). The program was verified by comparing the analysis results of the Morrow Point arch dam in the USA with forced vibration test experiments (Duron and Hall, 1988).

Arch Dam Analysis Program (ADAP) was improved by Ghanaat and Clough and the new version was called as EADAP, Enhanced Arch Dam Analysis Program (1989). The major modifications were including the hydrodynamic effects of water using equivalent added mass matrix assuming incompressible water. Previously, only V-shaped valleys could be modeled for arch dams built in for the mesh generator. However, U-shaped valleys were also considered in EADAP. In addition, there were some improvements for the foundation model having more realistic results near the crest of the dam. For the static analysis, gravity load, water load, temperature load, silt load and ice load were included. The results of the static analysis were the nodal point displacements and element stresses due to these loads applied.

Analyses methods until the end of 1980's for arch dams only focused on linear behavior. Fenves developed a nonlinear analysis method to model the opening and closing action of contraction joints during earthquake in arch dams (1989). ADAP88 program was developed to model the contraction joint behavior between the monoliths of concrete arch dams. Only joint movements were modeled with nonlinear constitutive laws, whereas the rest of the dam remained linear. Static analyses were conducted in two parts in order to represent the cantilevers transfer the weight directly to foundation by giving zero elastic modulus to other cantilevers. Then in second static analysis, moduli of elasticity of remaining cantilevers were defined. Figure 1.5 presents the arch dam model with nonlinear joint elements in program ADAP88. By modeling the joints, redistribution of stresses during earthquake by opening and closing was possible. Vibration period of the arch dam was found to increase due to the loss of arching action during opening of joints.

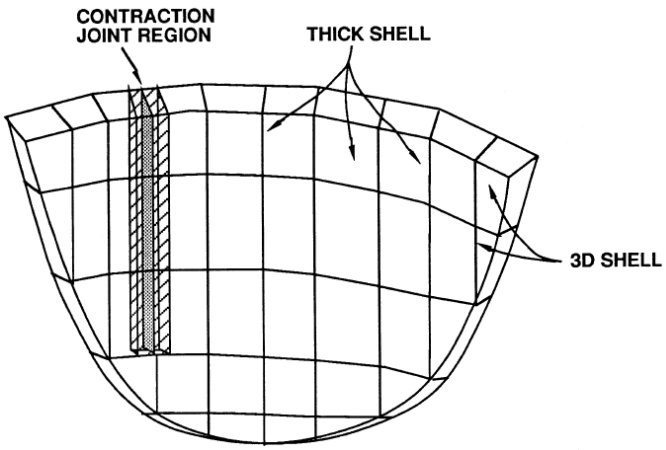

Figure 1.5 Arch dam model in ADAP88 with nonlinear joint elements (Fenves et. al. 1989)

Zhang and Chopra developed the frequency dependent dynamic stiffness matrix using the boundary element method for uniform cross section, infinitely long canyon in a homogeneous viscoelastic half-space (1991). Wave scattering was modeled for multi support excitation to consider spatially varying ground motion. A series of two-dimensional boundary problems were solved to determine the impedance matrix, which were more efficient compared to the three dimensional boundary element methods. Fourier transform of full space Green's functions were employed in these two dimensional boundary problems. The procedure followed for the development of impedance matrix at the degrees of freedom of interface of the dam- foundation using boundary element method can be summarized as follows:

1) The interface of dam-foundation was discretized into two dimensional surface elements and Fourier transforms were obtained. Then, canyon boundary of half space surface at x=0 was divided into line elements. 2) Three sets of linear algebraic equations related with displacements were solved for each of the node. 3) Nodal displacements were represented by the nodal tractions from the solutions of the linear algebraic equations. Then, flexibility influence matrix was obtained for each harmonic excitation frequency. Inverting the flexibility matrix for each frequency, dynamic stiffness matrix was obtained.

In 1995, EACD-3D program was further modified to include the inertial and damping effects of the foundation for the effects of interaction of the dam-foundation (Tan and Chopra, 1995) by using the procedure of Zhang and Chopra (1991). Substructure method was employed to consider the hydrodynamic effects in the frequency domain. Direct boundary element method was used according to Zhang's procedure, for the computation of the impedance matrix of foundation. Cubic interpolation was assumed for the determination of smooth impedance coefficients for intermediate frequencies. It was observed that fundamental resonant response of the dam was decreased by the frequency dependent foundation model. Symmetric vibration modes were more affected by the dam-foundation interaction when compared with the unsymmetrical vibrations modes (at cross-stream component of earthquake). If reservoir was almost full, then the effect of dam-foundation interaction on the reduction of fundamental resonant frequency was limited. Morrow Point Dam was investigated using the EACD-95 program. It was seen that previous procedures with massless foundation models overestimated stresses in arch dams. It was concluded that, as the ratio of modulus of elasticity of foundation to dam was reduced, effects on fundamental resonant frequencies of dam-foundation interaction increased compared to the rigid foundation case. The radiation damping of reservoir boundary absorption resulted in significant reduction in the dam response. It is noted that incorporating the mass and radiation effects of foundation in evaluation of seismic safety of existing dams was crucial.

SCADA, "Smeared Crack Arch Dam Analysis", was developed by Hall in 1997 for seismic analysis of arch dams. SCADA modeled the contraction joints closing and opening actions. It

provided time savings when compared with ADAP-88, due to the reduction in the number of degrees of freedom. Nonlinearity was included in terms of opening and closing of contraction joints and sliding of cracks in the concrete dam body. Gravity, temperature, water pressure, opening of contraction joints, filling the cracks with grouting were the major analysis steps in SCADA. Dam and foundation were discretized for the static analysis. Shell elements were employed for idealization of finite elements of the dam. In the smeared crack method, when a crack was formed, then modulus of elasticity of that portion of element was reduced to zero in the direction normal to the crack (Ralph, Graves 1987, 2008). Foundation was modeled using solid elements with linearly elastic behavior ignoring the mass. Spatially uniform earthquake ground motion was applicable. Damping effects in the dam was included with a backward difference method of Bossak's extension of the Newmark's method. Incompressible water was assumed for hydrodynamic effects. As a case study Pacoima Dam was studied using SCADA and no severe damage was observed on the dam.

Proulx and Paultre conducted a study on hydrodynamic effects on the dam seismic response in 1997. It was concluded that when incompressible water was used in the analyses corresponding to the Westergaard's solution with an additional mass on the upstream, the fundamental frequency of the system was overestimated. However, the damping of the system was underestimated (Proulx, Paultre, 1997).

Wieland (2004) studied the subject of earthquake safety of concrete dams. According to Wieland, seismic safety was also affected by the dynamic tensile strength of the concrete. Other than the uniaxial compressive strength of concrete; age effect, strain-rate effect and size effect are the other parameters influencing the dynamic tensile strength. Size effect was due to the thickness of the dam and fracture toughness of concrete (Wieland, 2004). Moreover, damping ratios can be changed with respect to the modes of vibration. It was suggested to use about 10 % damping ratio for the lowest modes of vibration and it may increase for the higher modes while considering the dam, foundation and reservoir interaction using the linear elastic analyses. Analyses done with incompressible reservoir and massless foundation including only the flexibility of the foundation with 5 % damping ratio might overestimate the stresses 2 or 3 times more than the dynamic stress under earthquake excitation (Wieland, 2004). If it is desired to reduce the seismic response of an arch dam, complicated dynamic interaction analyses should be studied.

1.3 EACD-3D-08

This section describes EACD-3D-08 program developed by Chopra and Wang in detail owing to the use of the program in the course of this study.

1.3.1 General

The computer program EACD-3D-2008 is the latest version of programs developed by Chopra and his colleagues for the three dimensional earthquake analyses of concrete dams. It is the continuation of the previous analyses procedures (EACD-3D and EACD-3D-96) including all (foundation-dam-water) interaction phenomenon "correctly" along with spatially non-uniform motion input capability. Not only flexibility of foundation, but also mass and damping effects were included. In addition, dam-water interaction was studied by considering the water compressibility and sediments absorption at the bottom and sides of the reservoir. However, foundation-water interaction was not considered since it was pointed to have no significant effect (Tan, Chopra, 95).

The main assumptions of the program are as follows: 1) concrete dam, foundation and impounded water behave linearly. 2) Thermal effects and possible crack generations of concrete are not considered. 3) Opening of the construction joints is ignored. 4) Water cavitation is not considered.

Ground motion can be spatially uniform or varying according to the user's desire where the earthquake data is specified as the free-field motion. It should be noted that over the reservoir bottom and sides, the ground motion is uniform in the cross-stream direction.

The analyzed system consists of three main parts in the EACD program. These are the concrete dam, foundation rock and impounded water substructures. For the selected coordinate system of the program, +x direction is on the upstream side, y axis is for the vertical direction along the height of the dam and finally z axis is for the cross-stream direction. Figure 1.6 shows the general view of the system of the dam, foundation and water.

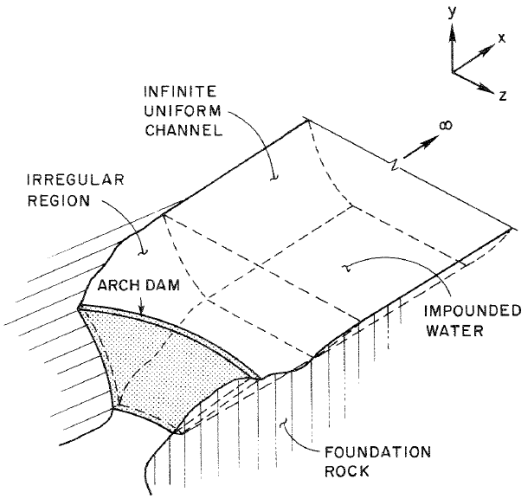

Figure 1.6 System of dam-foundation-water (Fok, Hall, Chopra, 86)

1.3.2 Finite Elements

Concrete dams can be modeled using three dimensional solid finite elements or shell elements (for arch dams). In order to assign the connection between the dam elements and foundation, transition elements may be used. Element library in the EACD-3D-08 program with quadratic shape functions are shown in the Figure 1.7. Each node has three degrees of freedom in the x, y and z directions for the solid elements. Minimum 8 nodes are required to define a rectangular prism element, (one node at the corner of the prism) and it may increase to 20 nodes for a fully quadratic element. Standard Gauss quadrature rule is used for the integrations of element stiffness matrix. There are 8 Gauss quadrature locations per elements. While numbering the nodes of an element, nodes should be numbered in the counter-clockwise direction from the upstream side. Figure 1.8 shows the proper node-numbering rule that should be followed. As the focus of this study is on gravity dam modeling in three dimensions, shell elements will not be further discussed.

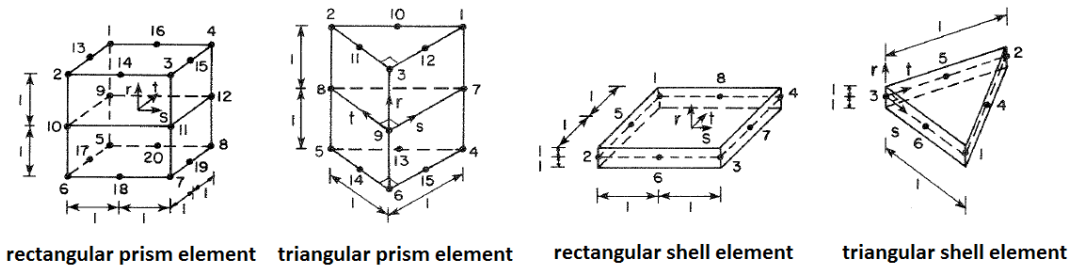

Figure 1.7 Element alternatives for modeling dam (Wang, Chopra, 2008)

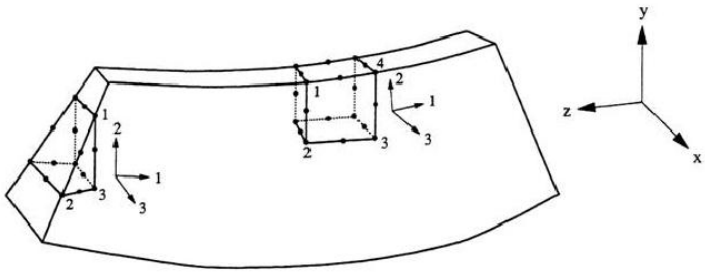

Figure 1.8 Node numbering of solid dam elements (Wang, Chopra, 2008)

1.3.3 Foundation

Complex valued frequency-dependent impedance matrix of the foundation is required for the analysis of earthquake on the dam-foundation interaction. Direct boundary element procedure was used for the interface between the dam and foundation rock (Zhang and Chopra, 1991). It is essential to note that nodal points of foundation should coincide with the dam nodes.

Total displacement was composed of the free-field motion (u_{ff}) and the scattered-field motion (u_s) when the canyon was present which was given (Zhang and Chopra, 1991) in Equation 1.4. Equation 1.5 represents the total traction vector

$$\{u(x)\} = \{u_{ff}(x)\} + \{u_s(x)\} \tag{1.4}$$

$$\{t^n(x)\} = \{t^n{}_{ff}(x\} + \{t^n{}_s(x)\} \tag{1.5}$$

Reciprocal theorem is used for the calculation of boundary integral equation for elastodynamic equilibrium state in Equation 1.6.

$$\int_{\Gamma_c \cup \Gamma_h \cup \Gamma_s} \int_{-\infty}^{\infty} \{t^{n*}(\vec{x}, \overrightarrow{x_{os}})\}^T \{u_s(\vec{x})\} dx d\Gamma = \int_{\Gamma_c \cup \Gamma_h \cup \Gamma_s} \int_{-\infty}^{\infty} \{u^*(\vec{x}, \overrightarrow{x_{os}})\}^T \{t^n{}_s(\vec{x})\} dx d\Gamma \tag{1.6}$$

Where Γ_c is the cross section of the canyon at x=0, Γ_h is on the surface of the half-space with x=0 line and Γ_s is the small contour of radius. Then, discretization of integration domain was obtained which extends to a finite distance on the surface of the half-space surface, dividing into M line elements with M+ 1 nodes on the system when the linear interpolation functions are employed.

Rectangular or triangular surface elements can be used for modeling the dam foundation interface (Figure 1.9). There are three displacement degrees of freedom for each node of the elements. In the Figure 1.9, the undistorted and parent forms of the elements are shown. There exists maximum of 8 nodes for rectangular and 6 nodes for triangular elements. They can be condensed to 4 and 3 respectively by eliminating the intermediate nodes. These elements are also isoparametric and can be used in distorted shapes. Quadratic shape functions are employed for these elements. For the numbering of the nodes of these elements, no specific rule is defined.

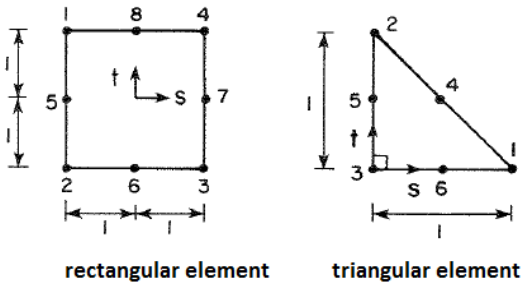

Figure 1.9 Surface boundary elements for foundation rock (Wang, Chopra, 2008)

When considering the compressibility of water, effect of the reservoir absorption may also be included. Impounded water and foundation rock interaction becomes important in this consideration and due to sedimentary materials deposit on the reservoir bottom which are highly saturated with a low shear modulus (Fok and Chopra, 1985). One-dimensional wave absorption model is used for the representation of the absorption.

1.3.4 Impounded Water

The impounded water is limited by the upstream side of the dam on the x direction and defined by the natural topography, the valley on the z direction. Irregular reservoir domain may be complicated but using the finite element models, the fluid is modeled up to a finite boundary and then it extends to infinity in the x direction.

Three dimensional fluid elements with pressure nodes are used to model the finite part of the impounded water. The interaction between the dam nodes and water nodes are satisfied through equilibrium. Three dimensional wave equation (Equation 1.7) expresses the motion of water in the reservoir.

$$\frac{\partial^2 P}{\partial x^2} + \frac{\partial^2 P}{\partial y^2} + \frac{\partial^2 P}{\partial z^2} = \frac{1}{C^2}\frac{\partial^2 P}{\partial t^2} \tag{1.7}$$

Hence, dam nodes with displacement degrees of freedom must match the fluid element nodes with pressure degrees of freedom. Transmitting plane is defined for connecting the irregular finite fluid with the infinite uniform channel.

Five sub-meshes were used for modeling different parts of the reservoir. Mesh 1 is the entire finite irregular region that models using three dimensional elements given in Figure 1.9 rectangular or triangular solid elements. Mesh 2 discretizes the transmitting plane, Mesh 3 spans the interface between the dam and water on the upstream side and Mesh 4 discretizes the bottom and sides of the reservoir. Mesh 2, mesh 3 and mesh 4 are modeled using two dimensional boundary elements shown in Figure 1.10. Finally, mesh 5 is the one dimensional line element

spanning the bottom and sides of the transmitting plane. General view of the impounded water meshes are plotted on Figure 1.10.

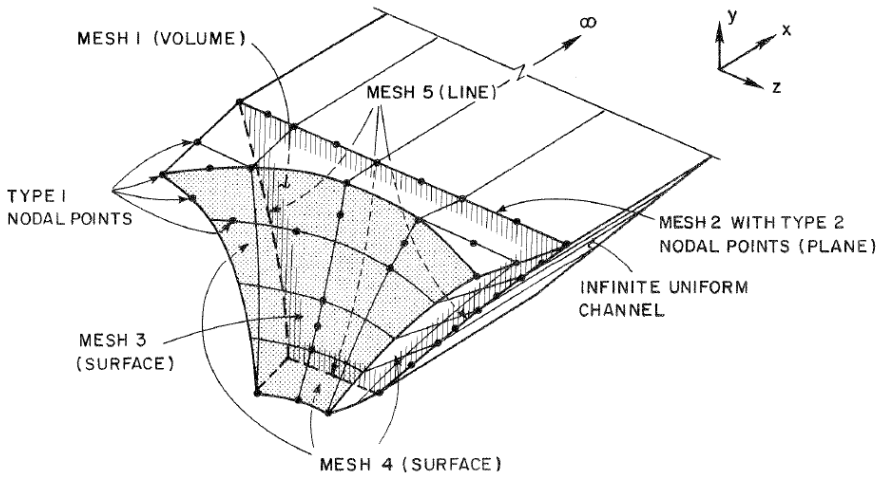

Figure 1.10 Meshes used for modeling the irregular fluid region (Wang, Chopra, 2008)

In the static analysis only the weight of the dam and hydrostatic pressure on the upstream side of the dam is included. For the dynamic analyses complete system including the dam, foundation rock and impounded water are considered.

1.3.5 Materials Models

The system is composed of concrete dam, impounded water and foundation rock. Linear behavior of these components is assumed.

The required parameters for the concrete properties are the unit weight, modulus of elasticity, Poisson's ratio and hysteretic damping factor. Hysteretic damping factor is the two times of the viscous damping ratio in percent. ($\eta=2\zeta$)

Damping is included in the modulus of elasticity as in Equation 1.8.

$$E' = E(1 + 2i\zeta) \tag{1.8}$$

where E is the modulus of elasticity, E' is the modified modulus of elasticity used in the calculations and ζ is the damping ratio.

Properties of the foundation rock are included by considering the unit weight, modulus of elasticity and Poisson's ratio of the rock. Again for damping, constant hysteretic damping factor for rock should be used.

For the reservoir, velocity of pressure waves in water, C and unit mass of water are the properties that should be included in the program for analyses.

1.3.6 Frequency Domain Equations

Frequency domain equations are summarized for EACD-3D-08 in this section (Chopra and Wang, 2008). The calculation procedure followed for the idealization system of EACD-3D-08 is described below:

General equation of motion for the dam is:

$$m_c \ddot{r}_c^t + c_c \dot{r}_c^t + k_c r_c^t = R_b(t) + R_h(t) \tag{1.9}$$

where, m, c, k are the mass, damping and stiffness matrices and subscript c denotes for concrete, R_b is the reaction force due to the dam-foundation rock interaction and R_h corresponds to the hydrodynamic effects.

Then using partitioning the total displacement into total displacement on dam-foundation rock interface and total displacement not on the interface are obtained. Total displacement not on the dam-foundation rock interface is the summation of structural displacement due to static earthquake induced free-field (quasi-static displacement) and instantaneous displacement. Quasi-static displacement can be obtained from the Equation 1.10 where k_b is the stiffness matrix of nodal points on dam-foundation rock interface; $\hat{r}_f^f$ is the free field displacements.

$$r^s = -k^{-1} k_b \, r_f^f \tag{1.10}$$

The general equation of motion then converts to equation given in Equation 1.11 by substituting Equation 1.10, transferring quasi-static displacement to other side of the equilibrium and taking Fourier transform where η_s is the constant hysteretic damping factor of the dam.

$$\left[-\omega^2 \begin{bmatrix} m & 0 \\ 0 & m_b \end{bmatrix} + (1 + i\eta_s) \begin{bmatrix} k & k_b \\ k_b^T & k_{bb} \end{bmatrix}\right] \begin{Bmatrix} \hat{r}(\omega) \\ \hat{r}_b(\omega) \end{Bmatrix} = \begin{Bmatrix} \hat{R}_h(\omega) \\ \hat{R}_b(\omega) \end{Bmatrix} + \left[\omega^2 \begin{bmatrix} m & 0 \\ 0 & m_b \end{bmatrix} - (1 + i\eta_s) \begin{bmatrix} 0 & 0 \\ k_b^T & k_{bb} \end{bmatrix}\right] \begin{Bmatrix} \hat{r}^s(\omega) \\ \hat{r}_f^f(\omega) \end{Bmatrix} \tag{1.11}$$

The complex valued impedance matrix of the foundation $S_f(\omega)$ is used to set the relation between the force and displacement of the free-field ground motion on the interface of dam-foundation.

$$S_f(\omega)\left[\hat{r}_f^t(\omega) - \hat{r}_f^f(\omega)\right] = \hat{R}_f(\omega) \tag{1.12}$$

In which subscript f denotes for foundation, superscript t and f are total and free-field displacements respectively.

$$\hat{R}_f(\omega) = -\hat{R}_b(\omega) \tag{1.13}$$

This equation ensures the equilibrium of the interaction forces between the dam and foundation rock at the interface of the dam-foundation.

The foundation displacements are calculated by subtracting the free-field displacement from the total displacement.

$$\hat{r}_f^t(\omega) - \hat{r}_f^f(\omega) = \hat{r}_b(\omega) \tag{1.14}$$

$$\hat{\hat{R}}_b(\omega) = -S_f(\omega)\hat{r}_b(\omega) \tag{1.15}$$

Then the equation of motion in terms of relative displacements r and $\hat{r}_f^f$ can be written as

$$\left[-\omega^2\begin{bmatrix} m & 0 \\ 0 & m_b \end{bmatrix} + (1+i\eta_s)\begin{bmatrix} k & k_b \\ k_b^T & k_{bb} \end{bmatrix} + \begin{bmatrix} 0 & 0 \\ 0 & S_f(\omega) \end{bmatrix}\right]\begin{Bmatrix} \hat{r}(\omega) \\ \hat{r}_b(\omega) \end{Bmatrix} = \begin{Bmatrix} \hat{R}_h(\omega) \\ 0 \end{Bmatrix} + \left[\omega^2\begin{bmatrix} m & 0 \\ 0 & m_b \end{bmatrix} - (1+i\eta_s)\begin{bmatrix} 0 & 0 \\ k_b^T & k_{bb} \end{bmatrix}\right]\begin{Bmatrix} \hat{r}^s(\omega) \\ \hat{r}_f^f(\omega) \end{Bmatrix} \tag{1.16}$$

A set of 3(N+N_b) frequency dependent complex valued equations exist in the Equation 1.16. Ritz method is performed in order to reduce the number of DOFs and then Fourier transform of the displacement equation of linear combination of Ritz vectors is taken and the following formula is obtained.

$$\hat{r}_c(\omega) = \sum_{j=1}^{J} \widehat{Z}_J\ (\omega)\Psi_j \tag{1.17}$$

The following eigenvalue problem is solved and the first J eigenvalues λ_j^2 and the eigenvectors Ψ_j are calculated.

$$\left[k_c + \widetilde{S_f}(0)\right]\Psi_j = \lambda_j^2 m_c \Psi_j \tag{1.18}$$

$\Psi_j^T m_c \Psi_j = 1$, normalization is obtained for the Ritz vectors.

Three dimensional wave equation of Helmholtz given in Equation 1.19 is used for harmonic ground motion effect on water where $\hat{P}$ (x, y, z, w) is the Fourier transform of hydrodynamic pressure and c is the velocity of pressure waves in water.

$$\frac{\partial^2 \hat{P}}{\partial x^2} + \frac{\partial^2 \hat{P}}{\partial y^2} + \frac{\partial^2 \hat{P}}{\partial z^2} + \frac{w^2}{C^2}\hat{P} = 0 \tag{1.19}$$

It can be expressed as linear form of

$$\hat{P}(x,y,z,\omega) = \hat{P}_0(x,y,z,\omega) + \sum_{j=1}^{J} \widehat{\ddot{Z}_{jn}}\ (\omega)\widehat{P_j^f}\ (x,y,z,\omega) \tag{1.20}$$

The boundary conditions of $\hat{P}_0(x,y,z,\omega)$ for rigid dam, in Equation 1.20 are as follows:

$$\frac{\partial}{\partial n}\hat{P}_o(s,r,\omega) = -\rho\widehat{\ddot{r}_n^s}\ (s,r,\omega)$$

$$\left[\frac{\partial}{\partial n} - i\omega q\right]\hat{P}_o(s,r,\omega) = -\rho\widehat{\ddot{r}_{fn}^f}\ (s^t,r^t,\omega)$$

$$\overline{P_0}\ (x,H,z,\omega) = 0$$

The boundary conditions of $\hat{P}_j^f(x,y,z,\omega)$, in Equation 1.20 are as follows:

$$\frac{\partial}{\partial n}\hat{P}_j^f(s,r,\omega) = -\rho\Psi_j^f(s,r)$$

$$\left[\frac{\partial}{\partial n} - i\omega q\right]\hat{P}_j^f(s',r',\omega) = 0$$

$$\hat{P}_j^f(x,H,z,\omega) = 0$$

$$S(\omega)\,\hat{Z}(\omega) = L(\omega) \tag{1.21}$$

Ritz vector simplifies the solution of Equation 1.19. Dam-foundation-reservoir interaction for each excitation frequency solution is expressed in Equation 1.21. S(ω) includes the flexibility effects except the hysteretic damping given in Equation 1.22 and L(ω) term includes the water effect for the limit cases of imposed mass and water given in Equation 1.23.

$$S_{nj}(\omega) = [-\omega^2 + (1+i\eta_s)\lambda_n^2]\delta_{nj} + (\Psi_n^b)^T\left[S_f(\omega) - (1+i\eta_s)S_f(0)\right]\Psi_j^b + \omega^2(\Psi_n^f)^T\hat{R}_j^f(\omega) \tag{1.22}$$

$$L_n(\omega) = (\Psi_n^f)^T\hat{R}_o(\omega) + \omega^2(\Psi_n)^T m_c\hat{r}_c^s(\omega) - (1+i\eta_s)(\Psi_n^b)^T[k_b^T k^{-1}k_b + k_{bb}]\hat{r}_f^f(\omega) \tag{1.23}$$

After $\hat{Z}(w)$ is calculated, Fourier transform is determined and it is repeated for each excitation frequencies of the earthquake ground motion considered. Then inverse Fourier transform is determined in time domain as Z (t).

Displacement response is obtained using Equation 1.24 as r_c (t).

$$r_c(t) = \sum_{j=1}^{J} Z_j\ (t)\Psi_j \tag{1.24}$$

Finally, stresses in the dam are computed related to the nodal displacement vector as in Equation 1.25 where T_p is the transformation matrix of stress-displacement for a finite element.

$$\sigma(t) = T\,r(t) \tag{1.25}$$

The procedure followed for the analysis of the seismic response of dams is summarized on the Figure 1.11.

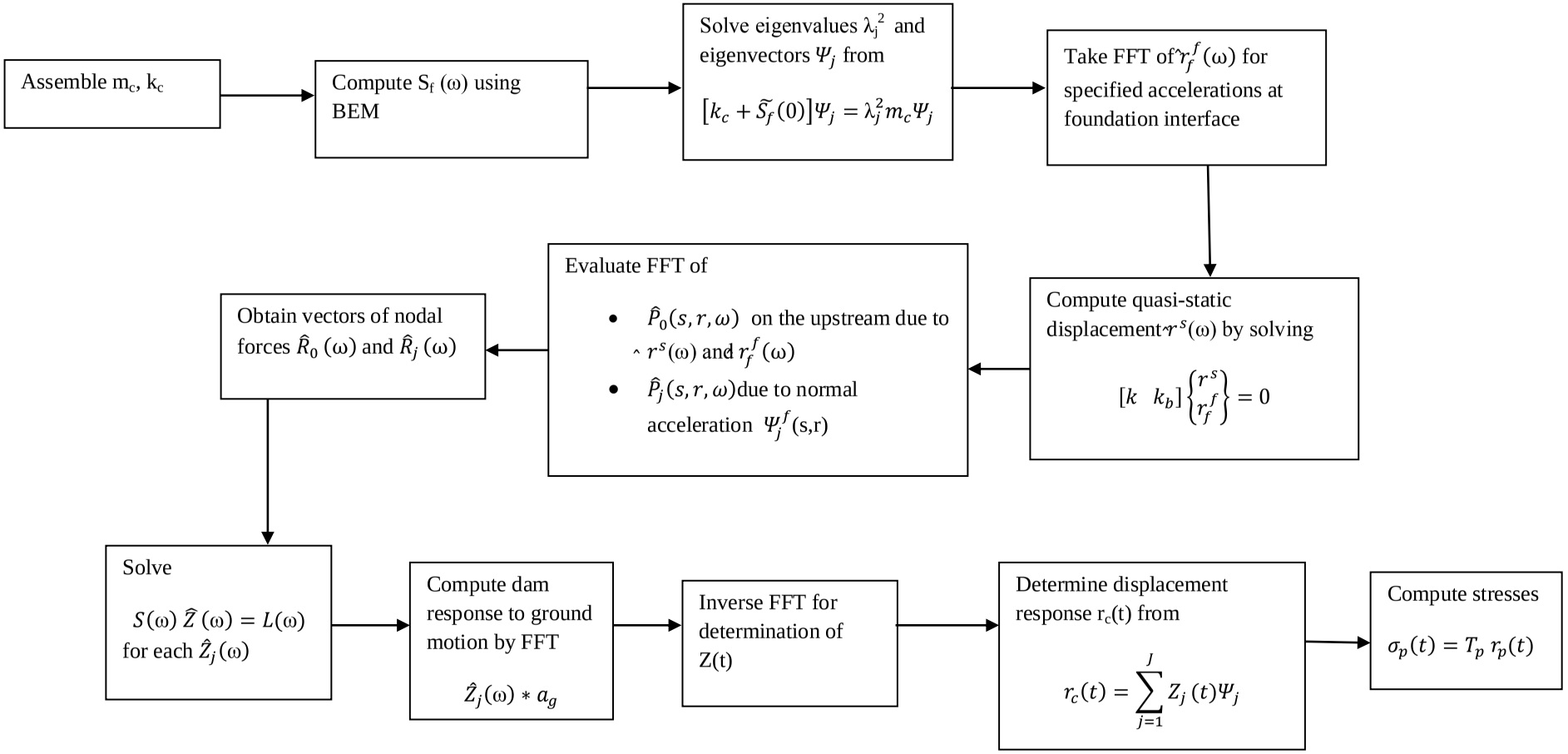

Figure 1.11 Analysis Procedure

1.4 Scope and Objective

Seismic analysis of dams requires complex solutions for the linear analysis of three dimensional systems of containing dam-foundation-water interactions. For the dam-foundation interaction problem, flexible foundation with mass and damping is essential. Water compressibility and wave absorption capacity of reservoir should be included to have a correct representation of dam-water interaction in the model. Commercial software does not consider these key points and they are inadequate. In the literature, three dimensional analysis conducted for gravity dams considering all these interactions is very limited, since most of the three dimensional analyses were conducted for arch dams.

The object of this study is

- To analyze a concrete gravity dam planned to be constructed in a relatively narrow valley considering three dimensional geometry and all interactions.

- To understand the seismic response of a concrete gravity dam response subjected to seismic ground motion including the effects of flexible foundation with inertial and damping effects, compressibility of water and reservoir bottom and sides absorption with a comprehensive dam-water-foundation interaction idealization.

- To study the parameters influencing the seismic behavior of the considered concrete gravity dam.

- To assess the seismic performance criteria by using the procedures suggested by BK Guidelines (2012).

- To examine the three dimensional analysis results in light of the results obtained from a rigorous two dimensional dam-reservoir-foundation analysis for the dam considered.

In chapter 2, a case study of a concrete gravity dam analyzed using EACD-3D-08 is presented. Andıraz Dam, in Kastamonu, Turkey was selected and using three dimensional solid elements the seismic response was studied. Additionally, assessments of use of linear analyses are presented according to USACE (2005). Chapter 3 summarizes the main conclusions of the study.

CHAPTER 2

SEISMIC ASSESSMENT STUDY OF ANDIRAZ DAM

In this chapter, seismic response and assessment study of Andıraz Dam is presented. These analyses are conducted using EACD-3D-2008. Stress plots, displacement time histories and seismic assessment using linear analyses are discussed. Parametric studies are performed in order to observe the effects of foundation flexibility, bottom absorption of foundation and the downstream slope on the seismic response. Comparisons of three dimensional seismic analyses results with two dimensional time history analysis are made. Effect of valley geometry on the seismic response is studied to demonstrate the importance of three dimensional analyses for gravity dams with no transverse joints.

2.1 General

Roller compacted concrete (RCC) has been commonly used in dam construction in Turkey in the last decade. RCC has zero slump and is consolidated by external vibration usually with rollers. RCC dams have several benefits compared to the conventional concrete dams. RCC is a low slump concrete which can support equipment during placement and develop minimum temperature rise during hydration. In addition, it can develop strength, impermeability and durability similar to conventionally vibrated concrete. Therefore, RCC is a logical choice to be constructed for mass concrete construction.

Andıraz Dam is a roller compacted concrete (RCC) dam in Kastamonu in the Black Sea Region of Turkey. Andıraz Dam's main design purpose is to protect Düzce and Kastamonu from seasonal floods. It also has some hydropower potential, but that is secondary in the design criteria. Some explanation on the section of RCC instead of other dam types is necessary: 1) No clay source nearby, 2) Significant slope stability risk in the reservoir and a large possibility of overtapping in the dams design period. According to General Directorate of State Hydraulic Works (DSİ), the dam is expected to have a capacity of 214 million cubic water storage, and 36 MW of electricity production capacity. Moreover, the dam will play an important role for mitigation of the flood hazard.

Andıraz Dam is located near the North Anatolian fault region. Therefore, it is essential to pay a great attention to earthquake risk. According to the Turkish earthquake map prepared by the General Directorate of Natural Disasters, Kastamonu has different degree of earthquake zones from 1 to 4. The Figure 2.1 shows the regions of earthquake zones of Kastamonu. Andıraz dam is located in the highest seismic hazard zone of the region. Further information on seismicity of the region and the earthquakes considered are provided in section 2.5.

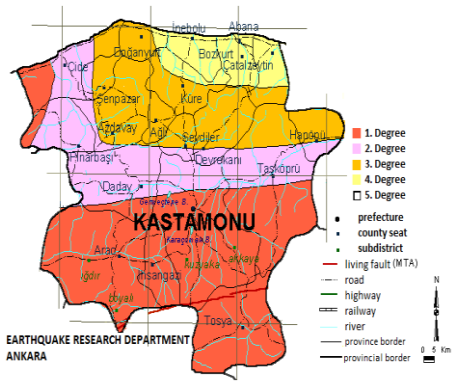

Figure 2.1 Earthquake zones of Kastamonu

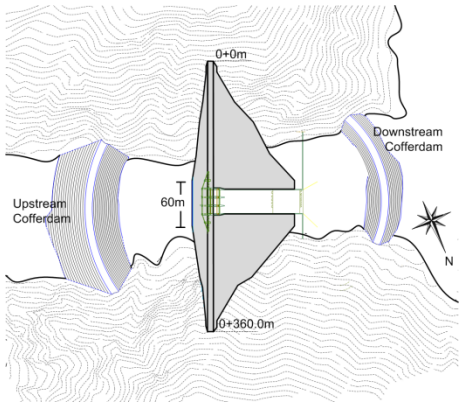

Figure 2.2 Andıraz Dam

Andıraz Dam (Figure 2.2) is designed as a 138 meter RCC gravity dam and has a crest length of 362 meter as shown in Figure 2.3. Located in a narrow valley, the mid part is 64 meter wide. The slopes of the valley sides have slightly different slopes 0.85 and 1.015 on two sides respectively. The dam is designed with a vertical upstream face and a downstream face slope of 1. The width of the crest is 10 m. In the course of this study, downstream slope of the dam is varied between 0.8-1.05 to investigate the change in stress demands in Section 2.7.3.

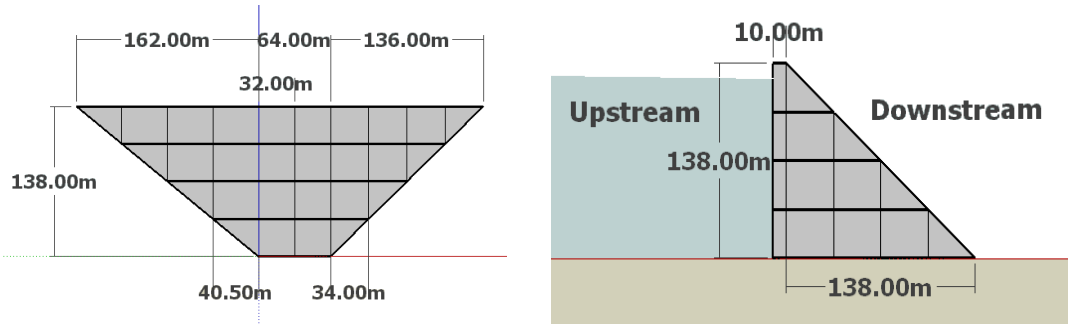

a) b)

Figure 2.3 Andıraz Dam Sectional Properties a) downstream view b) cross sectional view

2.2 Seismic Safety Assessment Methodology

Seismic design of dams can be conducted using linear elastic analysis methods owing to the brittle nature of concrete (USACE, 2003). Recently, Concrete Dams Committee of DSİ published a design guideline following the similar principles of USACE (2003-2007). This methodology requires conducting linear elastic time history analyses. Afterwards, demand to capacity stress ratios and total duration exceeding the tensile stresses of the dam are calculated (Figure 2.4). Demand capacity ratio is the computed tensile stress from the analysis divided by the tensile strength of concrete. The maximum demand-capacity stress ratio that can be allowed is limited by 2. Another important parameter is the cumulative duration of time exceeding the tensile strength of concrete. It is calculated from the stress time history and shows the energy measure as a damage criterion. The cumulative inelastic duration limit is 0.4 sec for the capacity of the tensile strength where DCR=1 and decreases linearly as the DCR value increases. Figure 2.5 shows the limit line below which the dam can be considered as safe according to linear elastic analysis

results. If any point lies above this line, seismic safety should be checked using nonlinear analysis. The procedure is summarized in Figures 2.4 and 2.5. Red and blue points with DCR=1.0 and 2.0 respectively are not satisfied with the performance criteria of linear analyses, whereas for other two DCR values, the calculated cumulative inelastic duration are located below the limit line shown in Figure 2.5. Performance criteria of linear analyses of the Andıraz Dam were studied according to the procedure presented above for Operating Basis Earthquake and Safety Evaluation Earthquakes for 2 levels.

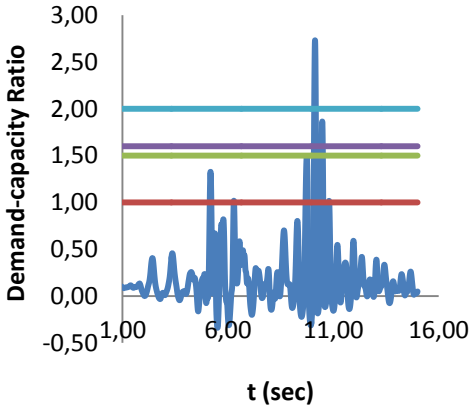

Figure 2.4 Calculation of time exceeding DCR

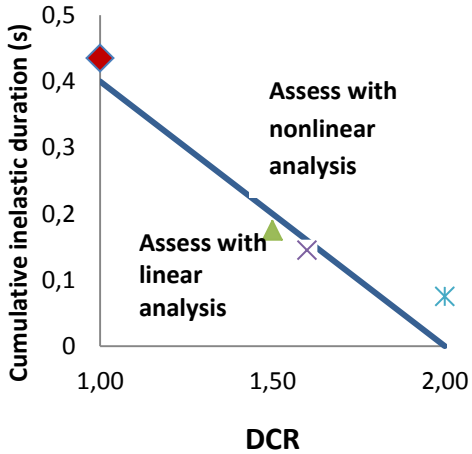

Figure 2.5 Performance criterion graph (USACE, 2003)

2.3 Finite Element Mesh

For the mesh of the three dimensional dam analyses, rectangular, prism and pyramid elements were used. A mesh with 41 solid elements, 28 foundation elements and 59 fluid/ transmitting plane elements was used initially in which the dam cross section and the length along the valley were divided into 4 and 7 elements, respectively. However, this mesh was considered as a coarse mesh and it was expanded to a finer mesh with totally 242 elements with 88 dam elements, 50 foundation elements and 104 water elements including all meshes. It was obtained by dividing the dam cross section into 5 elements in x direction and along valley direction into 10 elements in z direction. The views of the dam model from different perspectives are shown in detail in Figure 2.6. Foundation, water and dam meshes which are the components of the system can be observed for coarse (Mesh 1) and medium (Mesh 2) models in Figure 2.7.

Quadratic elements with 20 nodes were used for the three dimensional solid elements. The sufficiency of Mesh 2 (medium mesh) was checked by conducting modal and static analyses. Same mesh was translated to ANSYS, and then two finer meshes were prepared with 497 and 3141 dam elements as shown in Figure 2.8. Fine mesh was named as Mesh 3 with 497 dam elements and very fine mesh was called Mesh 4.

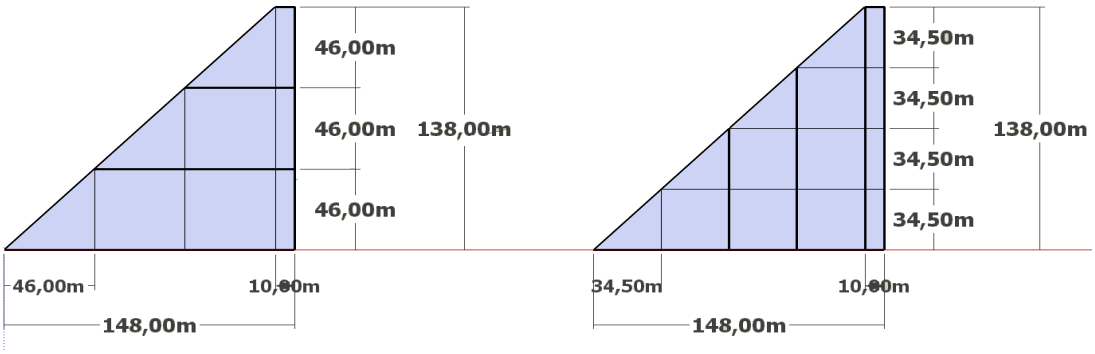

Mesh1 Mesh2

a) Dam cross section

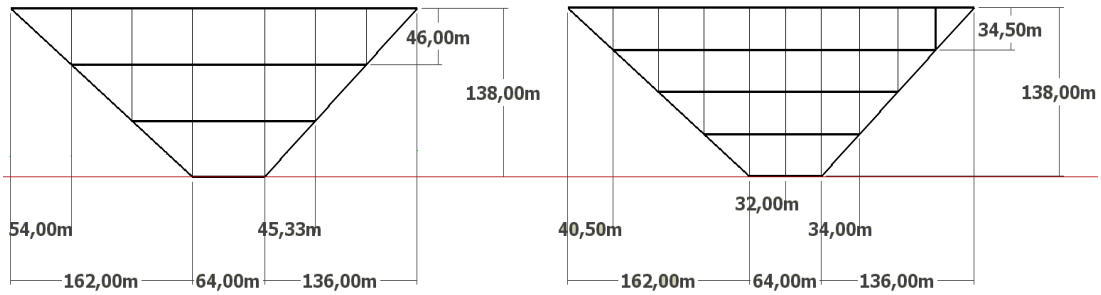

Mesh1 Mesh2

b) Front view of the dam

Figure 2.6 Dam cross section and valley from upstream views of coarse (Mesh1) and medium mesh (Mesh 2)

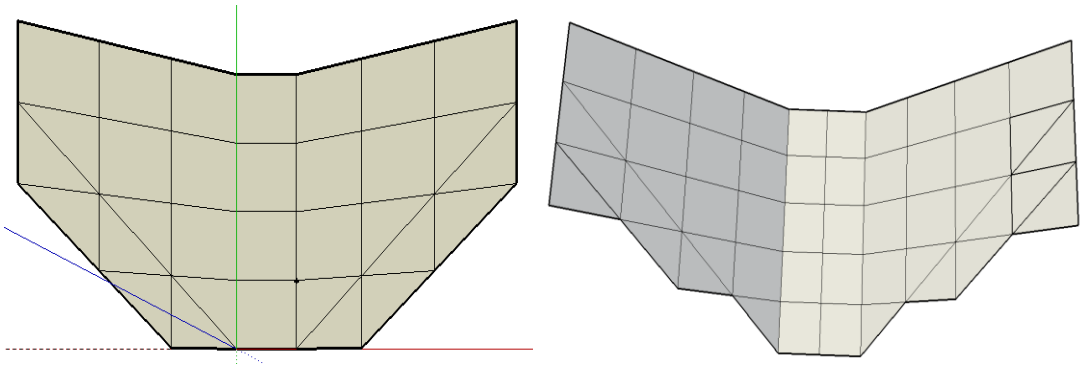

Mesh1 Mesh2

a) Foundation mesh for coarse and medium models respectively from top view

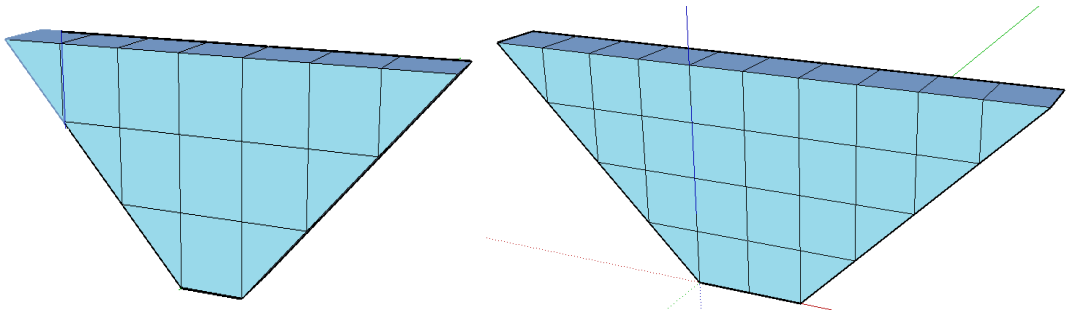

Mesh1 Mesh2

b) Water mesh for coarse and medium models respectively

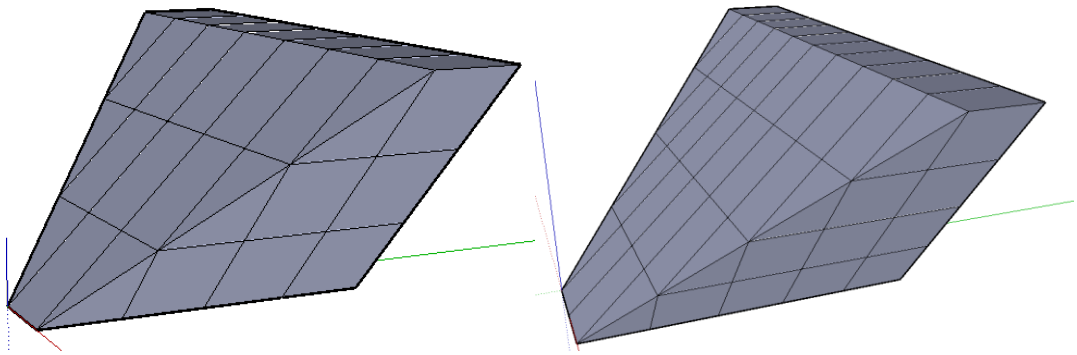

Mesh1 Mesh2

c) Dam mesh for coarse and medium models respectively in 3D

Figure 2.7 Mesh differences on the components of the coarse (Mesh 1) and medium (Mesh 2) models

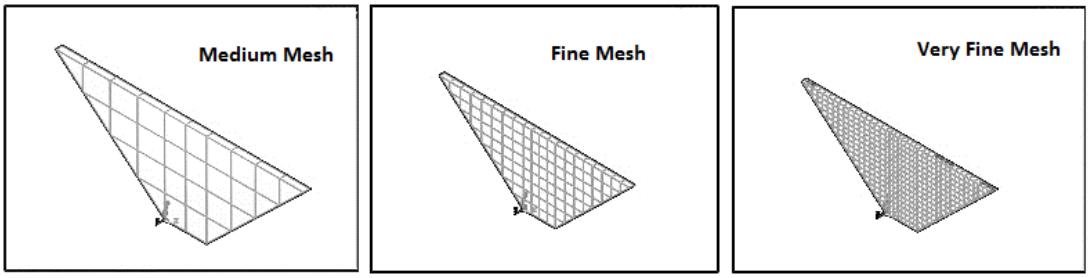

Figure 2.8 Different meshes for ANSYS (Mesh 2, 3 and 4 respectively)

Analyses were conducted under the gravity load and hydrostatic loads acting on the dam by using Mesh 2, Mesh 3 and Mesh 4 in ANSYS. Afterwards, the vibration frequencies and the mode shapes of each analysis were obtained. In Table 2.1 results of the frequencies of modes are listed for the model with different mesh densities. Results are very similar to each other with a maximum error of about 5% which is the tolerable range. Also, for the first five modes of the system, the maximum error is only 1.41 %.

Table 2.1 Modal analysis comparison of meshes on ANSYS and EACD

	EACD	**ANSYS**			**Error**		
Frequency (Hz)	**Medium**	**Medium**	**Fine**	**Very fine**	**Medium**	**Fine**	**Very fine**
Mode 1	4.641	4.629	4.625	4.624	0.25%	0.34%	0.36%
Mode 2	6.566	6.519	6.505	6.503	0.71%	0.93%	0.96%
Mode 3	8.325	8.258	8.214	8.21	0.81%	1.36%	1.41%
Mode 4	8.566	8.537	8.534	8.533	0.34%	0.37%	0.38%
Mode 5	8.788	8.761	8.745	8.744	0.31%	0.49%	0.51%
Mode 6	9.479	9.445	9.414	9.41	0.35%	0.69%	0.72%
Mode 7	10.514	10.357	10.233	10.223	1.52%	2.75%	2.84%
Mode 8	11.081	11.056	11.035	11.033	0.22%	0.41%	0.43%
Mode 9	12.193	12.096	11.995	11.987	0.80%	1.65%	1.71%
Mode 10	12.789	12.54	12.26	12.241	1.99%	4.32%	4.48%

Maximum crest displacement results and maximum principle stresses in two principal directions were also compared by using different mesh densities for the static analyses under gravity and hydrostatic forces. Maximum displacement results are very close to each other as shown in Table 2.2 with an error of less than 1 %. Table 2.3 shows the maximum principle stress comparison. The stress error is in the order of about 10 % between Mesh 2 with Mesh 4 and 25 % between Mesh 3 with Mesh 4 respectively.

Table 2.2 Maximum displacement comparison of meshes on ANSYS and EACD

			ANSYS		EACD	
Mesh	**No of Elements**	**No of Nodes**	**Δ (mm)**	**Error***	**Δ (mm)**	**Error****
Medium (Mesh 2)	88	439	8.79	-0.02 %	8.77	0.23 %
Fine (Mesh 3)	497	2234	8.787	0.01 %	-	-
Very Fine (Mesh 4)	3141	13430	8.788	-	-	-

*: Error calculated for meshes in ANSYS with respect to very fine mesh (mesh 4)
**: Error calculated for ANSYS and EACD results with respect to ANSYS with the same mesh.

Table 2.3 Maximum principles stresses comparison of meshes on ANSYS

	ANSYS				EACD			
Mesh	**σ 1 (MPa)**	**σ 3 (MPa)**	**Error 1***	**Error 3***	**σ 1 (MPa)**	**σ 3 (MPa)**	**Error 1****	**Error 3****
Medium (Mesh 2)	0.795	-3.13	27.06 %	6.85 %	0.557	-2.47	29.94 %	21.09 %
Fine (Mesh 3)	0.973	-3.22	10.73 %	4.17 %	-	-	-	-
Very Fine (Mesh 4)	1.09	-3.36	-	-	-	-	-	-

*: Error calculated for meshes in ANSYS with respect to very fine mesh (mesh 4)
**: Error calculated for ANSYS and EACD results with respect to ANSYS with the same mesh.

Based on the success of Mesh 2 in estimating the vibration frequencies with a high degree of accuracy (owing to the use of high order elements), it was decided to use Mesh 2 for the rest of the study. It should be kept in mind that stress errors may reach up to about 25% with this mesh, however computational effort needed for dynamic analysis using Mesh 4 is extensive compared to that with Mesh 2. A total of about 1000 dynamic analysis were conducted in this study. In order to solve all these cases within reasonable amount of time use of Mesh 2 was found to be sufficient for comparative analysis.

2.4 Material Properties

It was required to assign the proper material properties of the Andıraz Dam to be used for the analyses. These were the modulus of elasticity (Young's modulus), poisson's ratio and unit mass and hysteretic damping of the roller compacted concrete (RCC) and foundation rock. The modulus of elasticity of the foundation rock which was measured from the core samples taken from the site was 10800 MPa and the modulus of elasticity of RCC for the dam body was calculated according to the ACI 318-11 (2011) equations. Modulus of elasticity of concrete was used as 23750 MPa. The derivations from these properties were also studied in the parametric study section. Poisson's ratio was 0.2 for both foundation and dam. Unit mass of the concrete dam was 2400 kg/m^3 whereas it was 2500 kg/m^3 for the foundation rock.

The tensile strength of RCC was calculated as in Equation 2.1 according to BK guideline (2012b) with recommendations of USACE (1995). Since RCC was used in Andıraz Dam Equation 2.2 was considered for the tensile strength of RCC.

$$f_{ct} = R_c R_d R_{ab} f_{spt} \quad \text{(Eq. 2.1)}$$

$$f_{dct} = R_{dr} f_{ct} \quad \text{(Eq. 2.2)}$$

where f_{ct} is the dynamic direct tensile strength, f_{spt} is the static splitting tensile strength, R_c is the ratio of splitting to direct tensile strength, R_d is the factor converting static strength to dynamic in case of earthquake ground motion and R_{ab} is the reduction factor due to aggregate size. In Equation 2.2 R_{dr} is the factor related to the fluidity of RCC.

For the Andıraz Dam; f_{spt} was calculated as $0.6\sqrt{f_{ck}}$ with f_{ck}=35 MPa of RCC, R_c equaled to 0.8, R_d was 1.5, R_{ab} was 1.0 due to aggregate size smaller than 40 mm and R_{dr} was 0.67 with the use of pad mortar. Therefore, the tensile strength was obtained as about 3 MPa.

The analyses were conducted for full reservoir with 1000 kg/m^3 unit mass of impounded water. The level of water in reservoir was taken as full and empty to observe its influence on the seismic response. The velocity of pressure water waves was taken as 1442 m/s^2. Another important parameter which affected the analysis was the compressibility of the impounded water. The program offered two alternatives: either compressible impounded water or incompressible reservoir. Both cases were considered in the parametric studies to investigate the effect of water compressibility. In addition, the influence of wave reflection coefficient, α was also studied by varying its value between 0.9-1.0, which was the suggested range for new dams (Wang and Chopra, 2008).

2.5 Ground Motion Characteristics

A probabilistic seismic hazard analysis was conducted for the dam in which earthquake return period, uncertainties on ground motion parameters and uncertainties on earthquake seismic sources were included. Ground motion parameters for the specified annual rate of exceedance for the evaluation of performance or design, were determined (BK, 2012a). In the probabilistic seismic hazard methodology, ground motions are determined as follows:

First of all, magnitude, distance and occurrence rate of earthquakes were specified. Then, ground motion distribution was calculated and probability of this earthquake exceeding a certain level of ground motion is multiplied by the annual rate of earthquake. Finally, in order to obtain the rate of exceedance of each earthquake, different ground motions rates in the same model were considered.

Dynamic analyses are frequently used for the evaluation of design and seismic hazard assessment of dams. Expected ground motions compatible with the earthquake design spectrum should be used in such analysis. (BK, 2012a) states that if the design is conducted using the spectrum obtained from the probabilistic seismic hazard analysis, target earthquake scenarios can be obtained by considering the fundamental first period of the structure and using deaggregation (McGuire, 2001).

Different earthquake scenarios were developed with various risks of earthquakes. These were Operating Basis Earthquake (OBE) and Safety Evaluation Earthquakes (SEE) for two different hazard levels. These levels can be defined as follows:

Operating Basis Earthquake (OBE): Earthquake scenario with 144 years return period having a 30% probability of being exceeded in 50 years.

Safety Evaluation Earthquake-Level 1 (SEE1): Earthquake scenario with 475 years return period having 10% probability of being exceeded in 50 years. This level of earthquake is considered as SEE for dams under moderate risk (BK, 2012a).

Safety Evaluation Earthquake-Level 2 (SEE2): Earthquake scenario with 2475 years return period having 2% probability of being exceeded in 50 years. This level of earthquake is considered as SEE for dams under high risk.

BK guidelines introduce a method for the classification of risk levels of dams referring to ICOLD (1989) Bulletin. Risk levels are determined by a scoring methodology considering various factors and then according to these risk levels, dams were categorized into different risk groups. The main four factors included in designating the risk scores are as follows: 1) capacity of reservoir, 2) height of the dam, 3) necessity of evacuation considering human population and 4) potential downstream damage. Risk score is the summation of scores obtained from these factors. Risk factor values used for the calculation of the total risk score are given in Table 2.4 where the scores given in the parentheses are added with the proper class. Table 2.5 discretizes the risk classes according to the total risk score obtained from the summation of four factors (BK, 2012a).

Table 2.4 Determination of risk score by considering four risk factors

	RISK FACTOR			
Properties of Dam	**Very High**	**High**	**Medium**	**Low**
Reservoir Capacity (hm^3)	> 120 **(6)**	120-1 **(4)**	1-0.1 **(2)**	< 0.1 **(0)**
Height (m)	> 45 **(6)**	45-30 **(4)**	30-15 **(2)**	< 15 **(0)**
Necessity of evacuation of human population	> 1000 **(12)**	1000-100 **(8)**	100-1 **(4)**	No **(0)**
Potential downstream damage	High **(12)**	Medium **(8)**	Low **(4)**	No **(0)**

Table 2.5 Classification of risk groups according to total risk scores

Total Risk Score	**Risk Classification**		**Deterministic SEE percentile %**	**Probabilistic SEE return periods**
0-6	I	Low Risk Group	50%	224 years
7-18	II	Medium Risk Group	50%	475 years
19-30	III	High Risk Group	84%	975 years
31-36	IV	Very High Risk Group	84%	2475 years

Based on the tables offered by BK (2012a), risk class range of Andıraz Dam could be calculated in the following manner: Considering the reservoir capacity and dam height, Andıraz Dam is under very high risk. It is obvious that deciding on the risk factor for necessity of evacuation of human population and potential downstream damage in an extremely challenging task and requires dam break and inundation studies. From the point of necessity of human evacuation need and potential downstream damage, it can be stated that the risk score may range from low to no risk, since a significant population center does not exist in the downstream. As a result, one would calculate the total risk score as 6+6+0+4=16 as the lower bound value or 6+6+8+12=32 as the upper bound value. Based on these bounds SEE return period levels would be either 475 years or 2475 years. These two earthquake levels were considered as the two extreme scenarios and formed the basis of the ground motion definitions.

Table 2.6 Earthquake data characteristics

EQ DATA	ORIGINAL			MODIFIED			PGA VALUES
Name	**Δt (sec)**	**t end (sec)**	**# DATA**	**Δt (sec)**	**t end (sec)**	**# DATA**	**(g)**
OBE1	0.005	10	2000	0.025	10	400	0.220
OBE2	0.005	10	2000	0.025	10	400	0.199
OBE3	0.005	10	2000	0.025	10	400	0.231
SEE1-1	0.01	15	1500	0.05	15	300	0.352
SEE1-2	0.01	15	1500	0.05	15	300	0.408
SEE1-3	0.005	15	3000	0.025	15	600	0.314
SEE2-1	0.01	15	1500	0.05	15	300	0.661
SEE2-2	0.005	15	300	0.025	15	600	0.727
SEE2-3	0.02	10	500	0.02	10	500	0.973

In Table 2.6, the earthquake characteristics of the different earthquake scenarios are shown. At it can be seen, for each OBE, SEE1 and SEE2 levels there exists three different earthquakes to consider ground motion variability. Time increment of data obtained for the ground motion, the earthquake duration and the number of steps data used are listed on the table for the original ground motion.

Modified ground motion data were used in the analysis whose properties are summarized in the right-hand side of the Table 2.6. Modifications were made by selecting one data for every 5 time increments thereby reducing the frequency content of the motion to 10-20 Hz. Therefore, time increment values increased to five times of the time increment of the original data. Moreover, maximum peak ground acceleration values of each ground motion are listed. Figure 2.9 presents the time histories of the ground motions. Then, response spectra of these ground motions were prepared and shown in Figure 2.10.

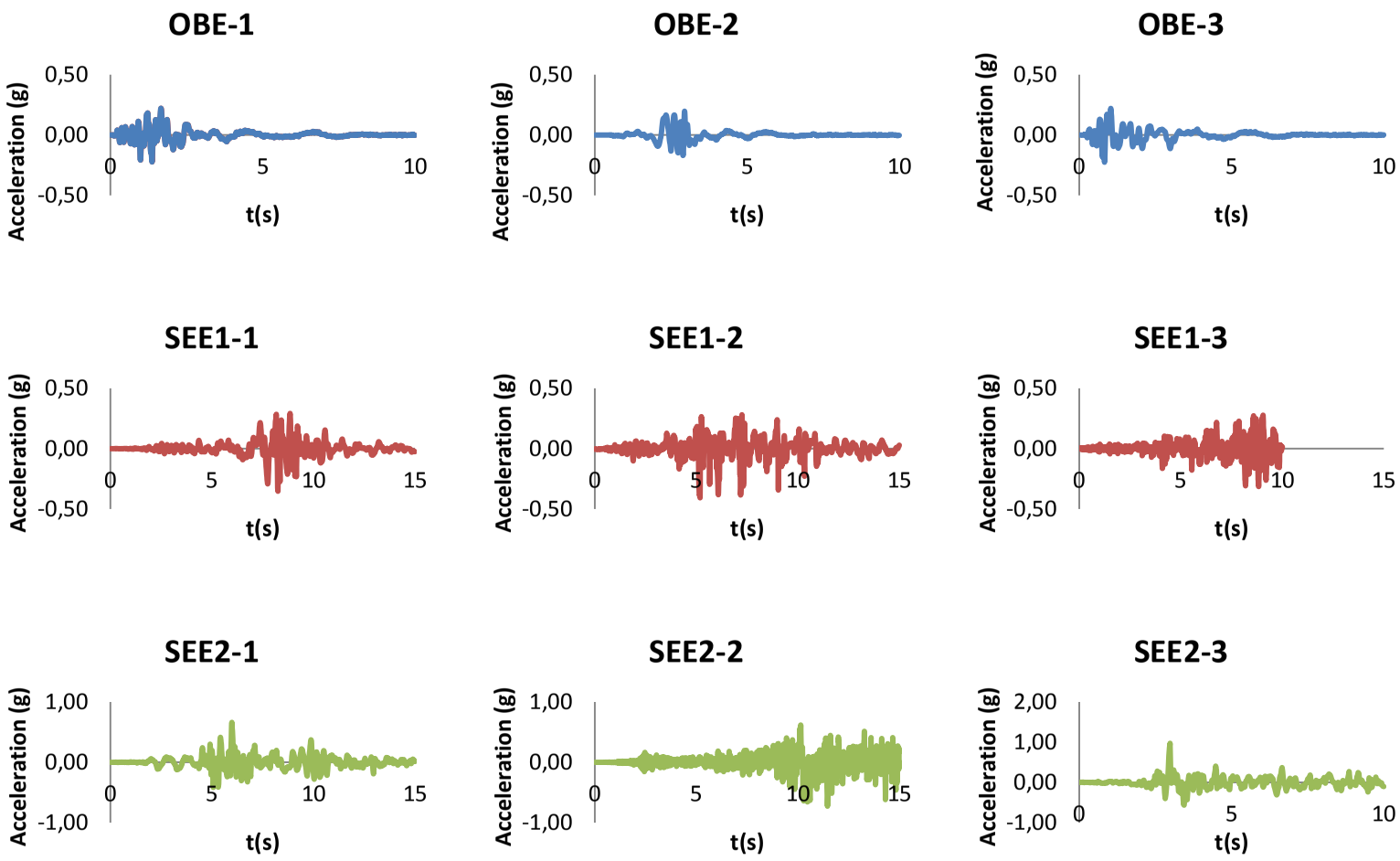

Figure 2.9 Ground motion time histories

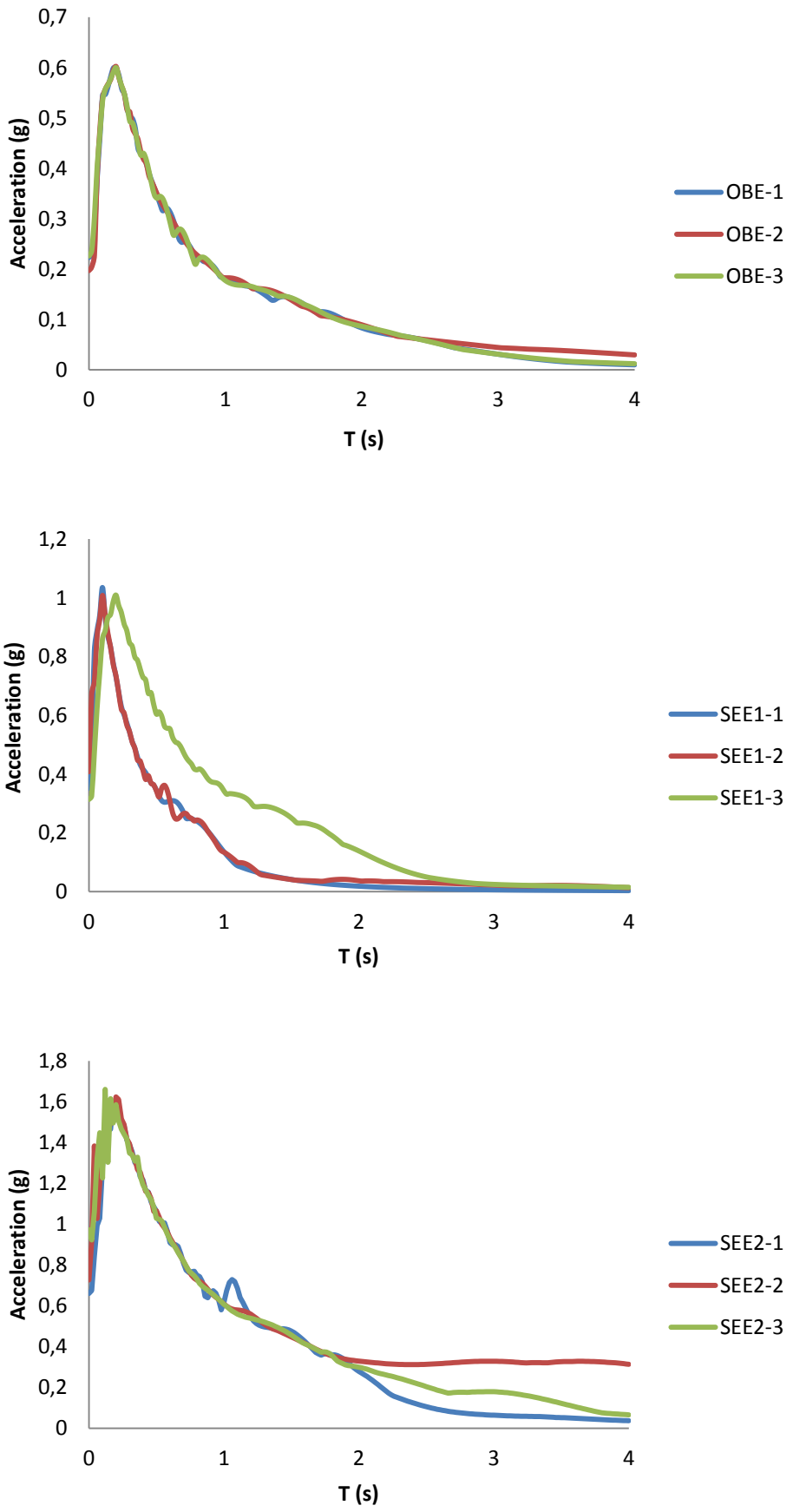

Figure 2.10 Response spectra graphs of earthquakes

USACE and BK guidelines require the use of all possible earthquake combinations in addition to gravity and hydrostatic load cases. In the absence of multi-directional ground motion data, it was decided to use 30 % rule of earthquake load combination for the lateral and vertical directions. Ground motions were chosen such that on the cross-stream (z) and vertical direction (y), the intensity of the ground motion was 30 % of the intensity on the upstream direction (x) if it existed in the combination. The combinations and their corresponding motions with respect to x, y and z directions are shown in Table 2.7. In the table, numbers show the multiplication factors in the load combinations then all of these combinations were analyzed. The most critical combinations resulting in highest stress demands are marked in Table 2.7.

Table 2.7 Earthquake Combinations

COMBINATIONS

	X upstream direction	**Z=(0.3x) cross-stream direction**	**Y=(0.3x) vertical direction**
Comb 1	1	0	0
Comb 2	0	1	0
Comb 3	-1	0	0
Comb 4	0	-1	0
Comb 5	1	1	0
Comb 6	-1	1	0
Comb 7	1	-1	0
Comb 8	-1	-1	0
Comb 9	1	1	1
Comb 10	-1	1	1
Comb 11	1	-1	1
Comb 12	-1	-1	1
Comb 13	1	0	1
Comb 14	-1	0	1
Comb 15	0	1	1
Comb 16	0	-1	1

2.6 Modal Properties

Mode shapes of the dam on flexible foundation with empty reservoir are shown in Figures 2.10 and Figure 2.11 for the first four fundamental modes. On the figures, blue line corresponds to undeformed configuration of the dam and red points are the locations of the nodes for the deformed situation for each mode.

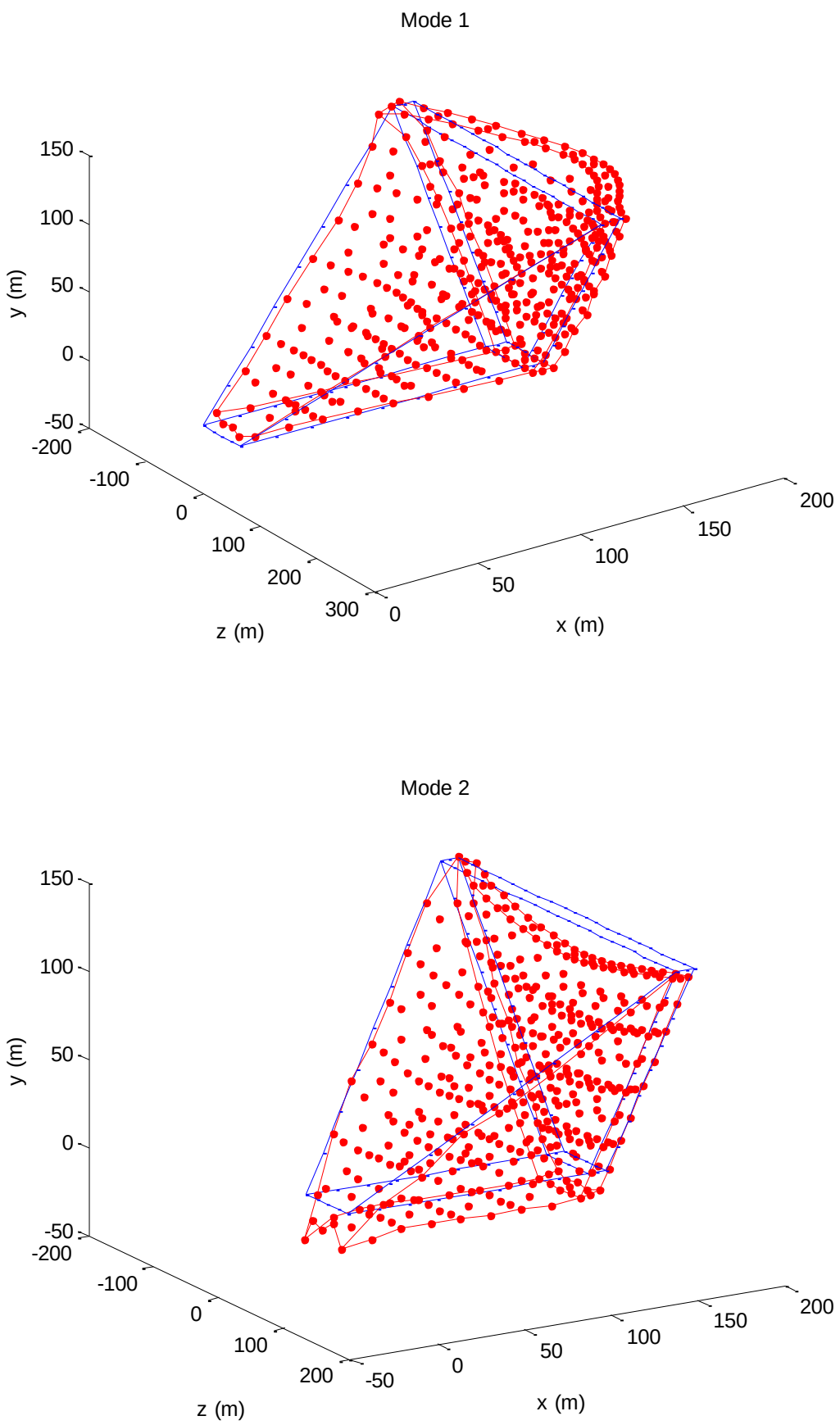

Figure 2.11 Mode shapes of the dam for first and second modes

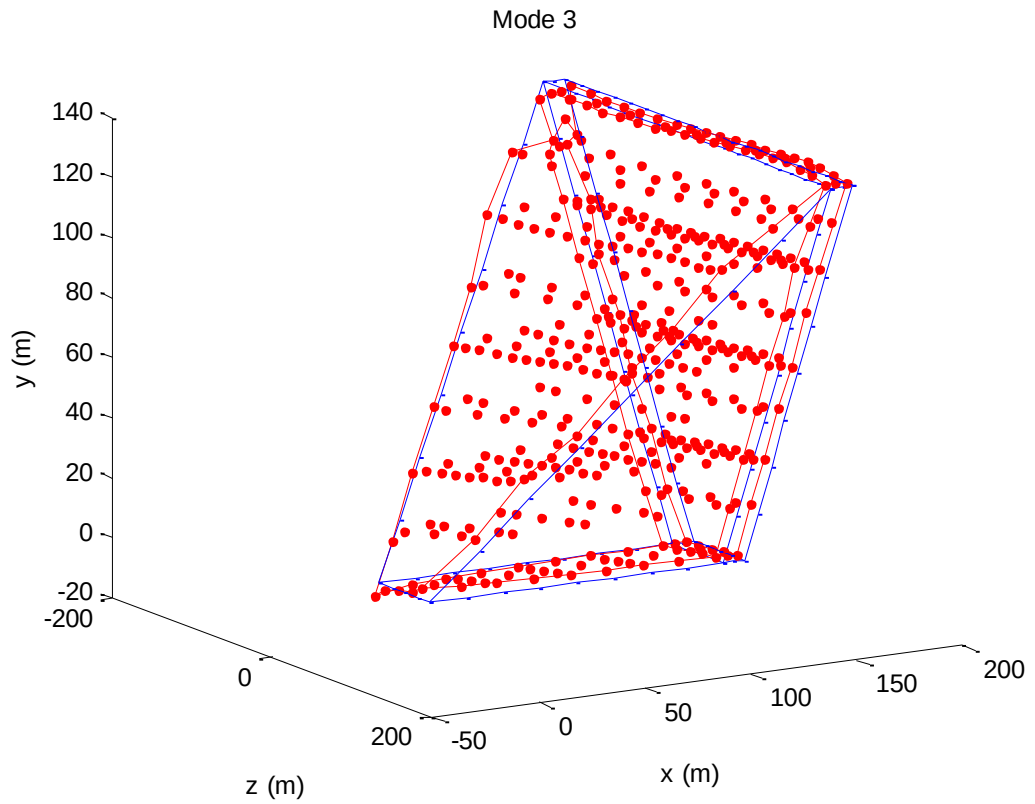

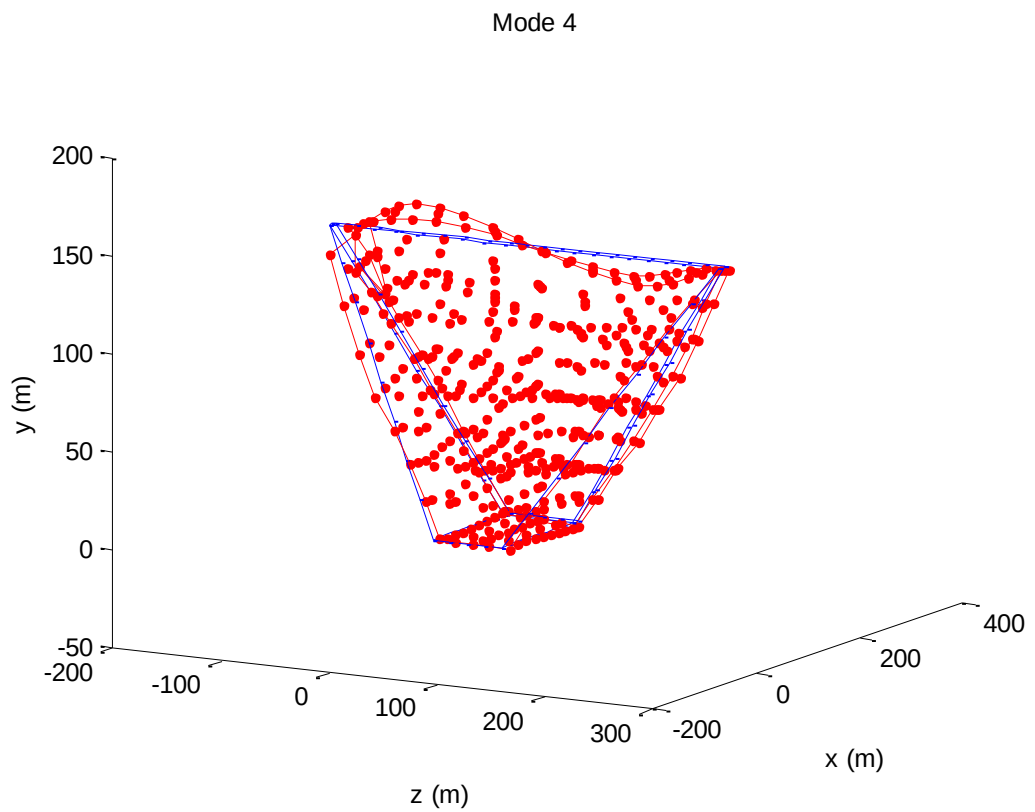

Figure 2.12 Mode shapes of the dam for third and fourth modes

The natural frequencies of the dam-foundation system (empty reservoir case) for the first five modes are listed in Table 2.8. The first mode period is found as 0.351 s. The modal properties of the dam-foundation-reservoir system cannot be found directly. To facilitate this, dam was analyzed under a pulse type loading and the crest acceleration was plotted against the frequency. (Figure 2.13) From this figure first five modes were identified as 2.29, 3.282, 3.74 ,4.695 and 5.573 Hz. According to these results presence of the reservoir decreases the fundamental frequency by about 20 %. The reduction of frequency of higher modes showed a decreasing trend as shown in Figure 2.13.

Table 2.8 Natural Frequencies and Periods of the dam-foundation system

	Empty Reservoir			**Full Reservoir**		**Difference**
Mode	**Wd**	**f (Hz)**	**T (s)**	**f (Hz)**	**T (s)**	**f**
1	1.79E+01	2.85	0.351	2.29	0.437	19.65%
2	2.47E+01	3.93	0.254	3.282	0.267	16.49%
3	2.66E+01	4.23	0.236	3.74	0.267	11.58%
4	2.92E+01	4.65	0.215	4.695	0.213	-0.97%
5	3.54E+01	5.63	0.178	5.573	0.179	1.01%

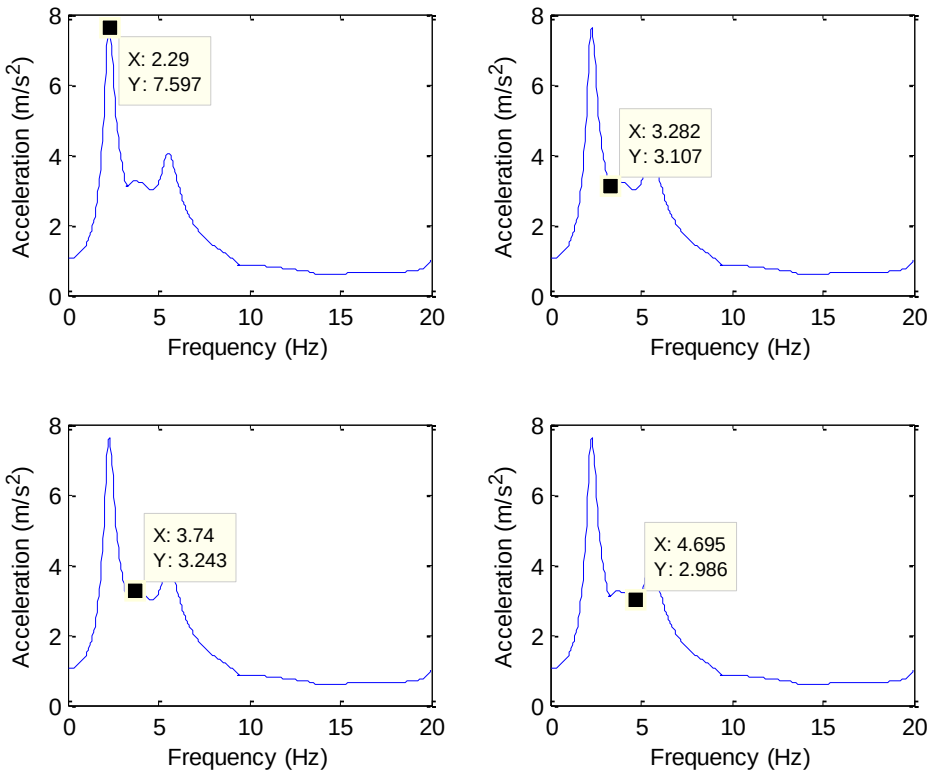

Figure 2.13 Frequencies of the dam with full reservoir

2.7 Analysis Results

In this part, analysis results are presented for the Andıraz Dam. Stresses on the cross sections of the dam are obtained. Maximum principle tensile stresses and vertical stresses are studied. In addition, displacement time histories are presented for each ground motion. Then, assessment of the dam using of linear analysis results is presented.

2.7.1 Stress Plots

The maximum stresses were generally observed on the edges of the canyon modeled by the pyramid-tetrahedral elements. EACD results on the Gauss Quadrature locations were used to prepare the stress plots of the two cross-sectional locations at z=6.76 m and z=38.8 m. Stress plots were prepared for each earthquake type and the most critical combinations 9, 11 and 13. Figures 2.14-2.19 present the results for the combinations that were the most critical ones for each earthquake type. Surprisingly, the results were very close to each other for combinations 9, 11 and 13. As a reminder, these combinations involve the motions in the x and y directions were same, the difference was the inclusion of z component or not in the positive or negative direction.

It should be reminded that these plots were from analyses with compressible impounded water with α=1, hysteretic damping ratio of 0.10 for dam and foundation (meaning 5% damping ratio). Modulus of elasticity of foundation and dam were 10800 MPa and 23750 MPa respectively as specified previously.

Maximum tensile stresses obtained from the maximum of the maximum principle stresses and also stresses on vertical direction (y) were studied. Titles of the vertical stresses graphs are presented as S22 stress. The sign convention for the stress follows the usual one, tensile stress are positive.

The stress values were obtained from the Gauss Quadrature locations of the elements of the dam model. The maximum and minimum stress values on each gauss quadrature point were taken from the EACD program. Maximum stress values were used in the plots. Two dimensional stress plots were obtained by using the contourf command in Matlab for cross sections of the dam. By the help of this command, isolines of the stress values at the gauss quadrature locations and the areas between these points were filled using corresponding colors.

Maximum stresses on the vertical directions were plotted through Figure 2.14-2.16 for different ground motions. It was observed that maximum tensile stress concentrations were on the body at the downstream side. From top to the bottom, the compression stress increased. Also at the toe of the dam, stress concentrations were observed. It was observed that compressive stresses were much smaller than the compressive strength of concrete. Therefore, compression regions are not critical.

The maximum tensile stresses of vertical stresses for OBE ground motions did not exceed 0.5 MPa which was tolerable and quite small (Figure 2.14). However, for SEE1 ground motions, maximum tensile stress values increased to approximately 1 MPa. Again stress concentrations on the body on the downstream and toe were observed. In addition, on the upstream side, additional tensile stress concentrations were seen (Figure 2.15). Mostly in SEE2 ground motion vertical stress results, the stress concentrations were dominant on the toe of the dam with a maximum value of 3 MPa tensile stresses. SEE2 analyses were more critical in terms of tensile stress considerations.

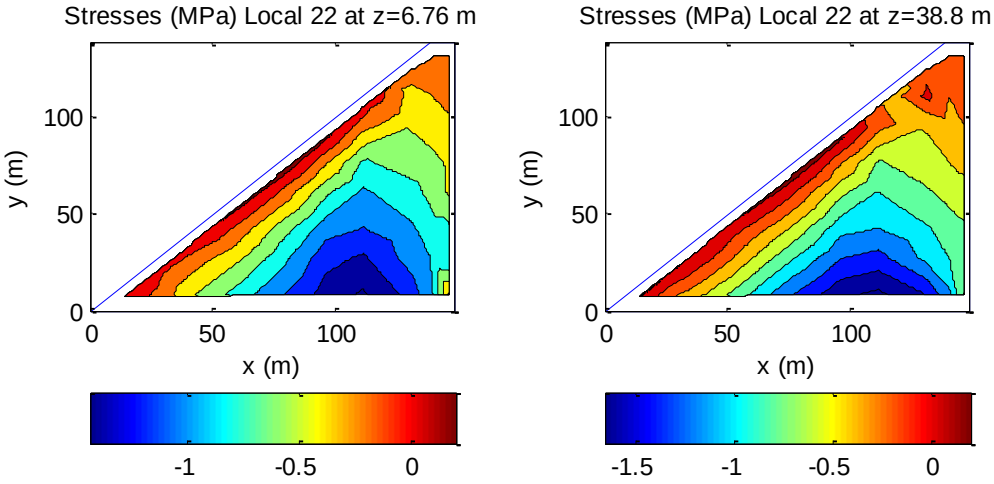

a) OBE-1 Combination 9

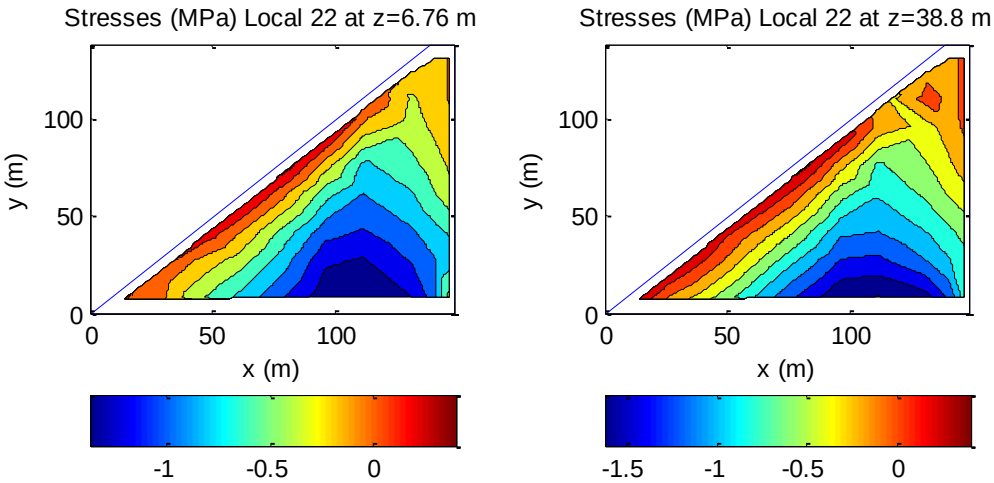

b) OBE-2 Combination 9

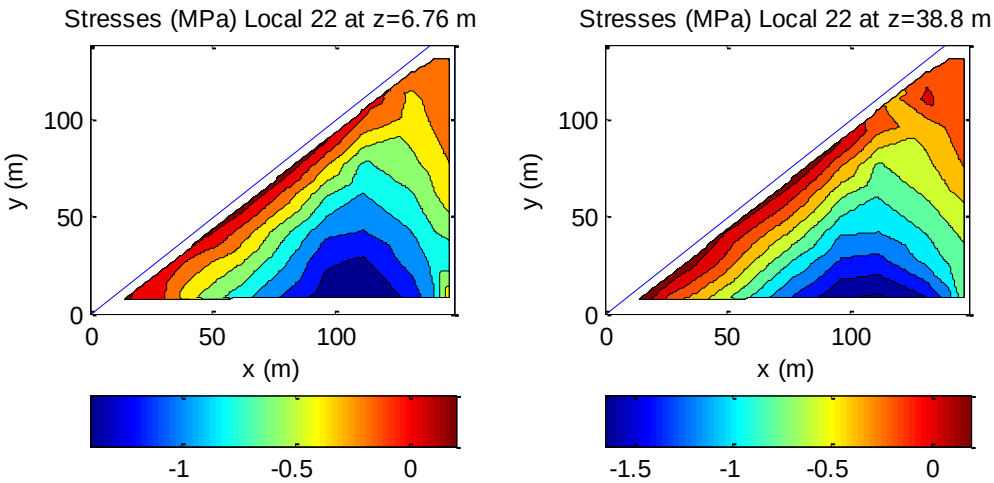

c) OBE-3 Combination 9

Figure 2.14 Maximum vertical stresses of OBE Analysis

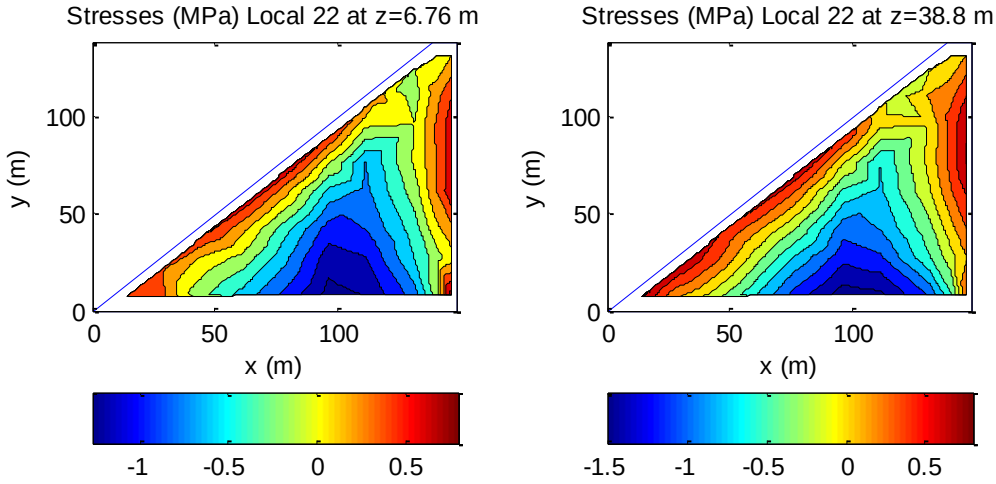

a) SEE1-1 Combination 9

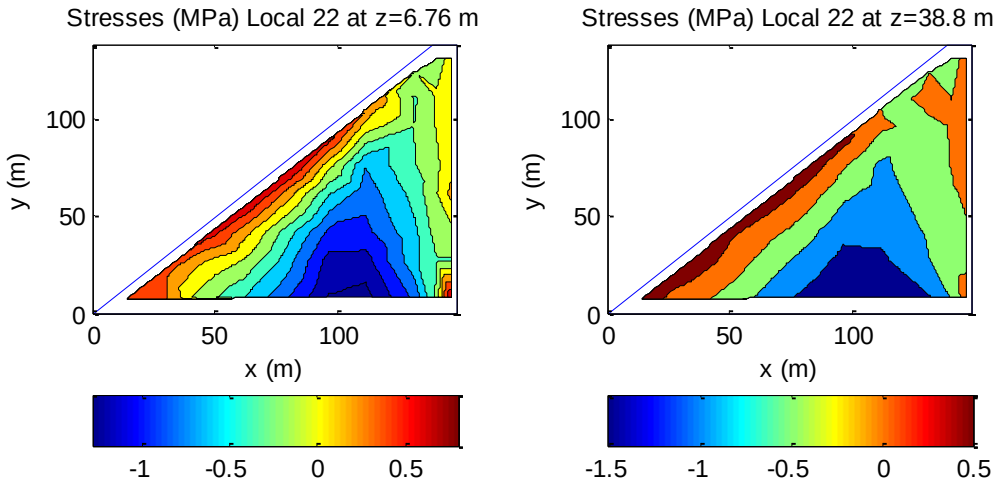

b) SEE1-2 Combination 9

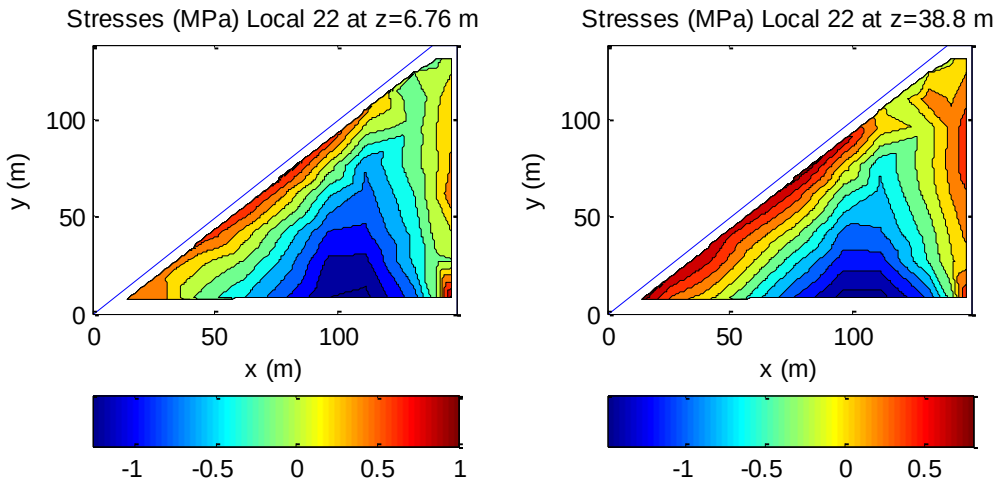

c) SEE1-3 Combination 9

Figure 2.15 Maximum vertical stresses of SEE1 Analysis

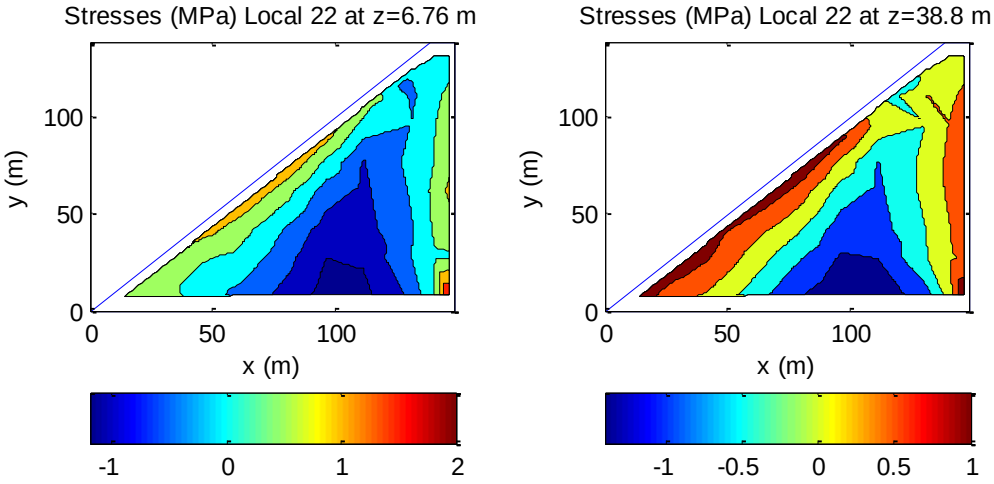

a) SEE2-1 Combination 11

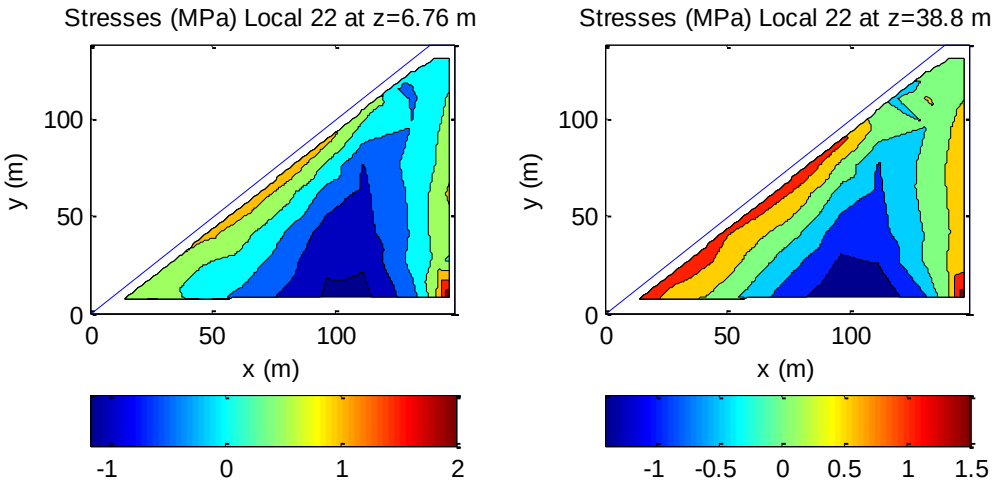

b) SEE2-2 Combination 9

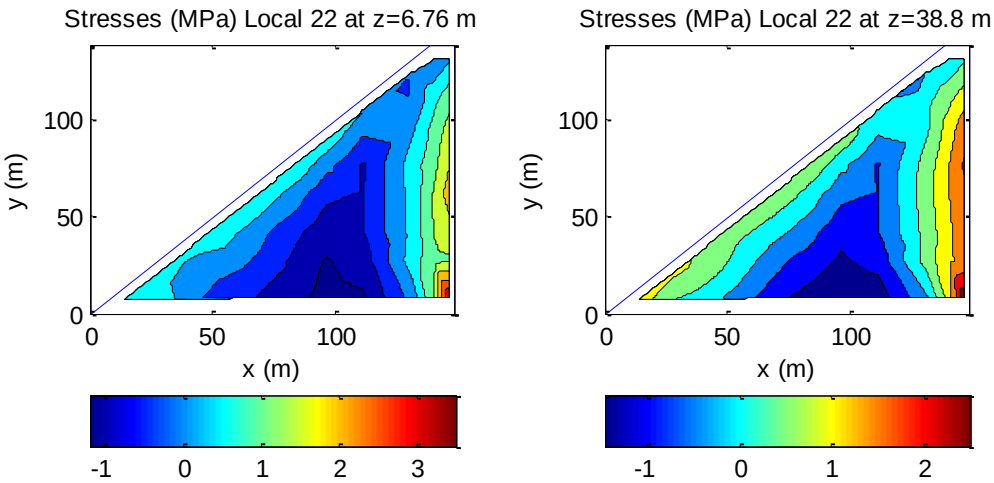

c) SEE2-3 Combination 9

Figure 2.16 Maximum vertical stresses of SEE2 Analysis

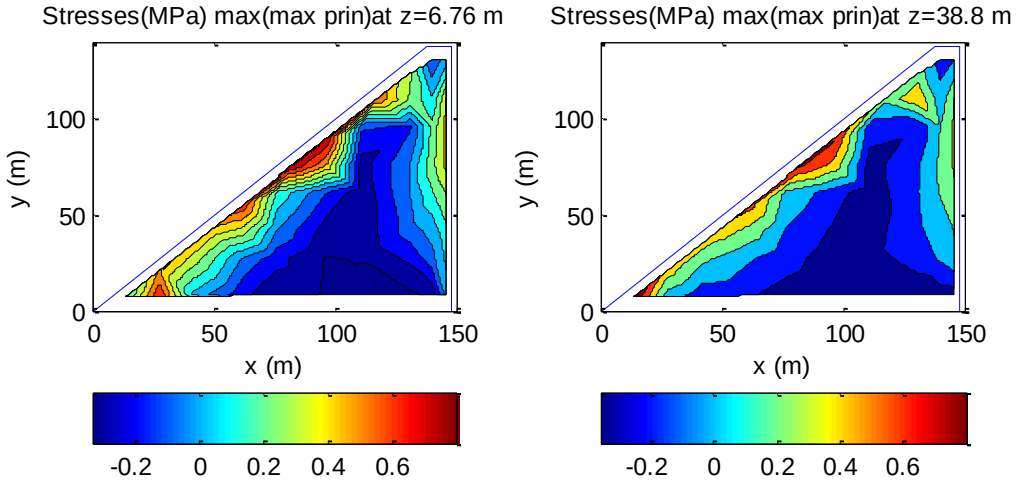

a) OBE-1 Combination 9

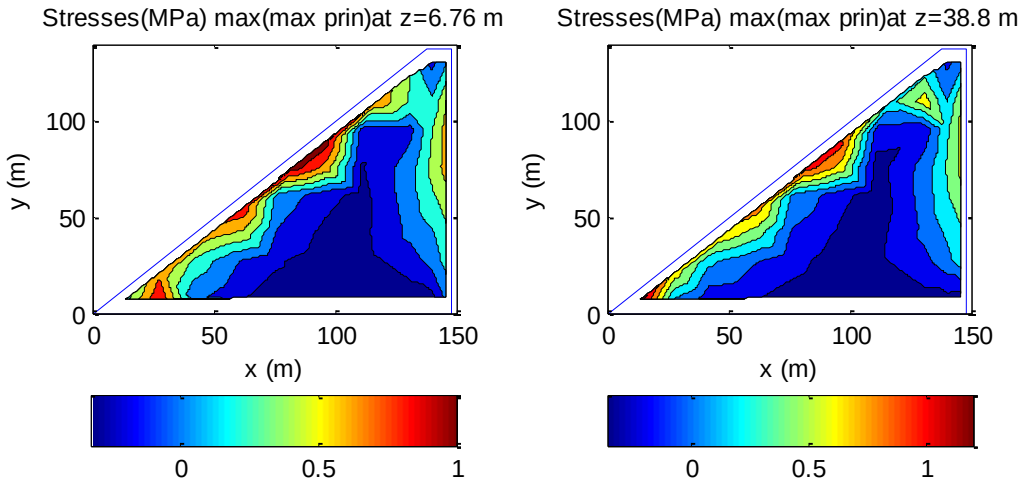

b) OBE-2 Combination 9

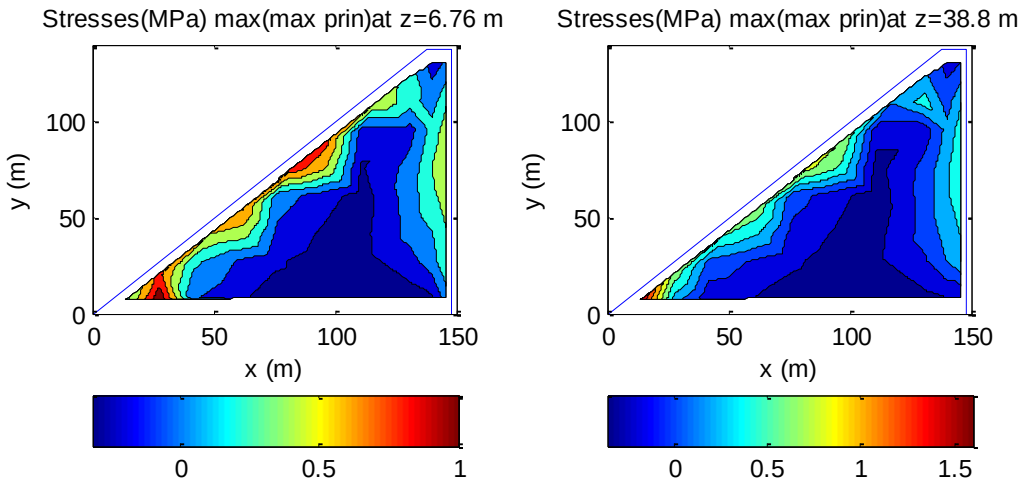

c) OBE-3 Combination 11

Figure 2.17 Maximum of maximum principle stresses of OBE Analysis

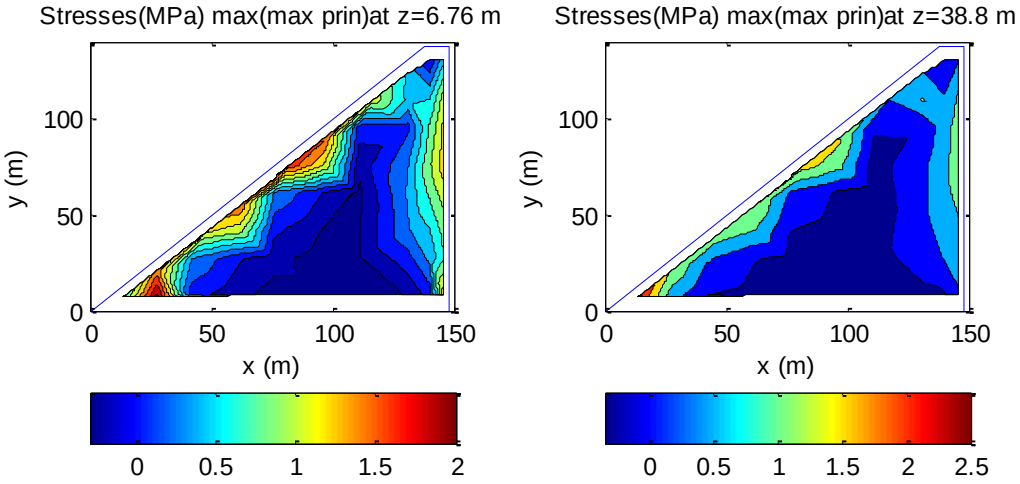

a) SEE1-1 Combination 9

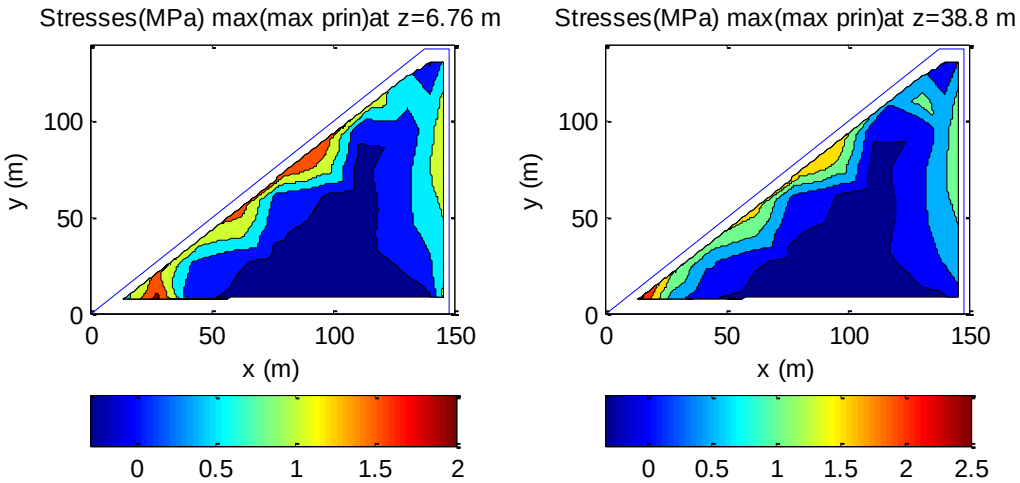

b) SEE1-2 Combination 9

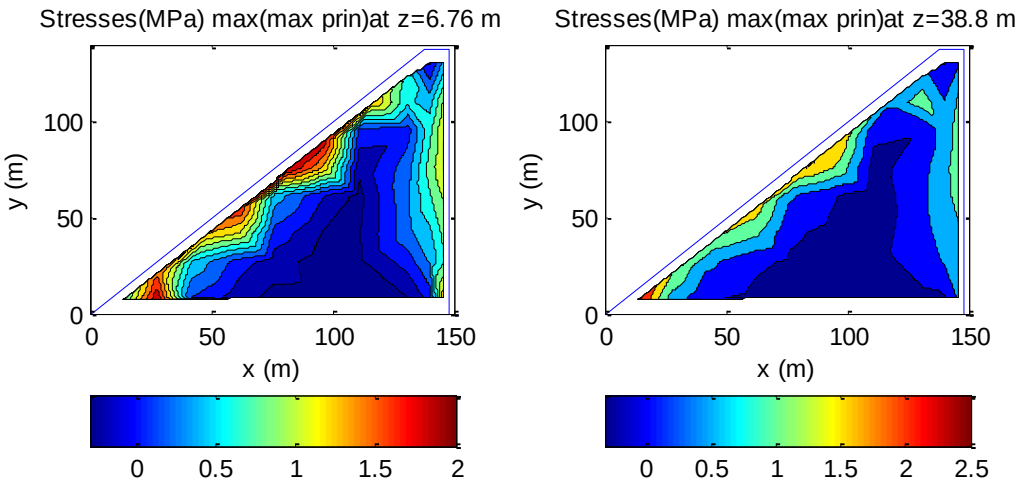

c) SEE1-3 Combination 9

Figure 2.18 Maximum of maximum principle stresses of SEE1 Analysis

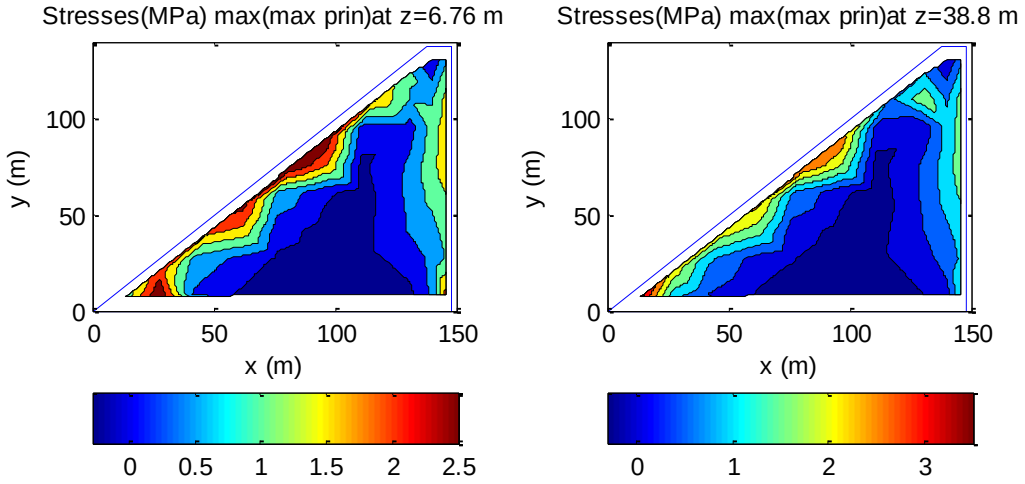

a) SEE2-1 Combination 9

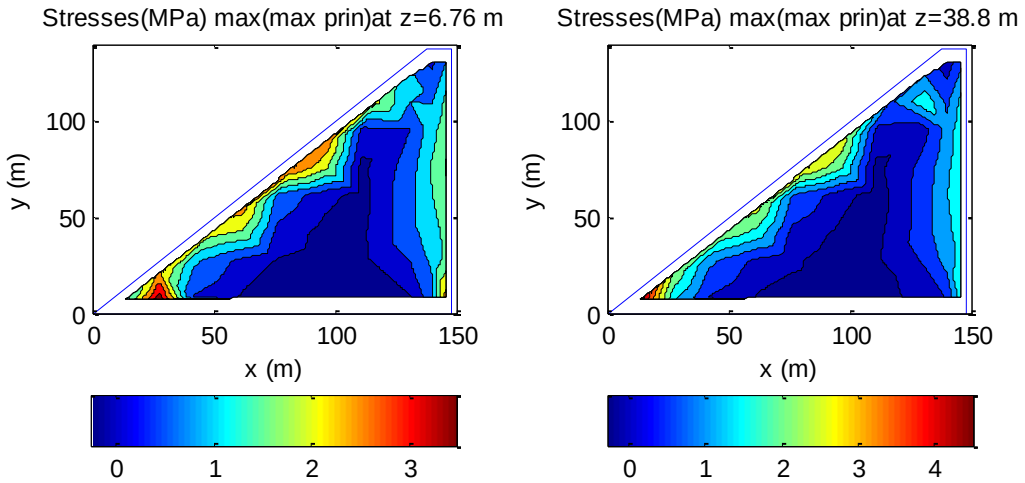

b) SEE2-2 Combination 9

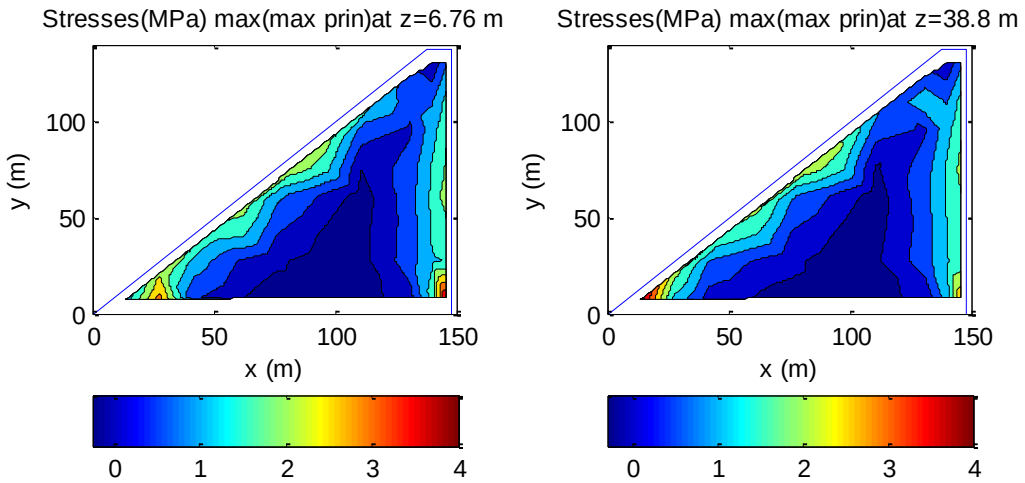

c) SEE2-3 Combination 11

Figure 2.19 Maximum of maximum principle stresses of SEE2 Analysis

Same procedure was repeated for plotting the maximum of the maximum principle stresses for each ground motion. Stress values were obtained from the gauss quadrature locations and contours were plotted by approximations between these points. The results are presented on Figures 2.17-2.19.

Critical stress concentrations are on the body of the dam on downstream side for the maximum of the maximum principle stresses. These locations are the possible crack regions on the downstream. For OBE ground motion, the maximum tensile stress was about 1.5 MPa and it was increased to 2.5 MPa for SEE1 and to about 4MPa for SEE2 ground motions respectively. Moreover, for SEE2-3 ground motion, maximum tensile stress was observed at the toe of the dam on the upstream side (Figure 2.19). It is important to note that larger stress concentrations were observed in the valley sides. Stress values reach to 10 MPa values as given in Table 2.9. This shows that three dimensional modeling is extremely important for capturing highly stressed regions as one would miss such high stresses with a two dimensional analysis.

Table 2.9 Maximum Principle Stresses for three dimensional analyses

Maximum Principle Tensile Stress (MPa)

Combination	**OBE**			**SEE1**			**SEE2**		
	OBE1	*OBE2*	*OBE3*	*SEE1-1*	*SEE1-2*	*SEE1-3*	*SEE2-1*	*SEE2-2*	*SEE2-3*
9	4.13	4.25	3.5	5.1	5.36	6.06	9.6	10.42	11.65
11	4.2	**4.32**	3.51	5.16	5.4	**6.08**	9.62	10.52	**11.88**
13	4.16	4.28	3.5	5.13	5.38	6.07	9.61	10.47	11.76

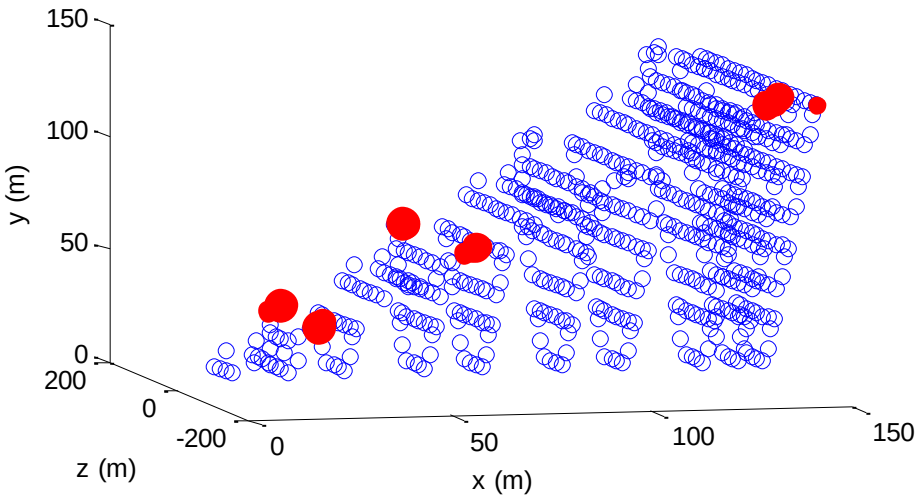

Figure 2.20 Stress Locations exceeding tensile capacity for SEE1-3 combination 11

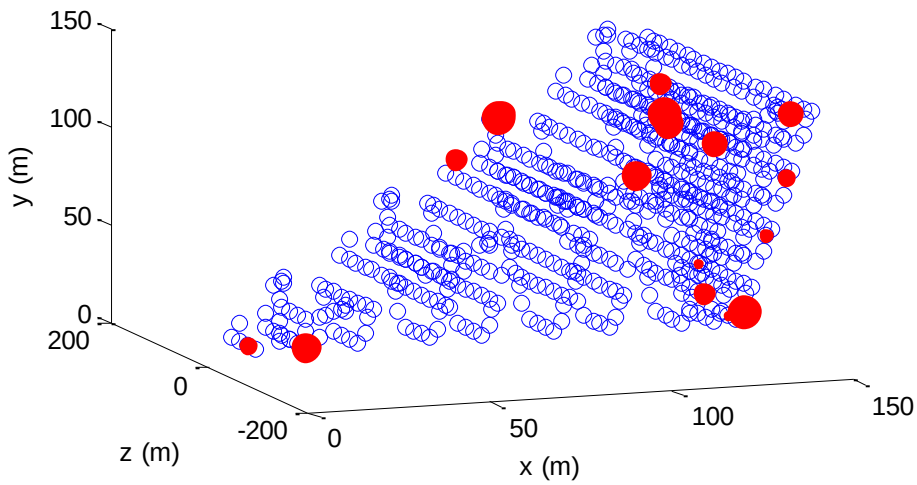

Figure 2.21 Stress Locations exceeding tensile capacity for SEE2-3 combination 11

2.7.2 Displacements

Displacement time history (dam body displacement with respect to base) in the stream direction at the crest of the dam (node with node number 194) is considered. The location of the dam node 194 is shown in Figure 2.22. Displacement time history responses are plotted in Figure 2.23 for each earthquake scenario.

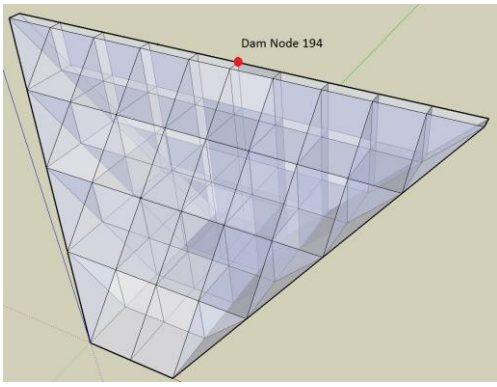

Figure 2.22 Location of Dam Node 194

OBE ground motions showed relatively small displacements than SEE1 and SEE2 motions as expected. The maximum displacement values were observed in the SEE2-1 and SEE2-2 ground motions. Peak value of displacements of OBE ground motion was about 3 cm in OBE-2. It was increased to 5 cm in SEE1-2 for SEE1 motions. The maximum displacement value was 8 cm in SEE2-2 for SEE2 motions. These displacements correspond to 0.023%, 0.038% and 0.056% of the dam height for OBE, SEE1 and SEE2 ground motions respectively.

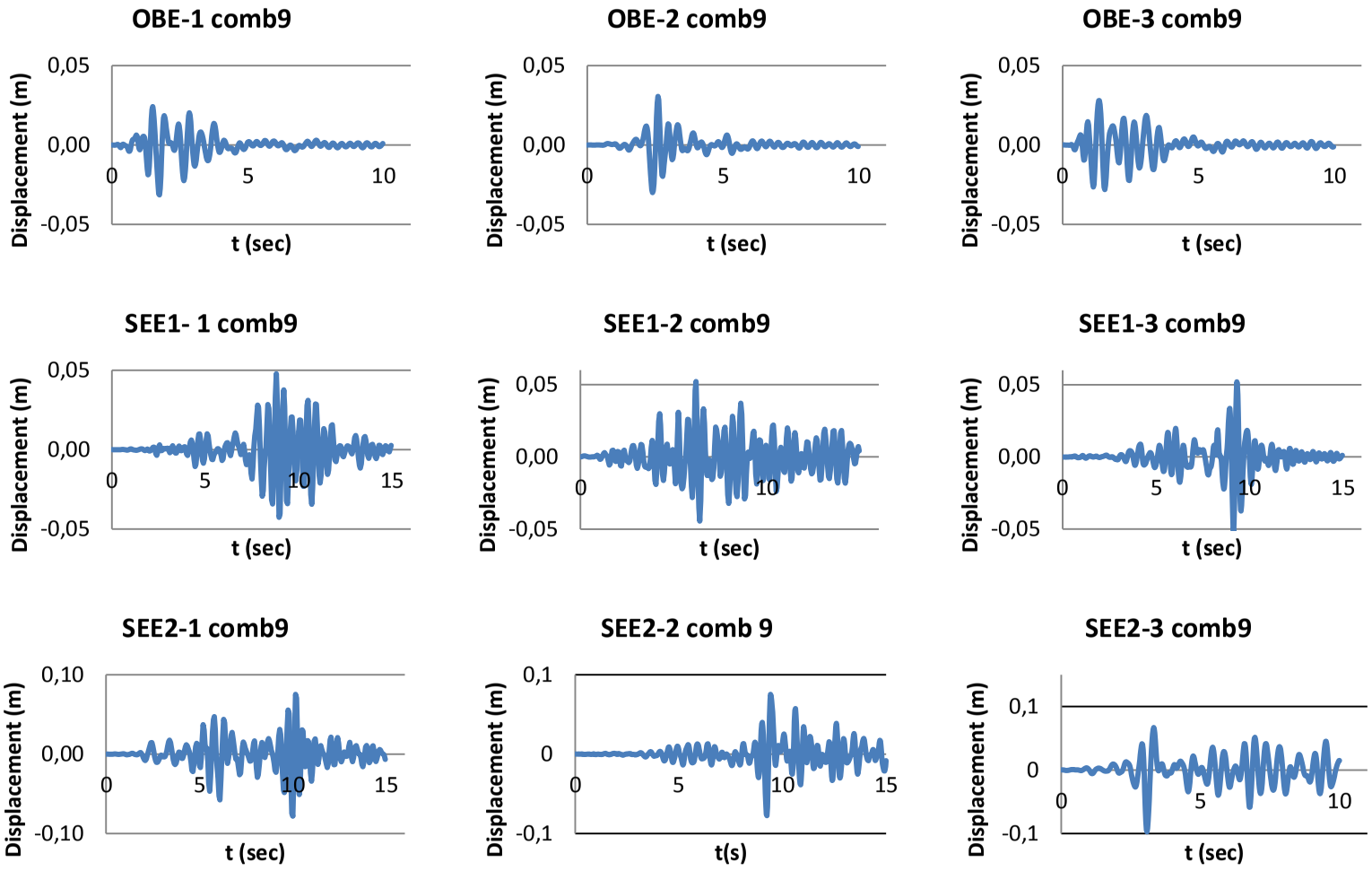

Figure 2.23 Displacement time history of node 194-x direction for each ground motion

2.7.3 Assessment Results

Stress based assessment was conducted for each ground motion following the methodology describe in Section 2.2. The most critical combinations were found as combinations 9, 11 and 13. Results providing the maximum stress locations along with assessment results are provided in Figures 2.24-2.26 with one combination giving the most critical result for each ground motion type. The performance criterion graphs of analyses with combination 9, 11 and 13 are given in Appendix for each ground motion type. If there existed more than one critical gauss quadrature location on the dam; then the most critical point is shown on the plot. It should be noted that gauss quadrature stress results were directly used without any smoothing.

The tensile strength of the roller compacted concrete was taken as 3 MPa as explained in the Section 2.4 under the title of "Material Properties". For the assessment the results of the compressible impounded water with rigid reservoir bottom and sides (α=1) were used. The maximum cumulative inelastic duration results for each earthquake type for the combinations 9, 11 and 13 were summarized in the Table 2.10.

Table 2.10 Summary Table of maximum cumulative inelastic duration

Maximum Cumulative Inelastic Duration Results (sec)

EQ Type	Combination 9	Combination 11	Combination 13
OBE-1	**0.1**	0.1	0.1
OBE-2	0.125	0.125	**0.125**
OBE -3	0.1	**0.1**	0.1
SEE1-1	0.55	**0.65**	0.6
SEE1-2	0.5	**0.55**	0.55
SEE1-3	**0.375**	0.35	0.35
SEE2-1	**0.5**	0.45	0.5
SEE2-2	0.25	**0.4**	0.275
SEE2-3	0.6	**0.7**	0.55

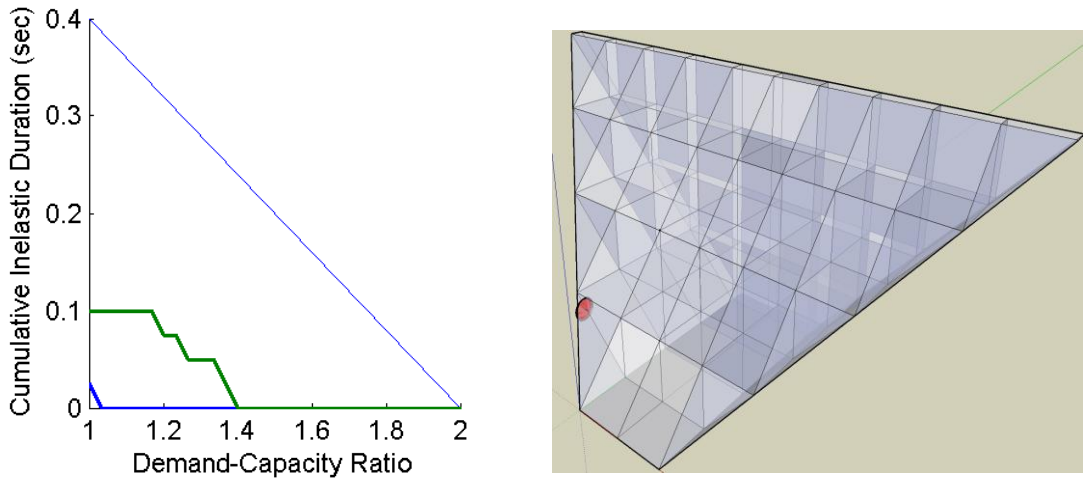

a) OBE-1_combination9

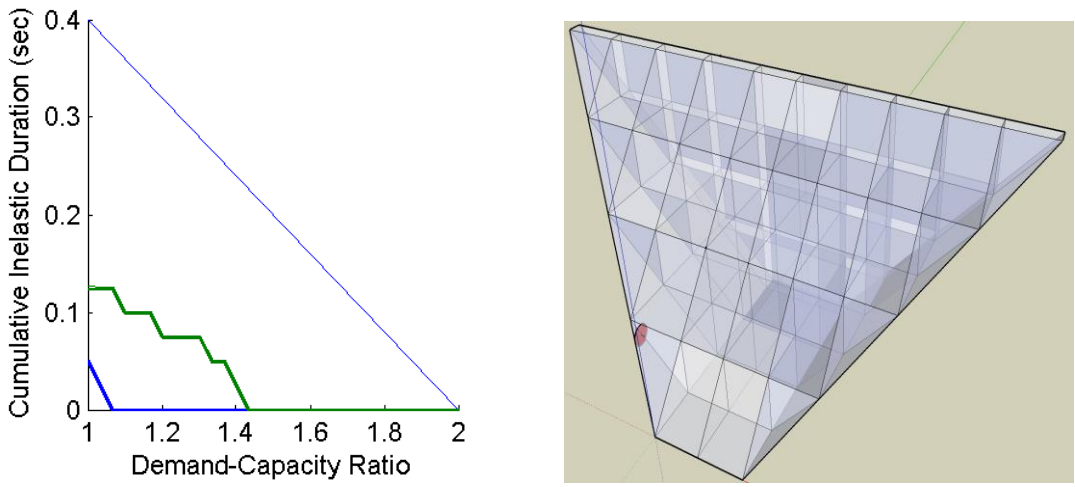

b) OBE-2_combination13

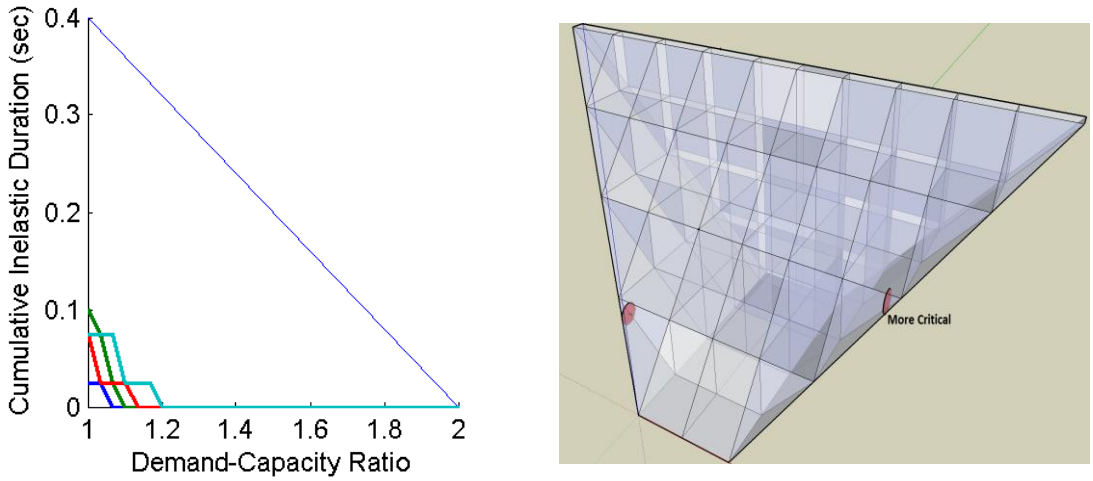

OBE-3_combination 9

Figure 2.24 Performance criterion graph and critical locations of OBE

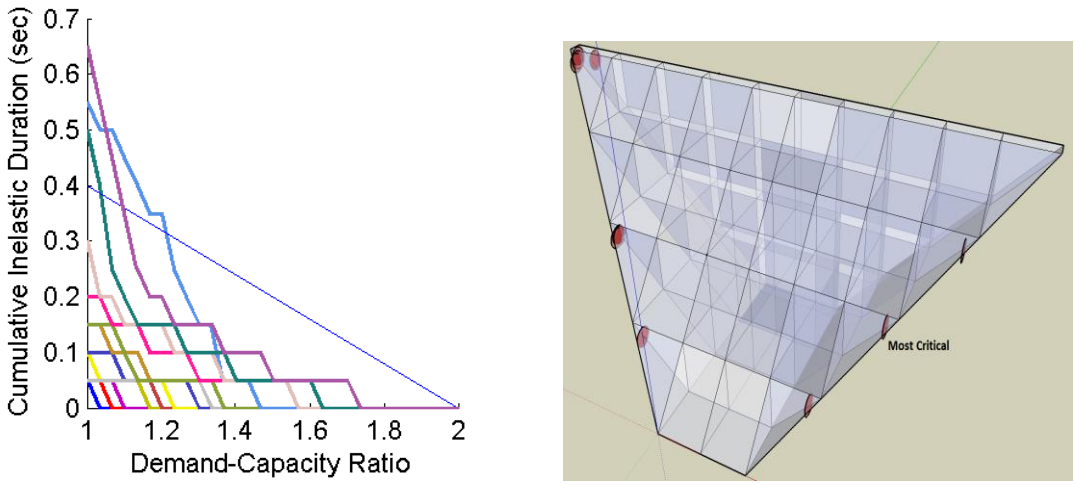

a) SEE1-1_combination11

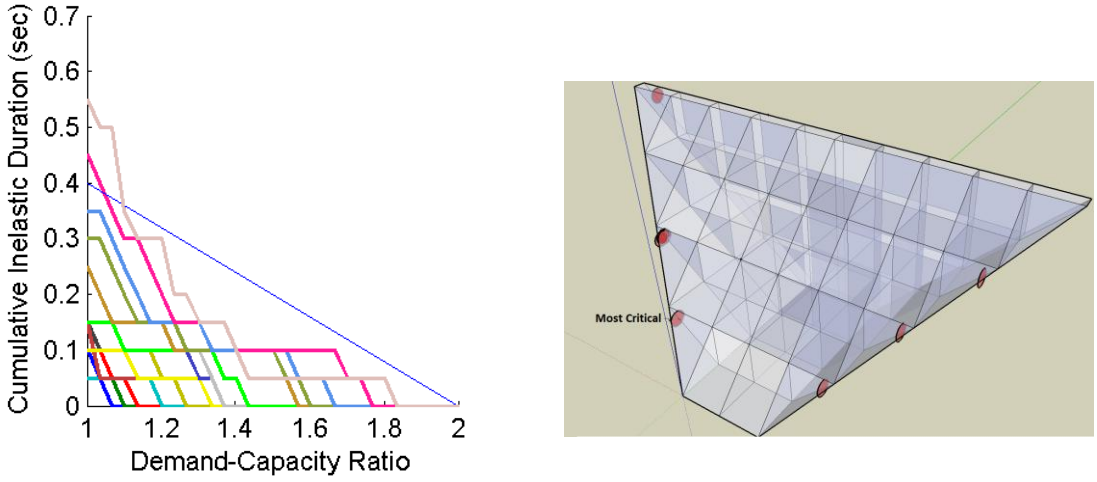

b) SEE1-2_combination11

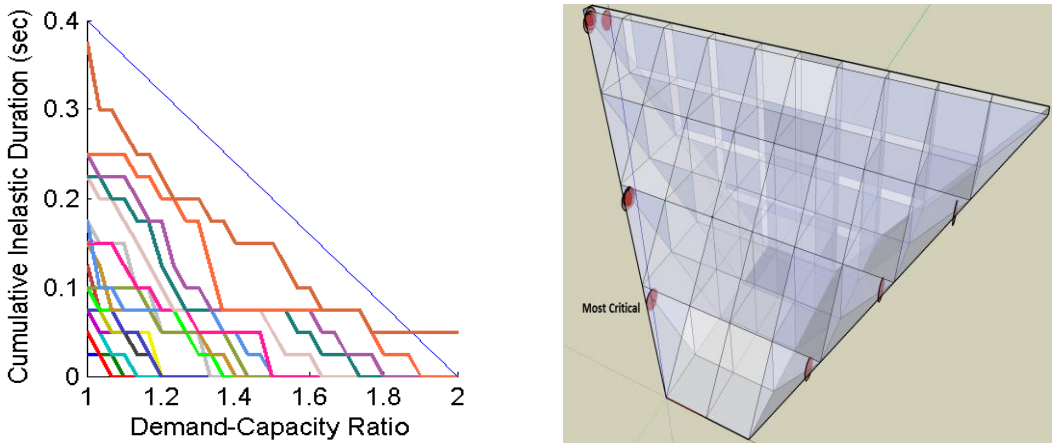

c) SEE1-3_combination9

Figure 2.25 Performance criterion graph and critical locations of SEE1 Analysis

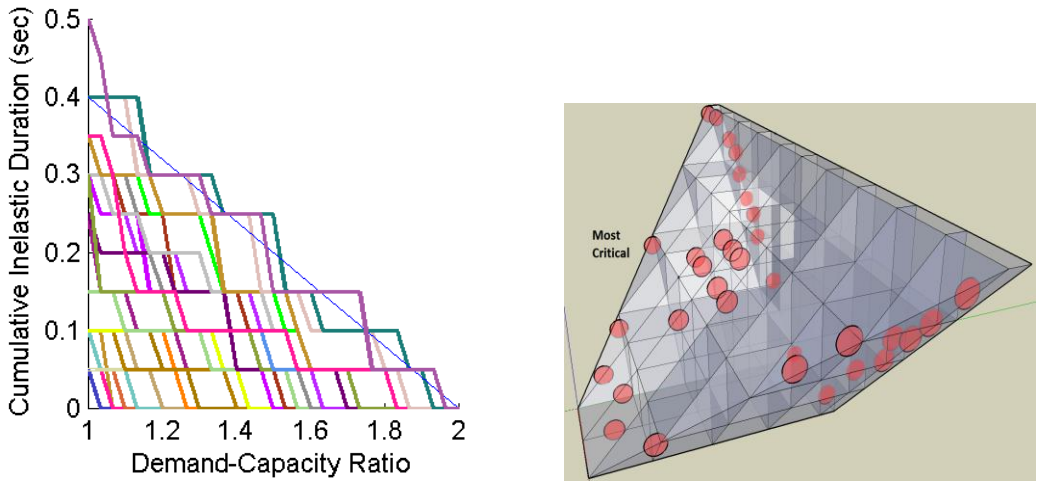

a) SEE2-1_combination9

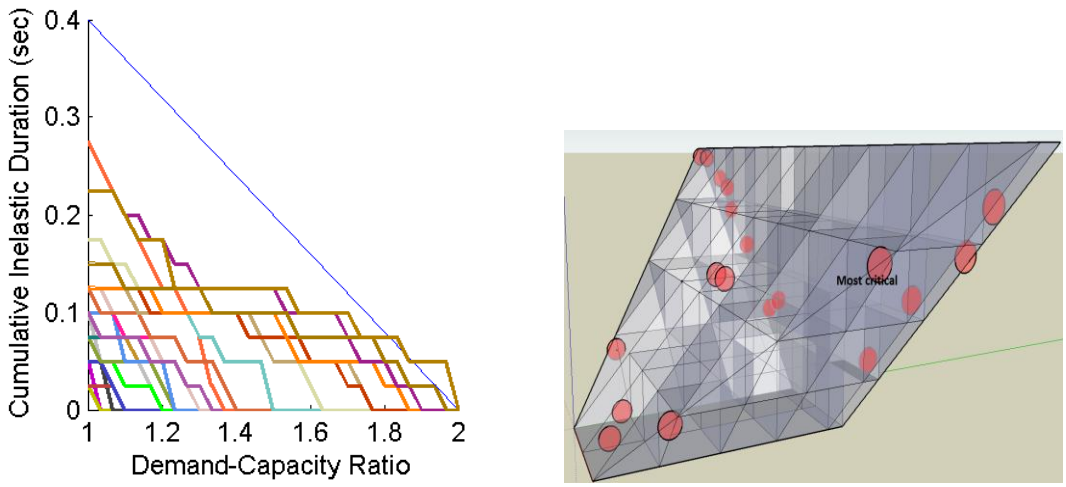

b) SEE2-2_combination13

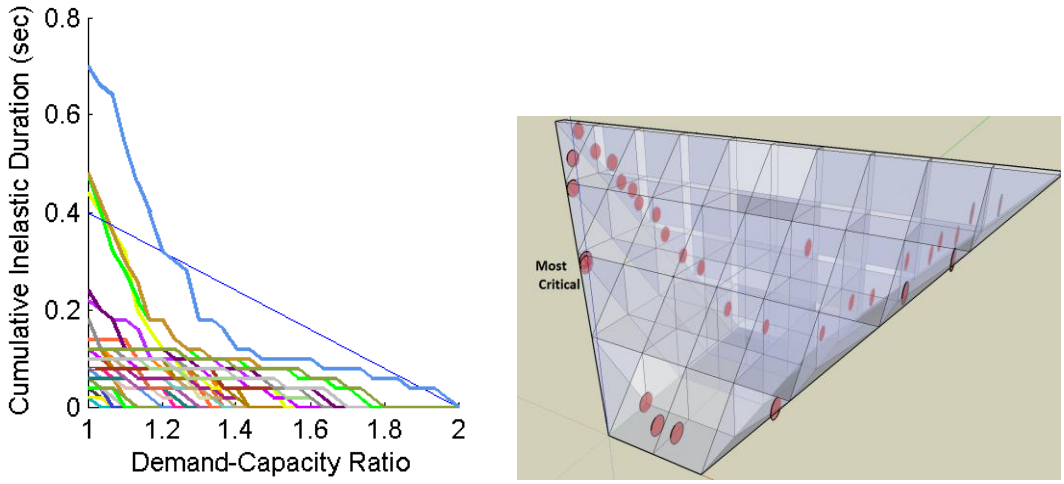

c) SEE2-3_combination11

Figure 2.26 Performance criterion graph and critical locations of SEE2 Analysis

By looking at the performance criterion graphs, it can be said that OBE (operating basis earthquake) data were not critical for further investigation. For each OBE ground motion and considering all these combinations, the linear analyses results yielded satisfactory elastic performance. While considering the SEE1, it was observed that the performance criterion was not satisfied especially for DCR values between 1 and 1.2. Therefore, limited nonlinear response in the form of cracking is expected. The designers should either increase the tensile strength of concrete or further nonlinear investigations must be made.

However, SEE2 performance criterion graphs exceeded the limitations generally on several locations. Especially, SEE2-1 ground motion had many points severely above the limit line. In such cases, it was required to perform nonlinear analyses or change the sectional properties of the dam.

It can be observed from the plots that the most critical points for the maximum cumulative inelastic durations located on the downstream side of the dam where the valley has a slope, in the proximity of the foundation. These regions are in the need of higher tensile strength material.

2.7.4 Effect of Peak Ground Accelerations (PGA) on Stress and Displacement

The effect of PGA values on the maximum principal stress and maximum displacement were studied. In order to observe the trends, analyses were conducted with the compressible impounded water case with wave reflection coefficient α=0.9 and incompressible impounded water. The analyses were conducted for combination 9 (x+0.3z+0.3y). OBE-1, SEE1-2 and SEE2-2 ground motions were considered for this investigation.

The maximum tensile stresses obtained from the analyses were used to plot the PGA versus stress graphs. The effect of ground motion on the expected crest displacement was also investigated. For this purpose, the displacement of dam node 194 was used. The location of the dam node 194 was shown in Figure 2.22 previously. PGA versus maximum tensile stress and PGA versus maximum crest displacement plots are shown in Figure 2.27 a and b respectively.

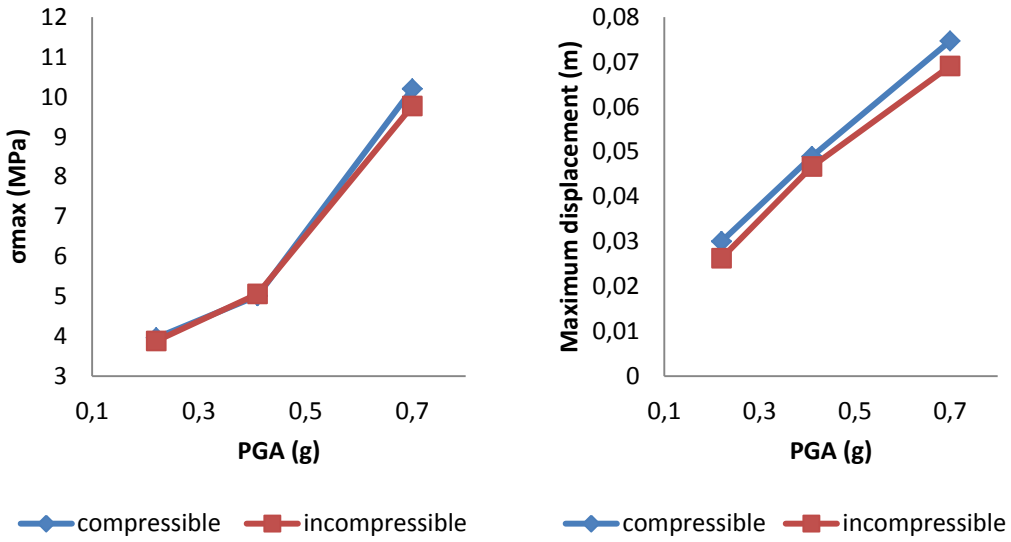

a) b)

Figure 2.27 PGA effect on a) maximum tensile stress b) maximum displacement at dam node 194 for compressible and incompressible cases

It can be seen from the Figure 2.27 that as the PGA values increase, both the maximum stresses and the maximum displacements increase. Plots show that there is almost a linear relationship between the demand parameters and PGA. Moreover, compressible impounded water results were slightly greater than the incompressible impounded water for both maximum stresses and maximum displacements.

2.8 Parametric Studies

2.8.1 Effect of Foundation Flexibility

A parametric study was conducted to examine the effect of foundation flexibility on maximum principle stresses and maximum crest displacements.

These studies were prepared for compressible impounded water with the wave reflection coefficient α=0.9 and for incompressible impounded water separately. Furthermore, the variations on the earthquake scenarios were considered. Operating basis earthquake (OBE), safety evaluation earthquake of level 1 (SEE1) and safety evaluation earthquake of level 2 (SEE2) were analyzed separately. Analyses were conducted for combination 9. Hysteretic damping ratio for foundation and dam were selected as 0.10 for both compressible and incompressible impounded water cases. The analysis parameters are summarized in the Table 2.11.

Figure 2.28 and 2.29 show the analyses results. It can be observed that as the foundation elasticity modulus decreases, the maximum tensile stresses on the dam body and maximum crest displacements decrease. This fact is the result of positive effect of foundation-structure interaction due to the radiation damping. It can be observed from Figure 2.28 that when the modulus of elasticity of foundation is reduced by half, the maximum principal stress is almost halved for OBE ground motion. This shows that for economical designs, consideration of dynamic foundation-dam interaction plays a crucial role.

On the other hand, maximum crest displacements do not follow the same trends discussed above. The crest displacement may increase or decrease, depending on the ground motion characteristics, when foundation flexibility is increased.

Table 2.11 Parameter values used for compressible and incompressible analyses

PARAMETERS	Compressible	Incompressible
Hysteretic Damping, c	0.10	0.10
Hysteretic Damping, f	0.10	0.10
α	0.9	-
Earthquake data	OBE-1, SEE1-2, SEE2-2	OBE-1, SEE1-2, SEE2-2

Table 2.12 Ec/Ef ratios and their corresponding values

Ec	Ef	Ec/Ef
23750	5800	4.095
23750	10800	2.199
23750	14100	1.684

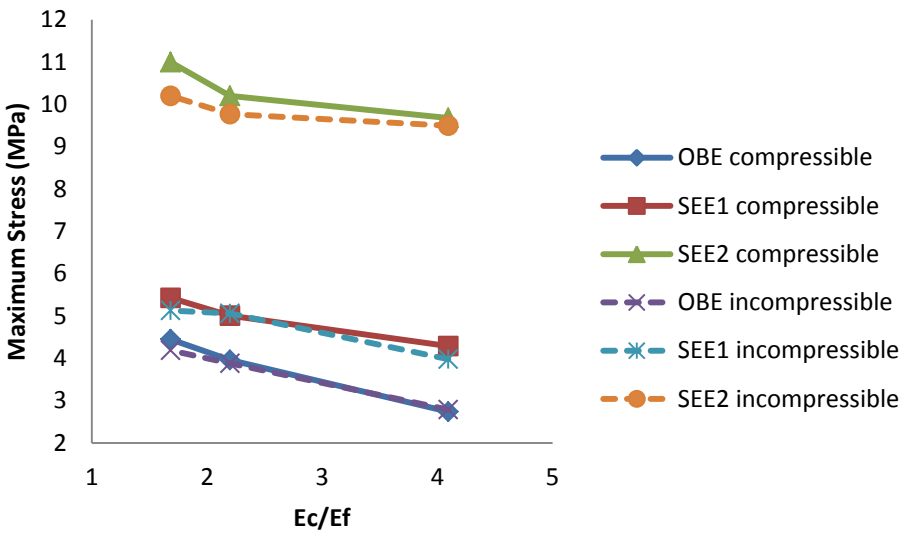

Figure 2.28 Ec/Ef effect on maximum tensile stress for compressible and incompressible cases

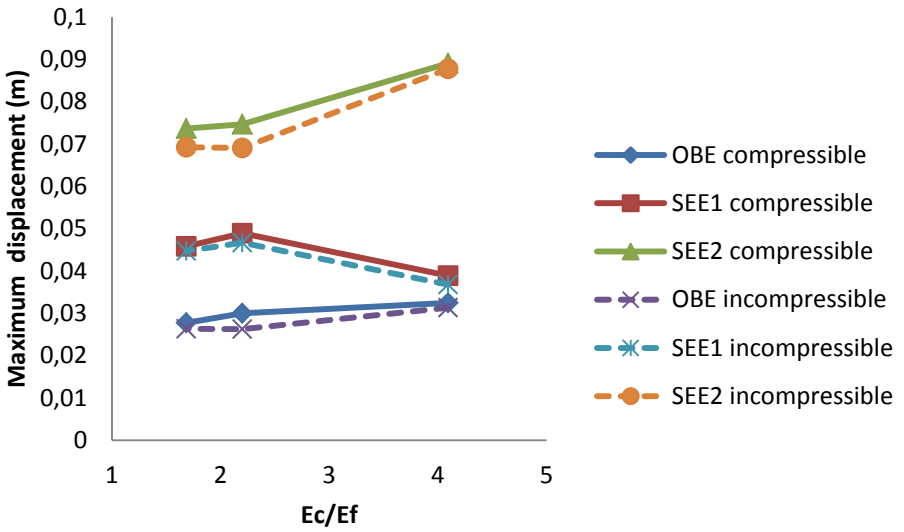

Figure 2.29 Ec/Ef effect on maximum displacement for compressible and incompressible cases

In addition, for the comparison of compressible and incompressible impounded water, it can be said that generally compressible water models show slightly higher displacements than the incompressible ones. However, the differences are marginal for practical purposes.

2.8.2 Bottom Absorption of Reservoir

Chopra (1985) advised to use wave reflection coefficient in between 0.8-0.9 for the models of new dams since the amount of sediment deposit is limited in new dams. However, while considering older dams, the used wave reflection coefficient may vary between 0.5-0.9 (Chopra,2008).

In order to show the effect of the absorptiveness different analyses were repeated by changing the wave reflection coefficient, α. These were done for OBE-1, SEE1-2 and SEE2-2 ground motions and the maximum stress values and maximum displacement values were calculated. Table 2.13 presents the results of the analysis.

Table 2.13 Results table of α effect on maximum stress and maximum displacement

α	**Maximum Stress (MPa)**			**Maximum Displacement (m)**		
	OBE-1	**SEE1-2**	**SEE2-2**	**OBE-1**	**SEE1-2**	**SEE2-2**
0.8	3.81	4.75	9.84	0.029	0.046	0.072
0.9	3.96	5.01	10.2	0.030	0.049	0.075
1	4.13	5.36	10.4	0.031	0.052	0.077
Maximum Difference (%)	**7.75%**	**11.38%**	**5.38%**	**8.53%**	**10.92%**	**7.32%**

It can be said that sedimentary materials play an important role on the behavior of the structure. For the completely reflected pressure waves, the maximum stress and maximum displacement values were greater than the absorptive ones. Therefore, as the wave reflection coefficient decreases, the values of maximum stress and maximum displacement decrease. Figures 2.30 and 2.31 were plotted to visualize this effect easily. The changes in the maximum stresses and maximum displacements for each ground motion are calculated as the variability percentages by considering 0.8 and 1 alpha results (Table 2.13). It can be stated that bottom absorption affects the maximum stress and displacement by about 10 %. Such variations in the response for new dams are not found to be significant due to the variations of alpha in the suggested range.

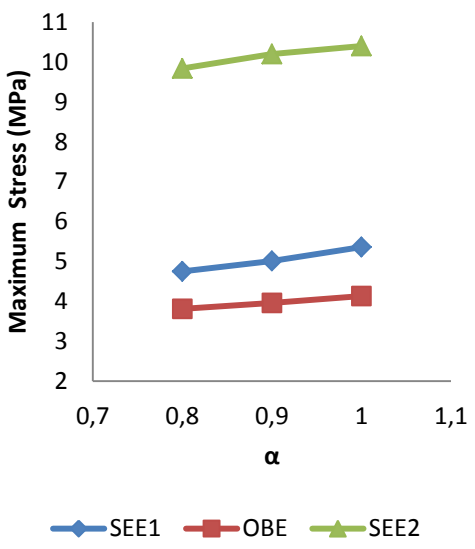

Figure 2.30 α Effect on max stress

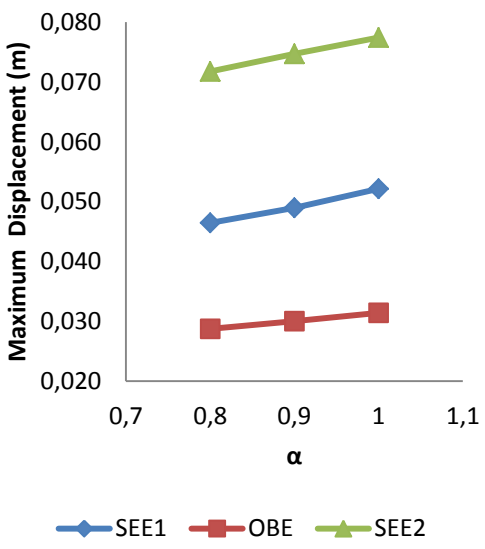

Figure 2.31 α Effect on max displacement

2.8.3 Effect of Slope of Cross-Section on the Behavior

The effect of section geometry has been studied by changing the downstream slope between 0.8 and 1.05. Analyses were conducted for SEE1-2 and SEE2-2 ground motions considering combination 9. OBE motions were not considered as they do not represent the safety evaluation earthquakes. In this part, the effect of the downstream slope of the dam's cross-section on the maximum tensile stress, maximum displacement taken place and the maximum cumulative inelastic duration were studied. Moreover, the performance criterion graphs were prepared according to BK (2012b) and USACE 2003 standards.

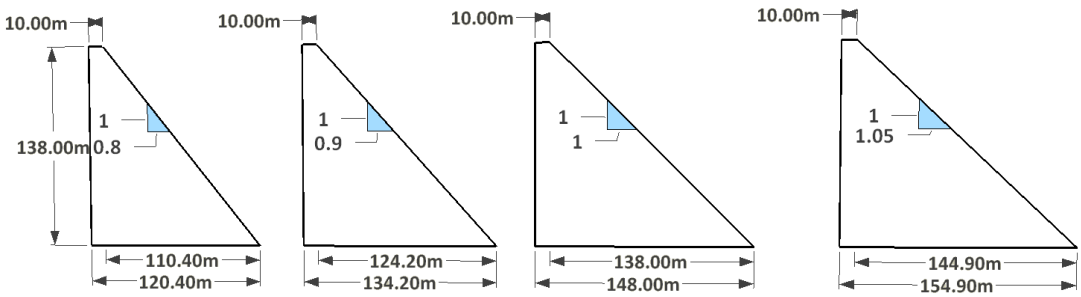

Figure 2.32 Various downstream slopes

The slope of downstream of the dam was varied between 0.8 and 1.05 as shown in Figure 2.32. The analyses were performed for incompressible impounded water and compressible impounded water with wave reflection coefficient 0.9. Results of analyses are presented in Tables 2.14 and 2.15.

Table 2.14 Effect of Slope of cross-section for SEE1-2 compressible analyses

SEE1- 2 Compressible	**Slopes**			
Engineering Demand Parameters	**m=0.8**	**m=0.9**	**m=1**	**m=1.05**
Node194 displacement (m)	6.51E-02	5.64E-02	4.89E-02	4.59E-02
Maximum principle stress (MPa)	5.46	5.16	5.01	5.54
Maximum duration (s)	0.85	0.5	0.45	0.4

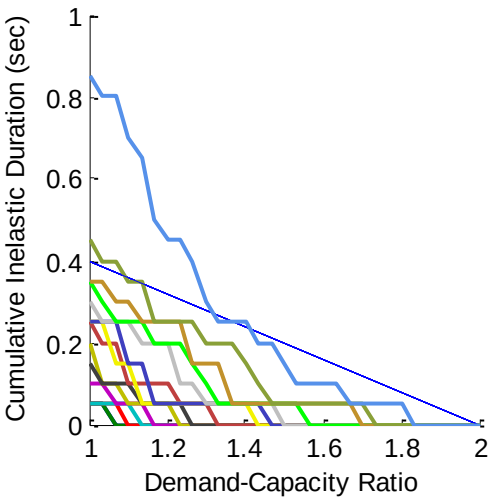

a) SEE1-2_comb9_compressible_m=0.8

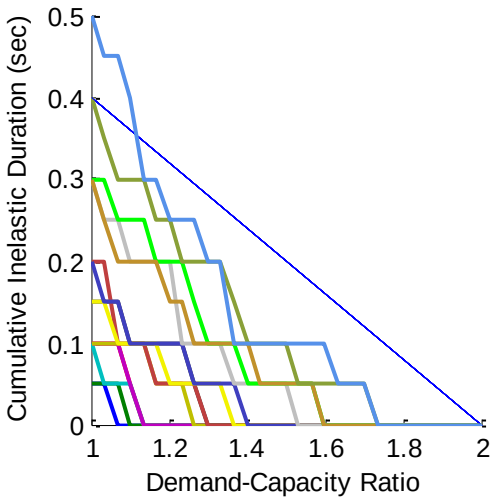

b) SEE1-2_comb9_compressible_m=0.9

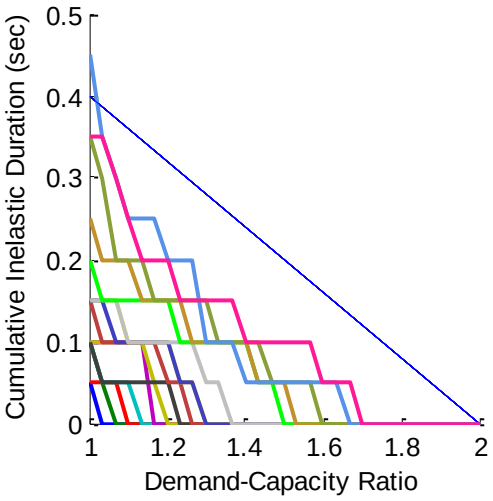

c) SEE1-2_comb9_compressible_m=1

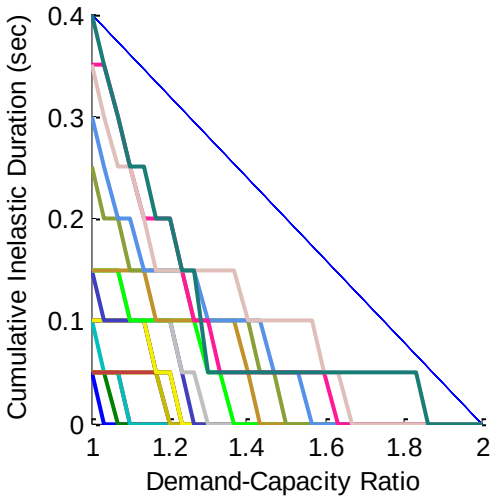

d) SEE1-2_comb9_compressible_m=1.05

Figure 2.33 Performance criterion curves of downstream slope effect of SEE1-2 with compressible

Table 2.15 Effect of Slope of cross-section for SEE1-2 incompressible analyses

SEE1- 2 Incompressible	**Slopes**			
Engineering Demand Parameters	**m=0.8**	**m=0.9**	**m=1**	**m=1.05**
Node194 displacement (m)	5.89E-02	5.09E-02	4.67E-02	4.47E-02
Maximum principle stress (MPa)	5.19	4.99	5.06	5.03
Maximum duration (s)	0.55	0.45	0.3	0.3

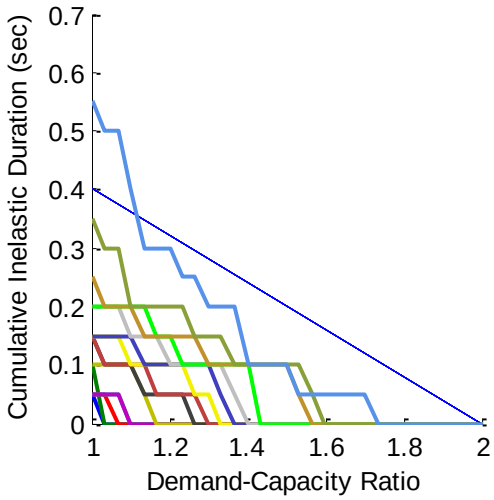

a) SEE1-2_comb9_incompressible_m=0.8

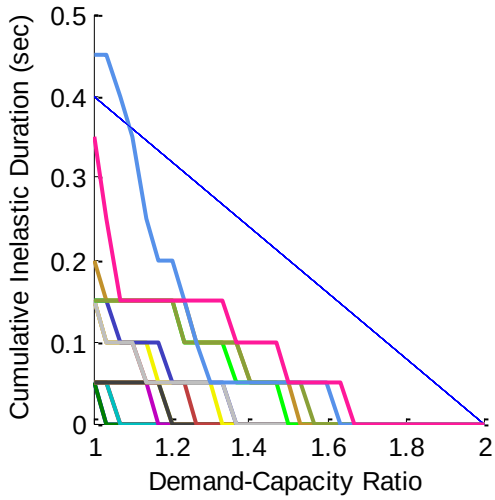

b)SEE1-2_comb9_incompressible_m=0.9

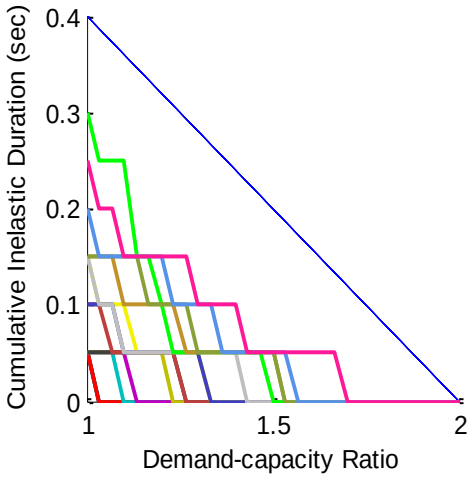

c)SEE1-2_comb9_incompressible_m=1

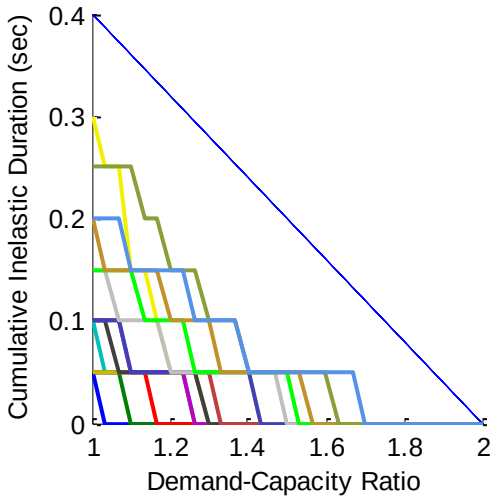

d) SEE1-2_comb9_incompressible_m=1.0

Figure 2.34 Performance criterion curves of downstream slope effect of SEE1-2 with incompressible

It was obvious that as the slope of the downstream was increased, the maximum stress decreased and DCR versus cumulative inelastic duration plots became less critical. In addition, maximum displacements were smaller for the higher slopes and also smaller maximum cumulative inelastic durations were obtained.

Figure 2.34 shows that when SEE1-2 combination 9 is considered, the optimum downstream slope is about 1.0. When the downstream slope is less than 1.0, the cumulative inelastic duration at low demand-capacity ratio values exceed the limit curve. It should be noted that such small changes in the downstream slope may affect the cost significantly. For Andıraz Dam a downstream slope change of 0.05, approximately corresponds to 77763 m^3 of extra RCC which correspond to a slope change from m=1 to m=1.05 shown in Table 2.16.

Table 2.16 Downstream slope effect on volume of the dam

Volume of dam	**m=0.8**	**m=0.9**	**m=1**	**m=1.05**
Concrete (m^3)	1538148	1693674	1849200	1926963
Difference (m^3)	311052	155526	-	-77763
Difference %	16.82%	8.41%	-	-4.21%

Another important issue was the compressibility of the impounded water. Slope effect was studied for incompressible and compressible with α=0.9 impounded water. It was observed that incompressible impounded water model experienced smaller maximum displacement, maximum stress and maximum cumulative inelastic duration than the compressible water for each different slope cases. However, results exhibit only about 10% change in the maximum stress values when one models the reservoir as incompressible as opposed to compressible fluid. Here neglecting the compressibility of the impounded water underestimated the stress results. The importance of including the compressibility of the water was emphasized by in relation to a study conducted on Monticello Dam by Chopra and Nuss (2009). Slope effect studies were repeated for the SEE2-2 records. The results can be investigated on the Tables 2.17 and 2.18 and Figures 2.35 and 2.36.

Similar conclusions may be drawn for the SEE2-2 records for the effect of slopes of the downstream with the SEE1-2 records. Again the maximum stress values are increased by the decrease in the downstream slope. Moreover, maximum displacements have an inverse relation with the slope of the downstream. The assessment by using linear analyses becomes less critical since the cumulative inelastic durations decrease, as the slope of the downstream increases. Again downstream slope equals 1 is the most optimum selection.

Surprisingly, different from the previous results for the maximum cumulative inelastic duration of the SEE1-2 records, model with SEE2-2 record of incompressible impounded water showed greater durations than the compressible model. Here, it may be concluded that in some situations incompressible model may overestimate the results. However, as mentioned before for the maximum stress and maximum displacement considerations, use of incompressible water model again underestimated the stress results.

There are many points exceeding the limit line, passing through 0.4 sec of cumulative inelastic duration for corresponding demand-capacity ratio 1 and zero tolerance of inelastic behavior for the DCR equals 2, in SEE2 analysis. Therefore, it should be concluded that optimization by using linear analysis from this assessment cannot be performed for SEE2 analysis.

Table 2.17 Effect of Slope of cross-section for SEE2- 2 compressible analyses

SEE2-2 Compressible	**Slopes**			
Engineering demand parameters	**m=0.8**	**m=0.9**	**m=1**	**m=1.05**
node194 displacement (m)	9.62E-02	8.64E-02	7.91E-02	7.56E-02
Maximum principle stress (MPa)	11.2	10.6	10.1	9.86
Maximum duration (s)	0.55	0.475	0.425	0.425

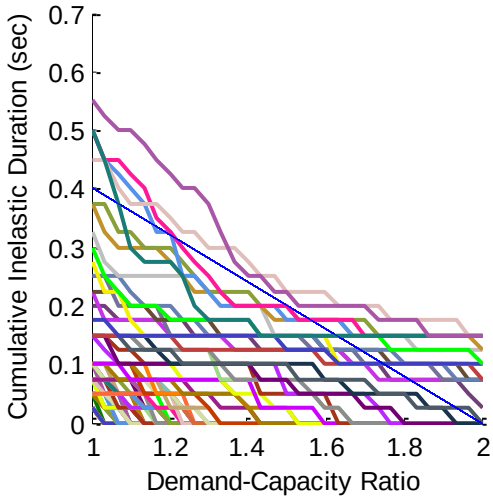

a) SEE2-2_comb9_m=0.8

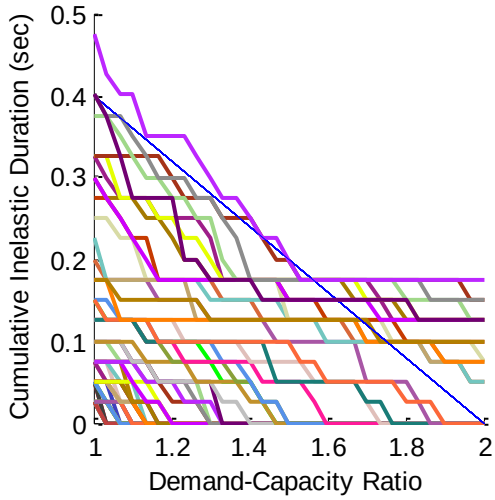

b) SEE2-2_comb9_m=0.9

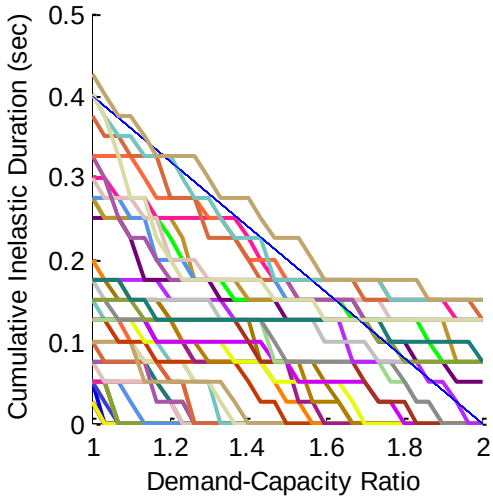

c)SEE2-2_comb9_ m=1

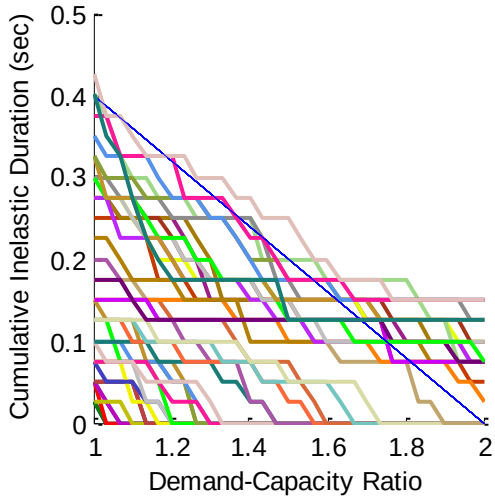

d) SEE2-2_comb9_m=1.05

Figure 2.35 Performance criterion curves of downstream slope effect of SEE2-2 with compressible

Table 2.18 Effect of Slope of cross-section for SEE2-2 incompressible analyses

SEE2- 2 Incompressible	**Slopes**			
Engineering demand parameters	**m=0.8**	**m=0.9**	**m=1**	**m=1.05**
node194 displacement (m)	9.16E-02	8.24E-02	7.47E-02	7.16E-02
Maximum principle stress (MPa)	10.7	10.3	9.8	9.57
Maximum duration (s)	0.575	0.6	0.525	0.475

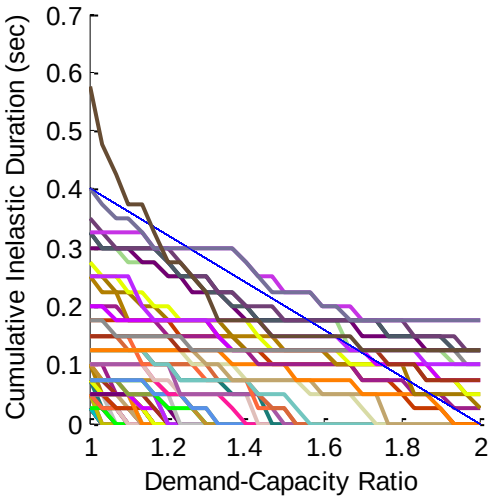

a) SEE2-2_comb9_incompressible_m=0.8

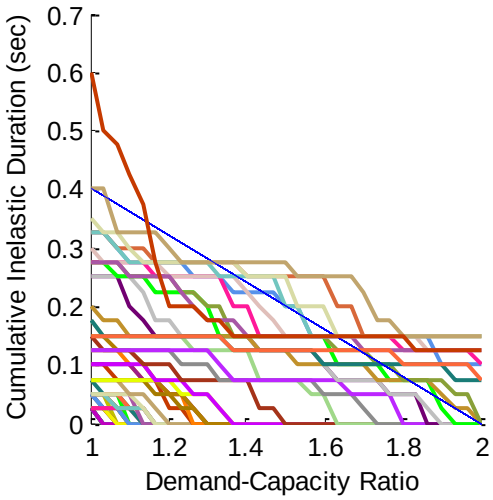

b) SEE2-2_comb9_incompressible_m=0.9

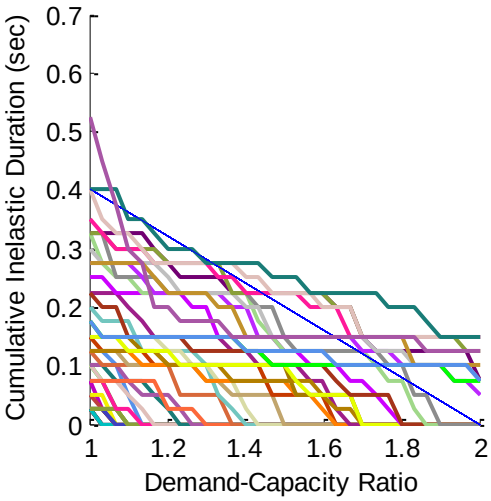

c)SEE2-2_comb9_incompressible_m=1

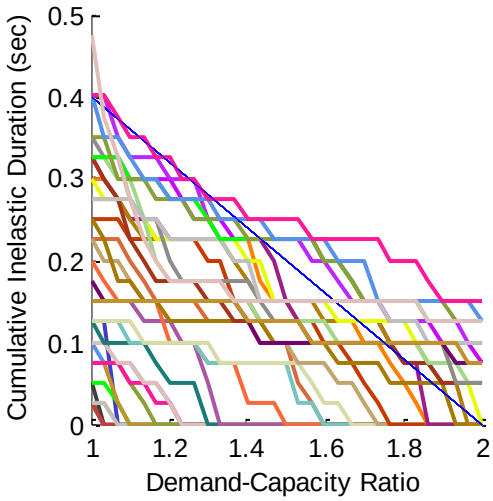

d) SEE2-2_comb9_incompressible_m=1.05

Figure 2.36 Performance criterion curves of downstream slope effect of SEE2-2 with incompressible

2.9 Tornado Diagrams

Tornado diagram approach, a deterministic sensitivity analysis method, is used for the determination of the effect of the random variables to the structural response. Tornado diagram shows the influence of different parameters, the most effective one at the top and with a descending order in which the least important parameter is located at the bottom. The procedure of obtaining the tornado diagram is as follows: Firstly, parameters to be investigated called as random variables are determined and several analyses are done in each case, only one parameter value changed at a time. For each independent parameter, there exist two boundaries as upper and lower values, and remaining parameters are taken in their median values, so that in each analysis the effect of the only one variable is investigated. The difference of the results of the two extreme values of a random variable gives the swing amount in absolute value. After determining the swings of each random variable, it is sorted according to the amount of swing with maximum swing one at the top. Figure 2.37 demonstrates the tornado diagram process. Variability of the results are shown as the length of the swing. The most effective parameter has the largest swing and is located at the top of the tornado diagram.

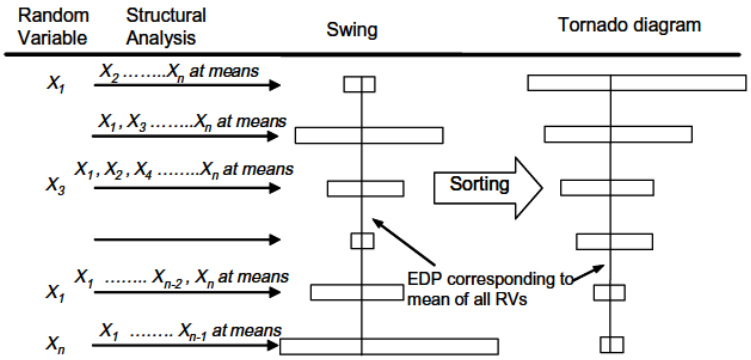

Figure 2.37 Tornado diagram preparation (Binici and Mosalam, 2006)

In this study, three engineering demand parameters were used: maximum principle tensile stress, maximum crest displacement (dam node 194) and the maximum value of the cumulative inelastic duration for the assessment of linear analysis usage.

While preparing the parametric study, the following parameters were included as the possible random variables:

E_c: Modulus of elasticity of dam
E_f: Modulus of elasticity of foundation
H.D.c: Hysteretic damping ratio of the dam
H.D.f: Hysteretic damping ratio of the foundation
Earthquake data type (EQ) (three different records are available)
α: wave reflection coefficient (only for compressible impounded water)

Analyses were also repeated for the incompressible impounded water situations. The parameters were same with the compressible impounded water excluding the α, wave reflection coefficient. Moreover, the variations on the earthquake scenarios were considered. Operating basis earthquake (OBE), safety evaluation earthquakes of level 1 and 2 (SEE1 and SEE2) were studied separately.

The control model parameters and their values can be observed in the Table 2.19, Table 2.24 and Table 2.29 for the compressible and incompressible impounded water situations. Same values

were used for both cases in order to compare the behaviors easily. For the analyses, combination 9 was used.

In addition, the same parameter values were used for the each ground motions; OBE, SEE1 and SEE2 analyses. OBE1, SEE1-2 and SEE2-2 were considered as the mean parameters.

After obtaining the results, the model results were normalized to 1 by dividing the demand parameter to the demand parameter obtained from the result of analysis conducted by using mean values. In this way the ratios of the change in the results to the control results gave the swing of the variation. It was important to sort the independent parameters such that the diagram looked like a tornado to reflect the highest swing causing parameter.

2.9.1 OBE Analyses

Tornado diagram study was first conducted for the OBE ground motion set. Andıraz Dam material properties were used for the mean model with the modulus of elasticity of the concrete and foundation rock taken as 23750 and 10800 MPa, respectively. For the modulus of elasticity of concrete a range of approximately 10000 MPa plus and minus to the mean parameter was selected. A similar strategy was employed to consider the variability of modulus of elasticity of foundation rock values as shown in Table 2.19.

Table 2.19 Input Parameters table for OBE analyses

Parameters	**Compressible**			**Incompressible**		
	MEDIAN	MIN	MAX	MEDIAN	MIN	MAX
Ec (MPa)	23750	13750	33750	23750	13750	33750
Ef (MPa)	10800	5800	14100	10800	5800	14100
Hysteretic Damping, c	0.10	0.04	0.14	0.10	0.04	0.14
Hysteretic Damping, f	0.10	0.04	0.20	0.10	0.04	0.20
Eq. Type (1,2,3)	1	2	3	1	2	3
α	0.9	0.8	1	-	-	-

The median model results for the demand engineering parameters considering OBE1 ground motion are presented in Table 2.20 where both compressible and incompressible impounded water results are shown. Analysis of compressible water case with wave reflection coefficient 0.9 resulted in slightly greater maximum principle stress than the analysis of incompressible water (2% difference). The maximum principle stress values were more than 3 MPa which was equal to the static tensile strength of RCC. The cumulative inelastic durations were calculated as 0.1 and 0.075 sec for compressible and incompressible water models respectively. Moreover, maximum displacement on the crest of the dam of compressible analysis was greater than the incompressible analysis.

Table 2.20 Median model results for OBE analyses

Median Model Results	**Compressible**	**Incompressible**
Maximum Principle Stress (MPa)	3.96	3.88
Maximum Deflection (m)* (x)	-0.03000	-0.02626
Maximum CID of assessment (s)	0.1	0.075

The results of the analyses are in Tables 2.21, 2.22 and 2.23 for the maximum stress, maximum top displacement and maximum duration of the nonlinear assessment respectively. Table 2.21 presents the results of maximum principle stresses for minimum and maximum values of the parameters for the OBE ground motion. According to Table 2.21, the maximum stress value was obtained when the maximum value of the modulus of foundation was considered. In addition, it was seen that modulus elasticity had a proportional relation with the maximum principle stress. The maximum stress values increased while both the moduli of elasticity of concrete and foundation rock increased. Hysteretic damping, on the other hand, was inversely proportional with the maximum stress. Compressibility of water, in terms of wave reflection coefficient, affected the maximum stress directly. As the wave reflection coefficient increased, greater stresses were obtained.

Table 2.21 Maximum Principle stress results for OBE analyses

Maximum Principle Stress (MPa)	**Compressible**		**Incompressible**	
Parameters	MIN	MAX	MIN	MAX
Ec	3.36	4.21	3.47	3.83
Ef	2.74	4.45	2.79	4.19
Hysteretic Damping, c	4.12	3.85	4.07	3.76
Hysteretic Damping, f	4.1	3.73	4.05	3.61
Eq. Type (1,2,3)	4.17	3.32	4	3.22
α	3.81	4.13	-	-

Maximum crest displacement values for upper and lower bound parameters are shown in Table 2.22. Some of the displacement values were negative. This was related to the direction of the maximum displacement. The absolute values of displacement were considered for the comparisons. It was observed that modulus of elasticity and hysteretic damping for both concrete and foundation rock affected the maximum displacements inversely. Moreover, incompressible water consideration resulted in smaller maximum crest displacements for each parameter than the compressible water.

Since maximum stress values exceeded the tensile strength of RCC, linear analysis assessment was conducted and the maximum cumulative inelastic durations are presented in Table 2.23. In this table, cumulative inelastic durations below the limiting exceedance time (i.e. 0.4 sec) for the OBE ground motion.

Table 2.22 Maximum top displacement results for OBE analyses

Maximum Displacement (m)	**Compressible**		**Incompressible**	
Parameters	MIN	MAX	MIN	MAX
Ec	-0.04154	-0.02435	-0.03893	0.02149
Ef	-0.03248	-0.02774	-0.03134	0.02636
Hysteretic Damping, c	-0.03122	-0.02920	-0.02766	-0.02539
Hysteretic Damping, f	-0.03121	-0.02810	-0.02754	-0.02426
Eq. Type (1,2,3)	-0.02940	-0.02684	0.02786	-0.02443
α	-0.02873	-0.03141	-	-

Table 2.23 Maximum duration of assessment results for OBE analyses

Maximum Duration of Assesment (s)	**Compressible**		**Incompressible**	
Parameters	MIN	MAX	MIN	MAX
Ec	0.075	0.125	0.075	0.1
Ef	not	0.125	not	0.025
Hysteretic Damping, c	0.1	0.1	0.1	0.075
Hysteretic Damping, f	0.1	0.1	0.1	0.075
Eq. Type (1,2,3)	0.125	0.05	0.1	0.025
α	0.1	0.1	-	-

The results given on the tables shown above were plotted on the tornado diagrams in order to see the most important parameter by observing the amount of the swing. Figure 2.38 represents the swing diagrams for OBE ground motion maximum stress, maximum crest displacement and maximum cumulative inelastic duration with compressible and incompressible water cases.

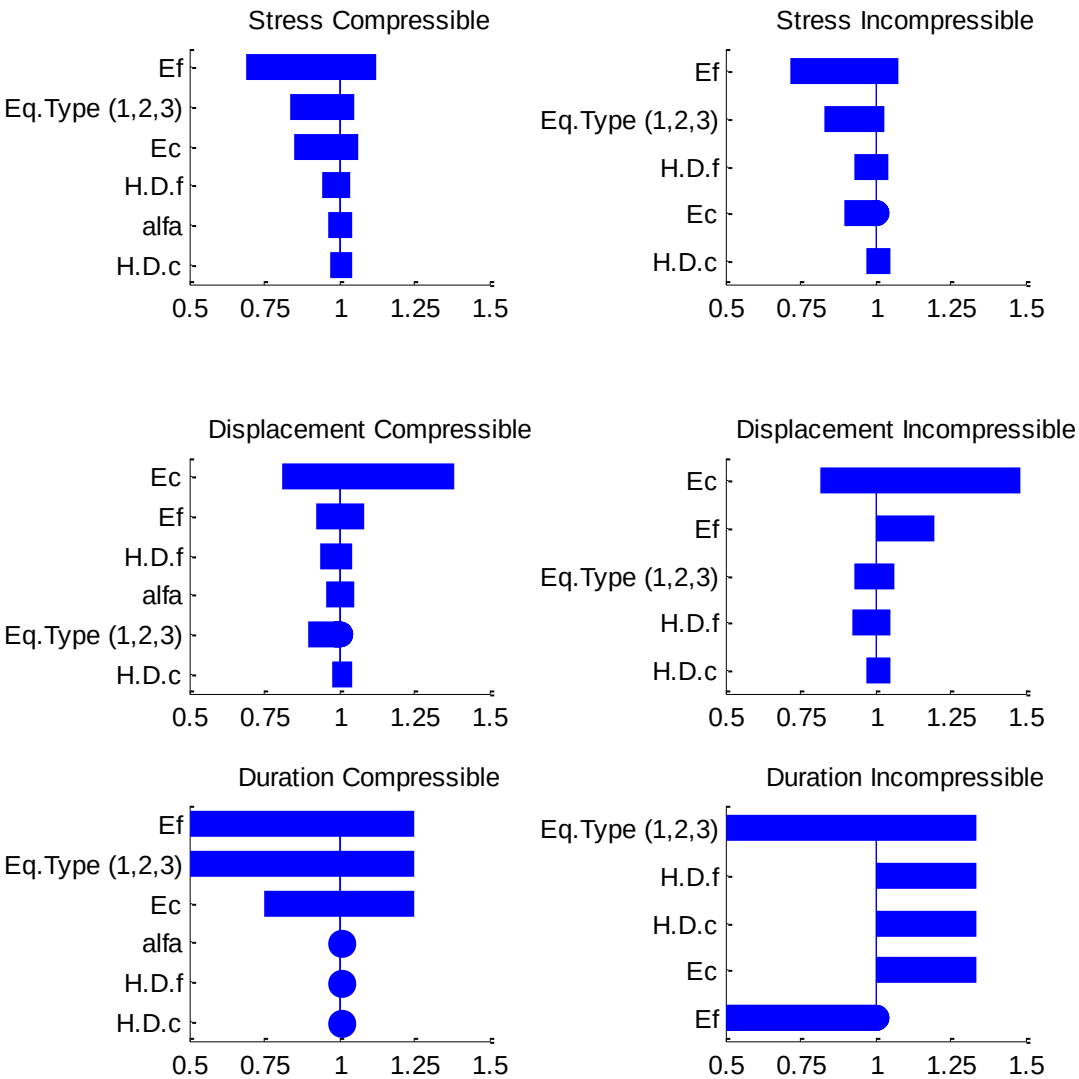

Figure 2.38 Tornado graphs of OBE analyses results

The most important parameter that affects the seismic response was the modulus of elasticity of the foundation rock for the maximum principles stress both for compressible and incompressible water cases. The second most influential latter parameter was the earthquake type influencing the results of stresses. The least important parameter was found as the hysteretic damping of concrete as can be seen in the tornado diagram.

It can be said that the modulus of elasticity of concrete was the important for the maximum crest displacement results. Then, modulus of elasticity of foundation appeared to be the next important variable. Similar to results of stresses, hysteretic damping of concrete was the least effective parameter. Ground motion type was more crucial than hysteretic damping of foundation rock for the compressible water, but the reverse was valid for the incompressible water.

It was not easy to decide on the most important parameter for cumulative inelastic duration. It can be said that ground motion type was the mostly effective since it was at the top of the tornado diagram for incompressible water and located on the second level for the compressible water.

2.9.2 SEE1 Analyses

Tornado diagram study was then performed for SEE1. Andıraz Dam properties were used for calculations which are listed in Table 2.24 under "Median" column. Same properties with previous OBE analyses were used. However, SEE1-2 ground motion was used as the median analysis results as this ground motion gave the median results.

Table 2.24 Input Parameters table for SEE1 analyses

Parameters	**Compressible**			**Incompressible**		
	MEDIAN	MIN	MAX	MEDIAN	MIN	MAX
Ec (MPa)	23750	13750	33750	23750	13750	33750
Ef (MPa)	10800	5800	14100	10800	5800	14100
Hysteretic Damping, c	0.10	0.04	0.14	0.10	0.04	0.14
Hysteretic Damping, f	0.10	0.04	0.20	0.10	0.04	0.20
Eq. Type (1,2,3)	2	1	3	2	1	3
α	0.9	0.8	1	-	-	-

The median model results for the demand engineering parameters are presented on Table 2.25 where both compressible and incompressible impounded water results are shown. Maximum principle stress of incompressible water was obtained to be greater than the compressible water analysis stress with a wave reflection coefficient of 0.9. The maximum principle stress values were more than 3 MPa. Therefore, it was possible to conduct the assessment of linear analysis. It was calculated that the cumulative inelastic durations were 0.45 and 0.3 sec for compressible and incompressible water models respectively. Moreover, maximum displacement on the crest of the dam of compressible analysis was greater than the incompressible analysis.

Table 2.25 Median model results for SEE1 analyses

Median Model Results	**Compressible**	**Incompressible**
Maximum Principle Stress (MPa)	5.01	5.06
Maximum Deflection (m)* (x)	0.04894	0.04670
Maximum CID of assessment (s)	0.45	0.3

The maximum stress, maximum top displacement and max duration of the assessment results are shown in Table 2.26, Table 2.27 and Table 2.28 respectively for SEE1 analyses. The maximum

stress value was obtained as 5.89 MPa in the SEE1-3 analysis from Table 2.26. 4.03 MPa stress value was reached with the consideration of minimum value for the modulus of elasticity of the concrete. The direct relation between the stress and modulus of elasticity of concrete and foundation rock was observed similar to the OBE results. Hysteretic damping had an adverse effect on the stress results. Compressibility of water, in terms of wave reflection coefficient, affected the maximum stress directly. As the wave reflection coefficient increased, greater stresses were obtained.

Table 2.26 Maximum Principle stress results for SEE1 analyses

Maximum Principle Stress (MPa)	**Compressible**		**Incompressible**	
Parameters	MIN	MAX	MIN	MAX
Ec	4.03	5.76	3.9	5.87
Ef	4.29	5.43	3.98	5.13
Hysteretic Damping, c	5.38	4.87	5.29	4.94
Hysteretic Damping, f	5.33	4.7	5.32	4.71
Eq. Type (1,2,3)	4.93	5.89	4.43	5.8
α	4.75	5.36	-	-

Table 2.27 presents the maximum crest displacement results obtained from the minimum and maximum values of the parameters for compressible and incompressible water. The absolute values of displacement were considered for the comparisons. Modulus of elasticity of concrete affected the maximum crest displacement adversely in contrast to the modulus of elasticity of the foundation rock. Incompressible water consideration resulted in smaller maximum crest displacements for each parameter than the compressible water.

In addition, Table 2.28 shows the maximum cumulative inelastic durations of the linear performance assessment required due to the excessive stress results. Some of the duration results are higher than the assessment limitations.

The results given on the Tables 2.26-2.28 were plotted on the tornado diagrams in order to see the most important parameter easily by the amount of the swing in Figure 2.39.

Table 2.27 Maximum top displacement results for SEE1 analyses

Maximum Displacement (m)	**Compressible**		**Incompressible**	
Parameters	MIN	MAX	MIN	MAX
Ec	0.06440	0.03895	0.06454	0.03901
Ef	-0.03891	0.04583	0.03680	0.04474
Hysteretic Damping, c	0.05088	0.04758	0.04947	0.04493
Hysteretic Damping, f	0.05124	0.04541	0.04893	0.04347
Eq. Type (1,2,3)	0.04638	-0.05095	0.04071	0.04814
α	0.04644	0.05213	-	-

Table 2.28 Maximum duration of assessment results for SEE1 analyses

Maximum Duration of Assesment (s)	**Compressible**		**Incompressible**	
Parameters	MIN	MAX	MIN	MAX
Ec	0.6	0.6	0.45	0.45
Ef	0.3	0.5	0.25	0.4
Hysteretic Damping, c	0.6	0.35	0.5	0.25
Hysteretic Damping, f	0.6	0.3	0.5	0.25
Eq. Type (1,2,3)	0.55	0.325	0.4	0.275
α	0.3	0.5	-	-

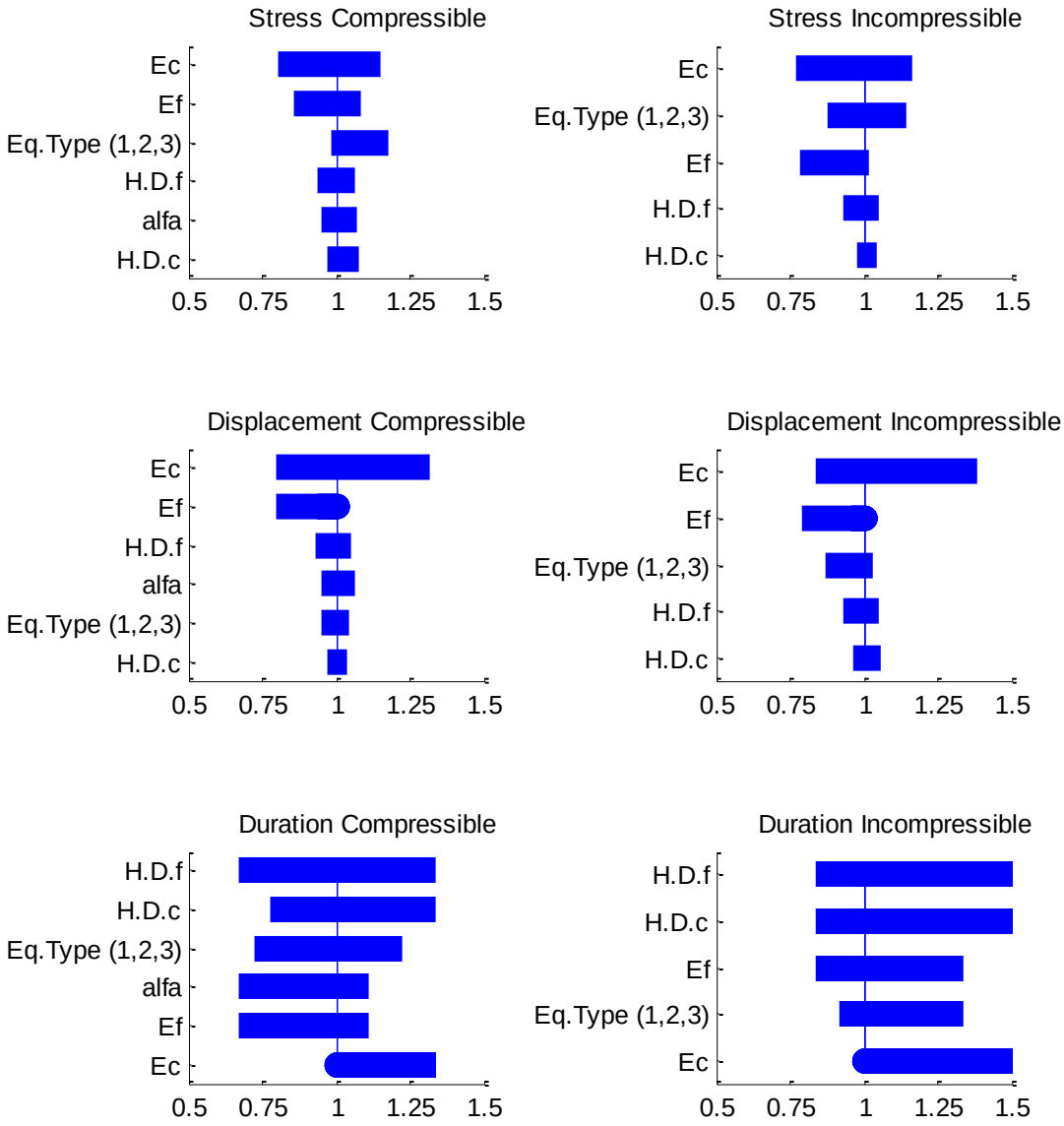

Figure 2.39 Tornado graphs of SEE1 analyses results

The most important parameters were the modulus of elasticity of concrete, foundation rock and earthquake type influencing the maximum stress. Moduli of elasticity of concrete and foundation rock were separately investigated. However, the ratio of modulus of elasticity of concrete to foundation rock was also crucial. Modulus of elasticity of concrete was in the first rank, then modulus of elasticity of foundation rock and ground motion type were the important variables affecting the variability in the engineering demand parameters for compressible and incompressible water. The parameter located at the bottom of the tornado diagram was hysteretic damping of concrete again.

Cumulative inelastic duration was mostly influenced by the hysteretic damping values of both concrete and foundation rock. Modulus of elasticity of concrete was the least important parameter on the CID.

2.9.3 SEE2 Analyses

Tornado diagram study was lastly performed for the SEE2 hazard level. Again, Andıraz Dam properties were used for the calculations which are listed on Table 2.29 under "Median" column. Same properties with previous OBE and SEE1 analyses were used. SEE2-2 ground motion was used for the median case as it gave the median values for the engineering demand parameters.

Table 2.29 Input Parameters table for SEE2 analyses

Parameters	**Compressible**			**Incompressible**		
	MEDIAN	MIN	MAX	MEDIAN	MIN	MAX
Ec (MPa)	23750	13750	33750	23750	13750	33750
Ef (MPa)	10800	5800	14100	10800	5800	14100
Hysteretic Damping, c	0.10	0.04	0.14	0.10	0.04	0.14
Hysteretic Damping, f	0.10	0.04	0.20	0.10	0.04	0.20
Eq. Type (1,2,3)	2	1	3	2	1	3
α	0.9	0.8	1	-	-	-

The maximum principle stress values were 10.2 MPa and 9.77 MPa for compressible and incompressible water which were more than 3 MPa (Table 2.30). Therefore, it was possible to conduct the assessment by linear analysis. It was calculated that the cumulative inelastic durations were 0.5 sec for both compressible and incompressible water models. Moreover, maximum displacement on the crest of the dam of compressible analysis was greater than the incompressible analysis. As expected, when compared with OBE and SEE1 analyses, SEE2 analyses resulted in the greatest maximum stresses, maximum crest displacements and maximum cumulative inelastic durations for both compressible and incompressible water.

Table 2.30 Median model results for SEE2 analyses

Mean Model Results	**Compressible**	**Incompressible**
Maximum Principle Stress (MPa)	10.2	9.77
Maximum Deflection (m)* (x)	-0.07468	-0.06909
Maximum CID of assessment (s)	0.5	0.5

The results of the analyses were given below for the maximum stress, maximum top displacement and max duration of the nonlinear assessment respectively.

Table 2.31 Maximum Principle stress results for SEE2 analyses

Maximum Principle Stress (MPa)	**Compressible**		**Incompressible**	
Parameters	MIN	MAX	MIN	MAX
Ec	8.29	10.6	8.38	9.88
Ef	9.68	11	9.5	10.2
Hysteretic Damping, c	10.4	9.94	10.1	9.55
Hysteretic Damping, f	10.4	9.7	10.1	9.25
Eq. Type (1,2,3)	9.17	11.4	9.05	10.5
α	9.84	10.4	-	-

Table 2.31 shows the maximum principles stress results due to the variability of the parameters. The maximum stress result was as high as 11.4 MPa obtained from the analysis of SEE2-3 ground motion with compressible water, and the minimum stress was obtained from the consideration of minimum concrete elastic modulus resulted in a value of 8.29 MPa.

Maximum crest displacement results of SEE2 analyses are listed on Table 2.32. It was observed that maximum displacement occurred in the SEE2-3 analysis. Moreover, compressible water considerations caused higher crest displacements than the incompressible water. Wave reflection coefficient increased the amount of maximum crest displacement.

Table 2.32 Maximum top displacement results for SEE2 analyses

Maximum Displacement (m)	**Compressible**		**Incompressible**	
Parameters	MIN	MAX	MIN	MAX
Ec	-0.09715	-0.06156	-0.09216	0.05571
Ef	0.08909	0.07365	0.08775	0.06924
Hysteretic Damping, c	0.07704	-0.07331	0.07291	-0.06744
Hysteretic Damping, f	-0.07749	-0.07054	-0.07202	-0.06478
Eq. Type (1,2,3)	-0.07396	-0.09540	0.07205	-0.09672
α	-0.07176	-0.07743	-	-

SEE2 analyses resulted in stresses well above the tensile strength of concrete. Therefore, it was possible to investigate the cumulative inelastic durations. These results are shown in Table 2.33 and the duration values are above the assessment limitations. The maximum duration was obtained from the SEE2-3 analyses was 1.16 sec.

Table 2.33 Maximum duration of assessment results for SEE2 analyses

Maximum Duration of Assesment (s)	**Compressible**		**Incompressible**	
Parameters	MIN	MAX	MIN	MAX
Ec	0.55	0.675	0.475	0.75
Ef	0.8	0.725	0.75	0.6
Hysteretic Damping, c	0.5	0.15	0.575	0.475
Hysteretic Damping, f	0.5	0.5	0.55	0.475
Eq. Type (1,2,3)	0.55	1.16	0.85	0.98
α	0.5	0.55	-	-

Then, tornado diagrams were prepared for SEE2 analyses results as shown in Figure 2.40.

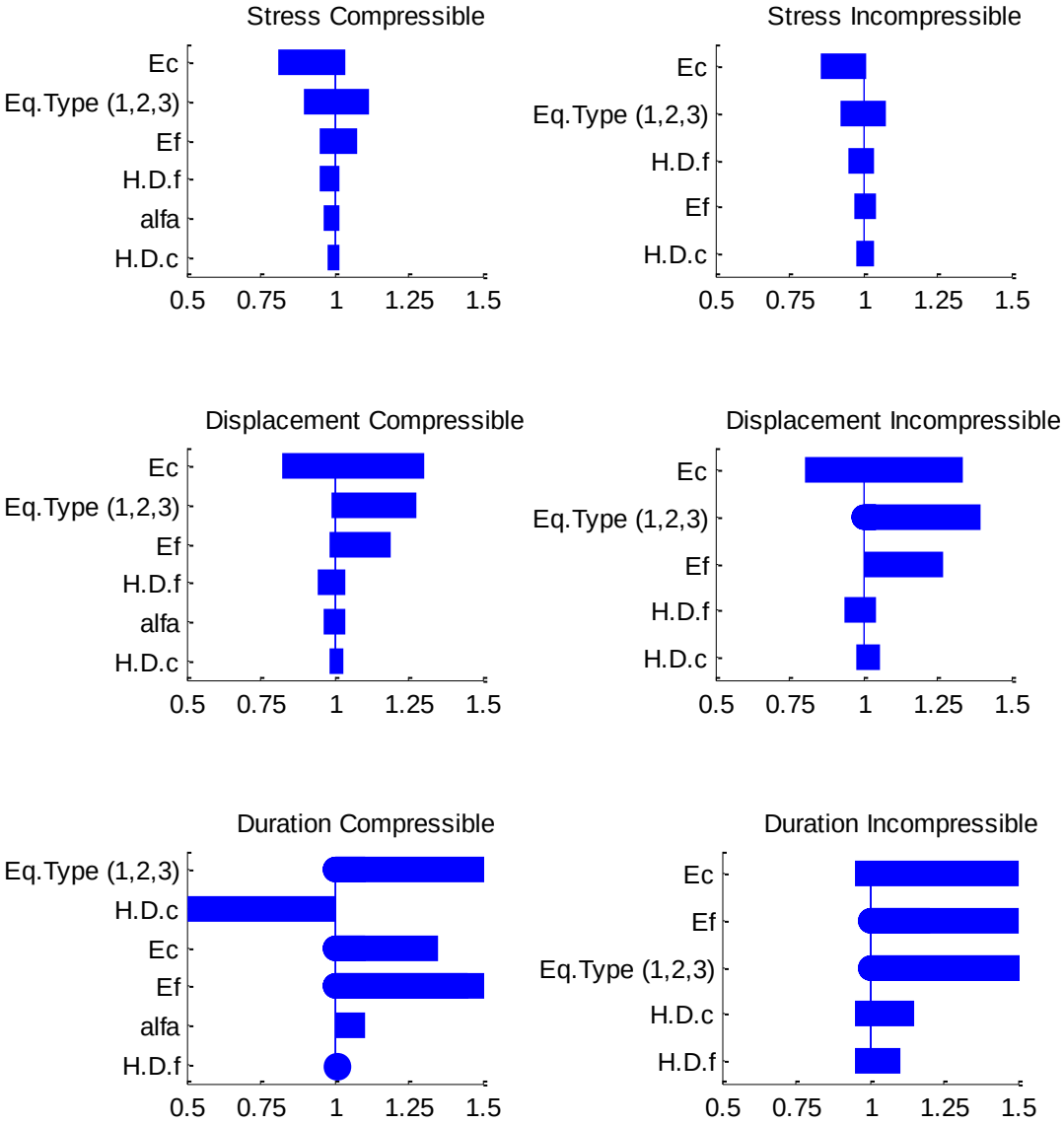

Figure 2.40 Tornado graphs of SEE2 analyses results

It was found that modulus of elasticity of concrete was the most important parameter affecting the SEE2 analyses except the maximum cumulative inelastic duration with compressible water. Then, ground motion type was the secondary parameter influencing the maximum stress and maximum crest displacement. Hysteretic damping of concrete was the least important variable creating the least swing for maximum stress and maximum displacement considerations. However, in terms of cumulative inelastic duration, the least important parameter was the hysteretic damping of foundation.

Following important conclusions can be drawn from the tornado analysis:

- Maximum principal stresses and maximum crest displacements are primarily sensitive to the moduli of elasticity of foundation rock and concrete and ground motion type for both the incompressible and compressible water cases and for all earthquake hazard levels. Damping ratios and wave reflection coefficient seem to be of secondary importance for the sensitivity of maximum principal stresses and maximum crest displacements. This result is a natural outcome of the importance of the dam-foundation rock interaction and radiation damping that can significantly influence the values of these two engineering demand parameters.

- The results indicate no clear vision of parameters that influences the maximum cumulative inelastic duration engineering demand parameter. However, damping ratios and ground motion types seem to be more important for cumulative inelastic duration compared to the maximum principal stress and maximum crest displacement engineering demand parameters.

2.10 Comparison of 3D Analysis Results with 2D Analysis Results

In order to demonstrate the importance of 3D modeling, results are compared herein with those obtained from rigorous 2D analyses.

Two dimensional analyses were conducted for concrete dam supported on the flexible foundation and impounded water in reservoir. Finite elements were used to model the dam in 2D. EAGD-84 program was used in order to model the dam as a two dimensional system (Fenves and Chopra, 1984, 1985). The limitation of EAGD-84 is that the upstream face of the dam should be vertical. It includes dam-foundation-water interaction, compressibility of reservoir bottom due to the sediment effects. Two dimensional analyses can be conducted alternatively with plane stress or plane strain assumptions. Generally, plane stress assumption is preferred for the case of independent vibration of monoliths due to the slips occurred in the joints when exposed to large-amplitude ground motions. However, for small amplitudes of earthquakes the dam system acts as a solid structure with limited slip of the joints between the monoliths. Plane strain assumption is more appropriate for dams with keyed contraction joints. For the static analyses, EAGD-84 program includes the dam weight and hydrostatic pressure due to reservoir in two dimensions, whereas the dynamic analyses involve the response due to earthquake ground motion.

Idealization of the foundation rock is homogeneous, isotropic and viscoelastic half-plane in EAGD-84. Two dimensional wave equations are solved to consider the hydrodynamic effects of impounded water. Fluid domain is assumed with a constant depth and upstream length extends infinitely with a horizontal reservoir bottom. Compressibility of reservoir was also included by wave reflection coefficient α, which was explained in Section 2.8.2. Four node linear finite elements were used for the dam monolith idealization. The modified version of EAGD-84 prepared by Yücel (2013) (in progress) was used in the analyses which provides an easy and user friendly interface simplifying the analyses procedure.

Andıraz Dam was modeled using the modified version of EAGD-84 and the mesh of the dam is shown in Figure 2.41 for two different cross sections of the dam with heights of 138 m (sections B, C, D and E) and 69 m (sections A and F) respectively. The dam was divided into 25 sections both in vertical and horizontal directions, totally 625 elements exist (Figure 2.42).

The necessary properties of the Andıraz Dam required for the two dimensional earthquake analyses are as follows: The modulus of elasticity and poisson's ratio of concrete was 23750 MPa, and 0.2 respectively. The tensile strength of concrete is selected as 3 MPa. Density of concrete is 2400 kg/m^3 and 0.10 hysteretic damping ratio is used. When considering the foundation, the modulus of elasticity of foundation was used as 10800 MPa with a 2500 kg/m^3 density. Hysteretic damping ratio of the foundation was similar to dam, as 0.10. Compressible impounded water was employed with the wave reflection coefficient of α=1. The ground motion was applied only on x, horizontal direction which was combination 1 given in Table 2.7. Three SEE1 records were studied which are shown in section 2.5 on the Figure 2.10. The results of the analysis were assessed according to USACE methodology of linear elastic analysis checks (2003). The performance criteria limitations of the assessment are 0.4 sec as the cumulative inelastic duration and a demand capacity ratio of 2. The two dimensional analyses were conducted for both plane stress and plane strain considerations.

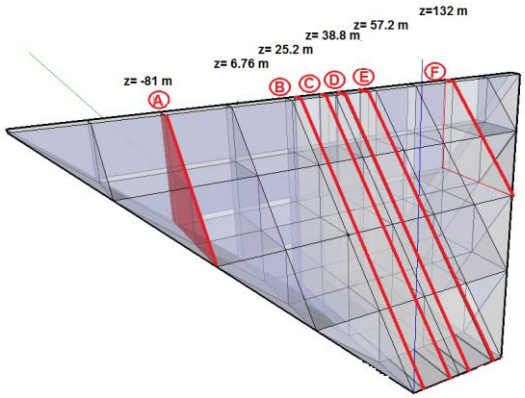

Figure 2.41 Different cross sections on the Andıraz Dam

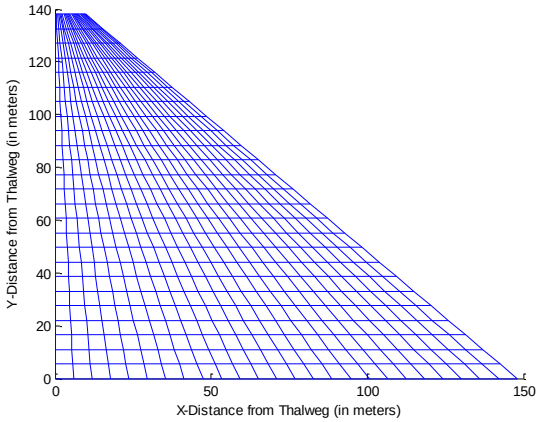

a) Cross section with h=138 m (sections B, C, D and E)

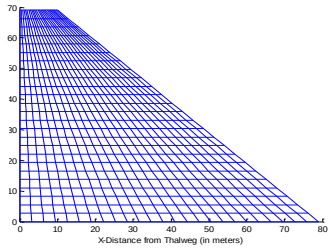

b) Cross section with h=69 m (sections A and F)

Figure 2.42 Dam element mesh on EAGD-84 (2D)

The response differences of 2D and 3D analyses were investigated by giving an impulse to both systems. Then, Fast Fourier Transformation (FFT) of results was prepared and these results were compared in Figure 2.43. It was observed that the first mode frequencies were slightly different which were 1.66 Hz, 2.29 Hz and 3.32 Hz for 2D (h=138 m), 3D and 2D (h=69 m) analyses respectively. Therefore, the periods were calculated as 0.602 sec, 0.436 sec and 0.301 sec for 2D (h=138 m), 3D and 2D (h=69 m) analyses respectively. Moreover, there was also significant difference in the amplitude of accelerations in Figure 2.43. The importance of 3D analyses can be examined from the response difference. 3D analyses behaved more rigid when compared to 2D analyses for the dam section with h=138 m. This difference in periods resulted in different spectral acceleration values. 3D analyses had greater spectral acceleration values as illustrated in Figure 2.44 when compared to 2D analysis (h=138m). Therefore, 3D analysis was exposed to greater earthquake accelerations which affect the behavior and results of the stresses. The spectral acceleration values for each ground motion for 2D and 3D analyses are listed on Table 2.34. The difference of spectral acceleration values was about 20-30%. As a result, stresses values obtained from 2D and 3D analyses may differ significantly. However, when 2D analysis with h=69 m was considered, it was observed that the acceleration values are greater than 3D analyses in the order of 20-30 %.

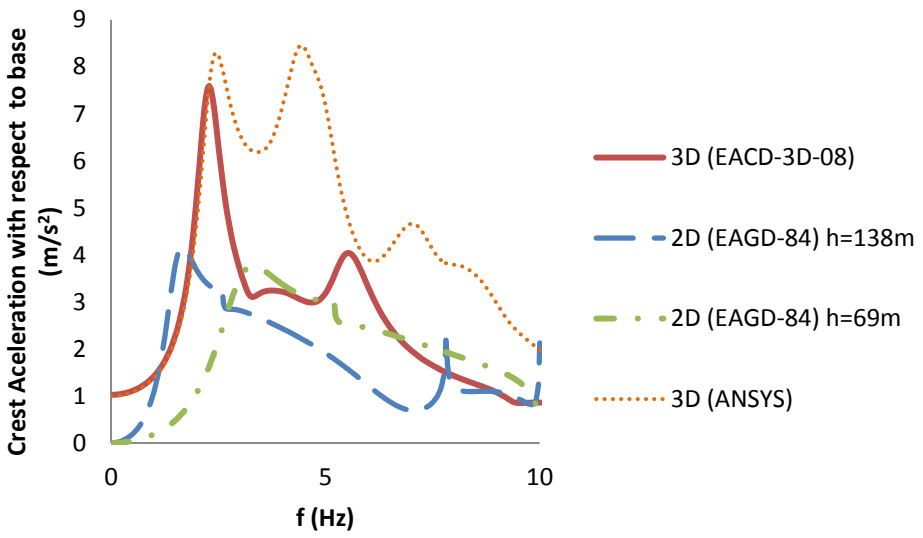

Figure 2.43 Comparisons of 2D (EAGD-84) and 3D (EACD-3D-08)

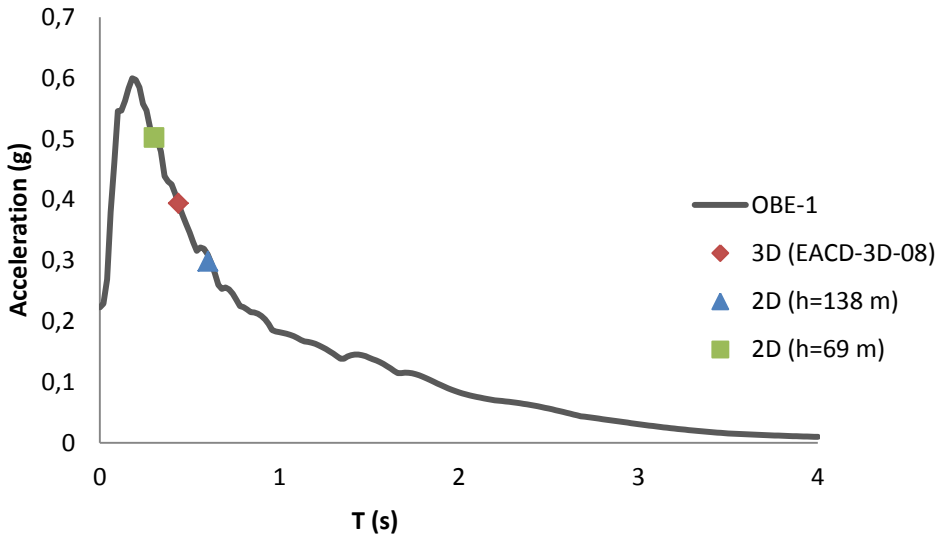

Figure 2.44 Spectral acceleration values for 2D and 3D analyses for OBE1 ground motion

Table 2.34 Spectral acceleration values obtained from the response spectra of ground motions

Spectral Acceleration (g)

	3D (EACD)	2D (h=138m)	2D (h=69m)	*Difference % (3D-2D h=138m)	*Difference % (3D-2D h=69m)
OBE1	0.394	0.298	0.499	24 %	-27%
OBE2	0.389	0.295	0.485	24%	-25%
OBE3	0.398	0.270	0.490	32%	-23%
SEE1-1	0.391	0.309	0.517	21%	-32%
SEE1-2	0.392	0.275	0.515	30%	-31%
SEE1-3	0.682	0.530	0.838	22%	-23%
SEE2-1	1.174	0.900	1.362	23%	-16%
SEE2-2	1.157	0.915	1.351	21%	-17%
SEE2-3	1.146	0.907	1.341	21%	-17%

*Differences are calculated according to 3D results.

The maximum principle stresses obtained from the two dimensional and three dimensional analyses at the highest dam section (h=138 m) for each ground motion type are plotted on Figures 2.45, 2.47 and 2.49. It is obvious from the plots that there is almost no difference in the stresses of plane stress and plane strain assumptions in two dimensional analyses. However, the two dimensional stresses are significantly different when compared with three dimensional stress results. Three dimensional analyses were conducted both by EACD-3D-08 including inertial effects of foundation and by ANSYS with incompressible impounded water massless foundation consideration. This model was called "Incompressible Fluid Massless Foundation" (IFMF) model. In order to approximately consider the radiation damping in the IFMF model, 15% Rayleigh damping matched for the first to tenth eigenfrequencies were employed in order to provide constant damping within the frequency range with minimum 90 % modal mass participation (Arıcı, Binici and Aldemir, 2011). 3D analyses results were available for z= 6.76 m, 25.2 m, 38.8 m and 57.2 m sections. The cross section at z=57.2 m away from the origin, which was almost at the center of the dam, was selected for comparison purposes. According to the plots, the distribution of stresses on the cross section of the dam is similar for 2D and 3D results. Critical points were on the upstream and downstream face of the dam body at similar locations for two cases. Some local stress concentrations were observed at the bottom of the dam near the foundation in 2D which was not observed in 3D results. SEE1-3 plots gave similar stress concentrations, where the critical stresses were observed on the toe and thalweg of the dam in addition to upstream and downstream regions.

Table 2.35 summarizes the maximum principle stresses for two dimensional plane stress and plane strain analyses and three dimensional cross sectional plot results for each section. The percentages differences between two and three dimensional analyses were calculated. The error was in the order of about 60% between 2D and 3D analyses (EACD-3D-08) when it was compared for the deepest cross section. Therefore, it may be concluded there is a significant underestimation of stresses in 2D analyses when compared to 3D analysis for the maximum principal stress. However, the error reduces to approximately to 35% for the consideration of stress comparison at the valley sides with h=69 m. The difference in stress results of three dimensional massless foundation incompressible fluid of ANSYS and EACD analyses is approximately 20 to 35% on average, ANSYS results being larger. This shows that massless foundation incompressible fluid modeling approach is conservative in estimating overstressed regions as apparent from the pulse response shown in Figure 2.43.

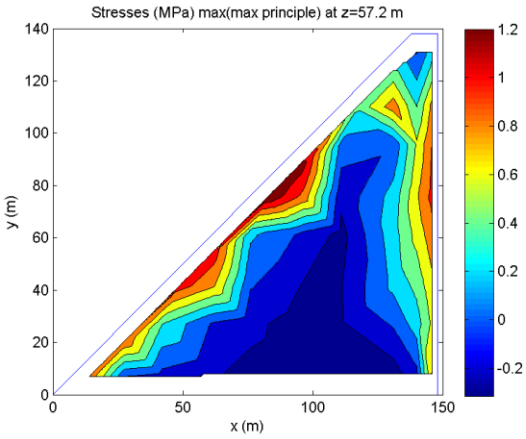

a) 3D (EACD-3D-08)

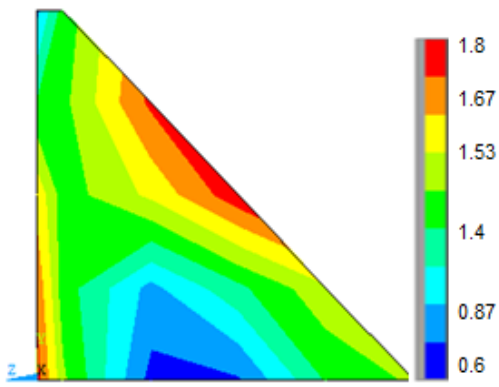

b) 3D (ANSYS)

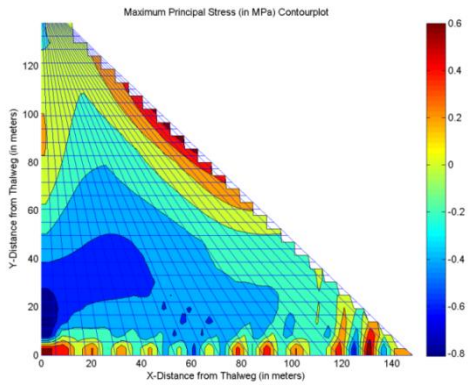

c) 2D (EAGD-84) Plane stress

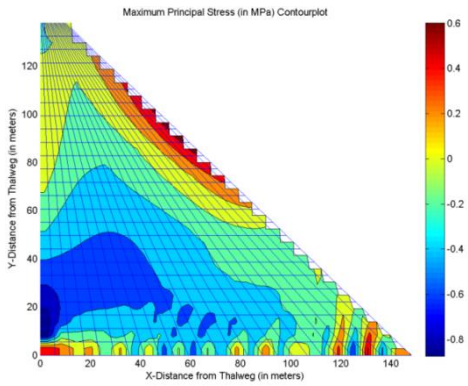

d) 2D (EAGD-84) Plane strain

Figure 2.45 Maximum principle stress plots of SEE1-1 ground motion for deepest cross section (h=138m) a) 3D EACD-3D-08 b) 3D ANSYS c) 2D plane stress d) 2D plane strain respectively

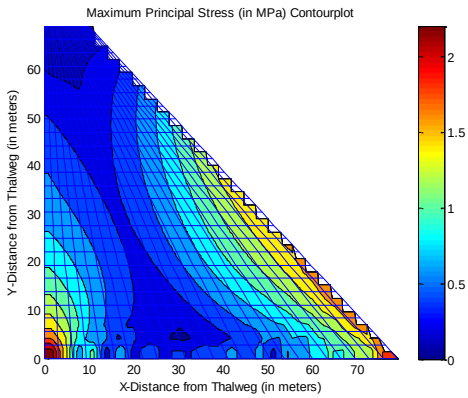

Figure 2.46 Maximum principle stress plot of SEE1-1 ground motion for y=69 m 2D plane stress for sections A and F

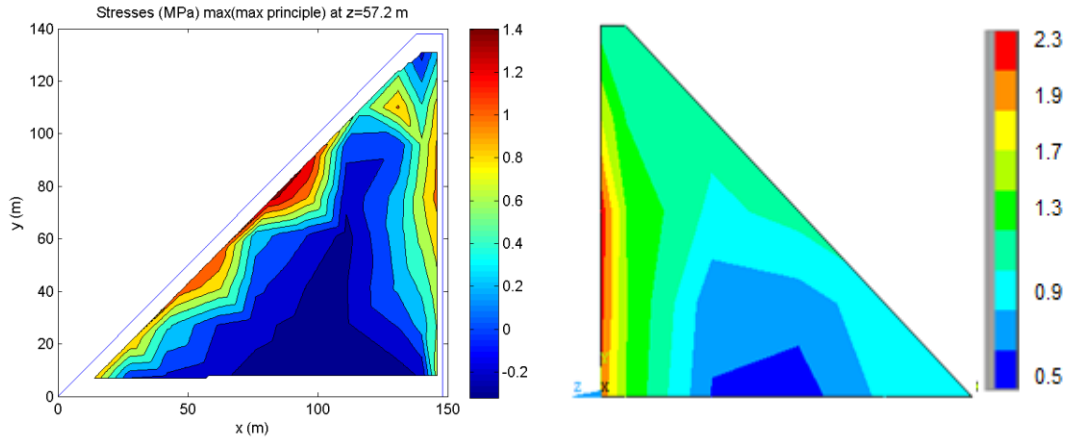

a) 3D (EACD-3D-08) b) 3D (ANSYS)

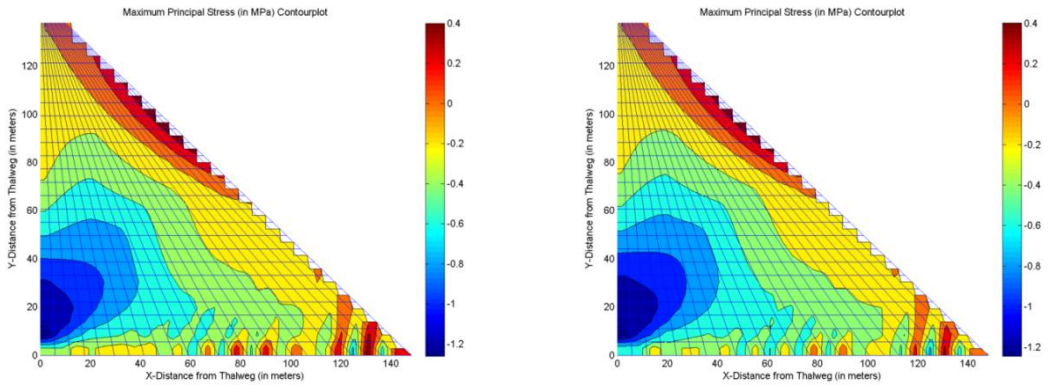

c) 2D (EAGD-84) Plane stress d) 2D (EAGD-84) Plane strain

Figure 2.47 Maximum principle stress plots of SEE1-2 ground motion for deepest cross section (h=138m) a) 3D EACD-3D-08 b) 3D ANSYS c) 2D plane stress d) 2D plane strain respectively

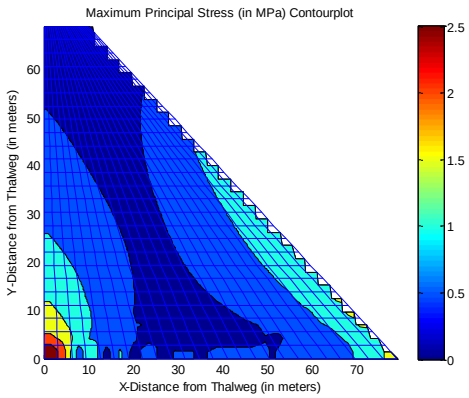

Figure 2.48 Maximum principle stress plot of SEE1-2 ground motion for y=69 m 2D plane stress for sections A and F

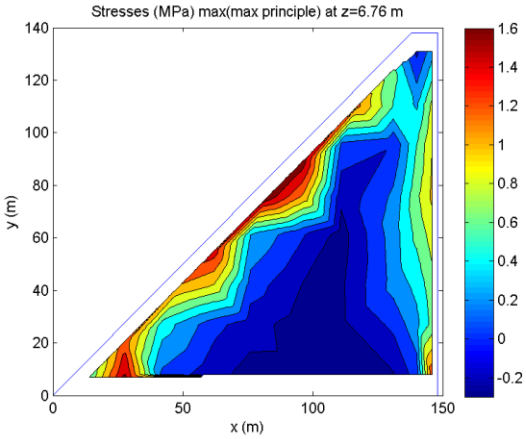

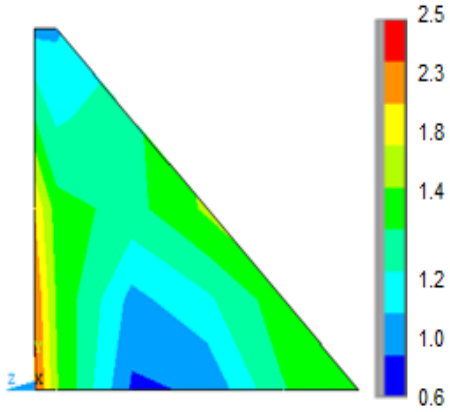

a) 3D (EACD-3D-08)

b) 3D (ANSYS)

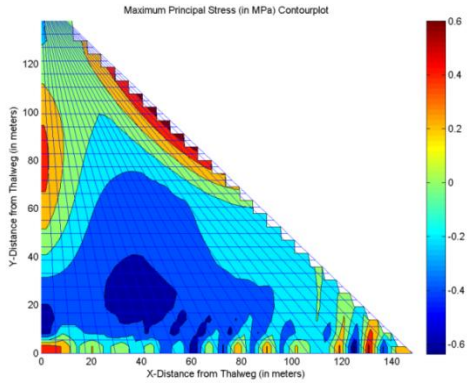

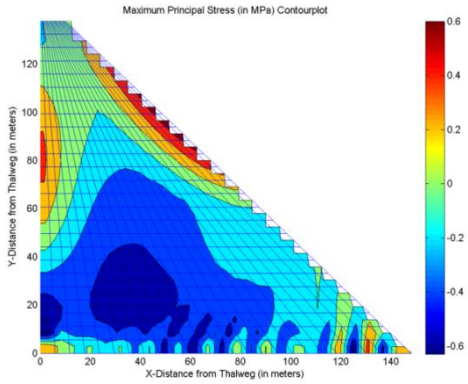

c) 2D (EAGD-84) Plane stress

d) 2D (EAGD-84) Plane strain

Figure 2.49 Maximum principle stress plots of SEE1-3 ground motion for deepest cross section (h=138m) a) 3D EACD-3D-08 b) 3D ANSYS c) 2D plane stress d) 2D plane strain respectively

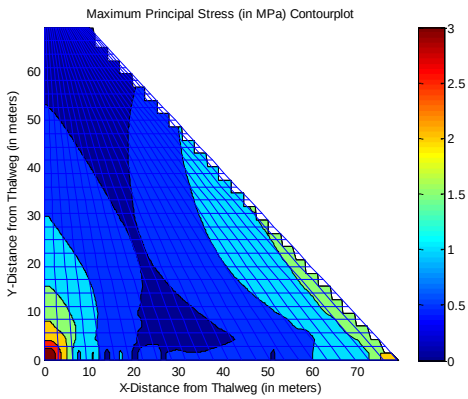

Figure 2.50 Maximum principle stress plot of SEE1-3 ground motion for y=69 m 2D plane stress for sections A and F

Table 2.35 Maximum principle stress results for 2D and 3D analyses

MAXIMUM PRINCIPLE STRESS (MPa)

	Sections*	SEE1-1	SEE1-2	SEE1-3
2D PLANE STRESS	A, F	2.1	2.5	3
	B, C, D, E	0.6	0.4	0.6
2D PLANE STRAIN	B, C, D, E	0.6	0.4	0.6
3D EACD	A	3.4	3.4	3.6
	B	1.7	1.7	1.8
	C	1.7	1.6	1.8
	D	2.2	2.2	2.2
	E	1.4	1.5	1.6
	F	4.4	4.4	4.5
3D ANSYS	B	1.9	2.3	2.5
	C	1.9	2.3	2.5
	D	1.8	2.3	2.3
	E	1.8	2.3	2.5
Difference 2D (h=138 m)-EACD**	B	64%	76%	66%
	C	64%	75%	66%
	D	73%	82%	73%
	E	57%	73%	63%
Difference 2D (h=69 m)-EACD**	A	38%	26%	17%
	F	52%	43%	33%
Difference EACD-ANSYS**	B	-13%	-38%	-43%
	C	-15%	-42%	-43%
	D	19%	-6%	-3%
	E	-29%	-55%	-52%

*: Section A, B,C, D, E and F refer to sections with z= -81 m, 6.76 m, 25.2 m, 38.8 m, 57.2 m and 132 m respectively as shown in Figures 2.41

**: Differences are calculated with respect to EACD results.

Maximum crest displacement is another important point that should be included in the comparison of two and three dimensional analyses. Displacement time histories of the crest node on the upstream face of the dam were prepared for each earthquake ground motion. Figure 2.51 presents the crest displacements of 2D and 3D analyses. The graphs of displacement time histories show similar trends for 2D and 3D cases, but two dimensional displacements were slightly greater than the 3D results. The maximum displacement values are listed on Table 2.36, where the differences between the analyses can be deemed acceptable.

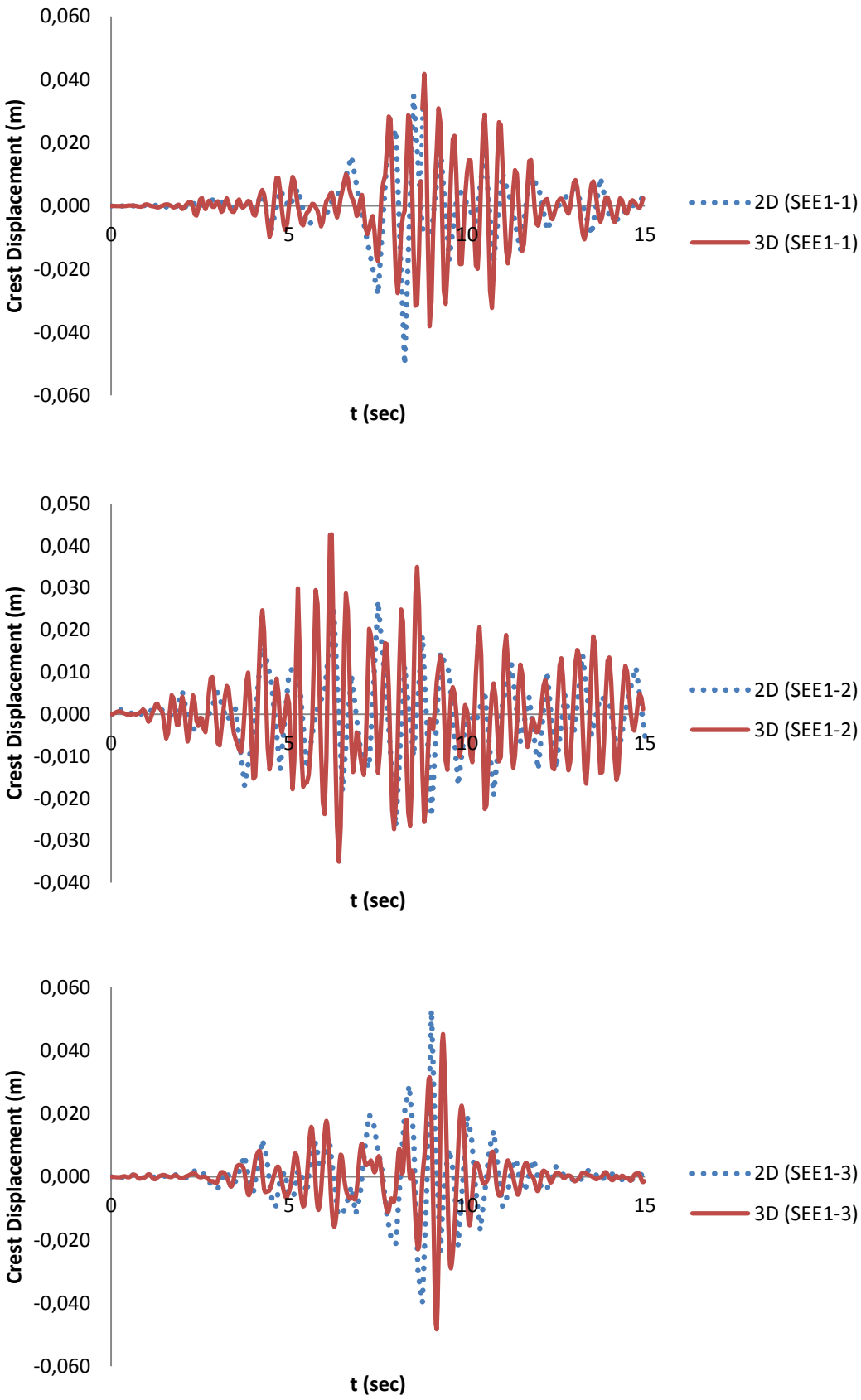

Figure 2.51 Crest displacement time histories for SEE1-1, SEE1-2 and SEE1-3 ground motions respectively

Table 2.36 Crest displacement time histories of 3D and 2D analyses

MAXIMUM CREST DISPLACEMENT (m)

Ground Motion	2D PLANE STRESS	2D PLANE STRAIN	3D* (EACD)	Error 1 with 3D	Error 2 with 3D
SEE1-1	0.045	0.042	0.04	-13%	-5%
SEE1-2	0.035	0.035	0.041	15%	15%
SEE1-3	0.061	0.06	0.048	-27%	-25%

According to analyses in two dimensions, linear analysis was sufficient and there was no point exceeding the tensile strength of concrete. This situation was also valid for the highest cross section of the dam in three dimensional analyses of EACD (Figures 2.45, 2.47 and 2.49 a). However, in three dimensional analyses, it was observed that some locations on the dam other than the deepest cross section had stress values greater than the tensile strength of concrete. These critical points exceeding the tensile capacity were located on the edges of valley sides on the corners. As a result, seismic safety assessment was studied for three dimensional analyses results (EACD-3D-08). The results of assessment plots are shown in Figure 2.52. Cumulative inelastic duration was 0.45 sec for SEE1-1 ground motion which exceeds the limitations. Therefore, it may be considered as critical and nonlinear analysis may be taken into consideration. However, this duration value can be healed easily by increasing the capacity slightly. Linear analyses can be used smoothly due to the results of SEE1-2 and SEE1-3 ground motions considering combination 1, since performance criterion graphs were convenience to the limitations.

These results highlight the importance of using three dimensional analyses for seismic response of dams. Stresses may be underestimated by using two dimensional analysis methods. Moreover, in two dimensional analyses only the cross section of the dam can be considered. The valley properties are disregarded.

The results indicate that 3D analysis results are significantly different from the results of 2D analyses results. This fact can be attributed to the following sources:

- When the dam is located in a narrow valley, interaction with the valley sides plays an important role.
- Foundation impedance calculations based on plane strain half space may not be realistic for the actual 3D geometry.
- Dam-water interaction in the presence of narrow valley sides may be different than a strain type assumption.

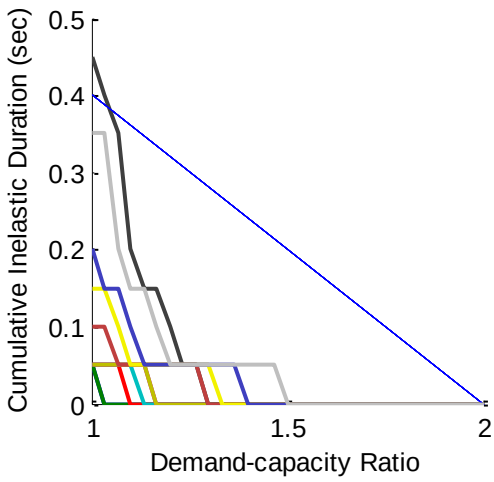

a) SEE1-1 combination 1

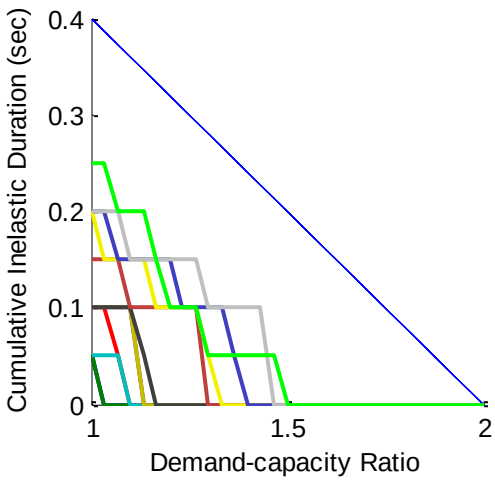

b) SEE1-2 combination 1

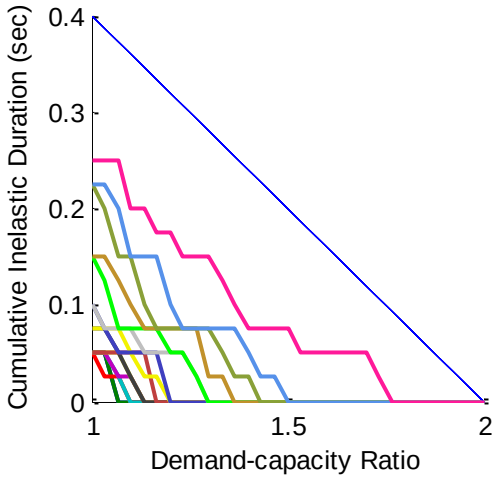

c) SEE1-3 combination 1

Figure 2.52 Performance criterion graph of SEE1 in combination 1 (3D)

2.11 Comparison of Nonlinear Results with Linear Analyses

Up to now, linear elastic response of Andıraz Dam was considered. Assessments of Andıraz Dam presented in Section 2.7.3 indicate that nonlinear analysis is necessary for SEE2 hazard level. Nonlinear dynamic analyses of Andıraz Dam were conducted by Arıcı et. al. (2013) in order to investigate the dam stability. Three dimensional analyses were conducted using DIANA for estimating the cracking (Arıcı, Binici and Aldemir, 2011). Dam behavior was studied both for the monolith (without transverse joints) and separated monolith (multi monolith) behavior with transverse joints and these results were compared with the two dimensional analyses. While modeling the dam foundation was taken massless and water was assumed incompressible (IFMF). In order to decide on the damping value, analysis results were compared with EACD-3D-08 results and a 15 % Rayleigh damping ratio was assigned. Figure 2.43 presents the comparison of IFMF and EACD-3D-08 results. Afterwards, nonlinear analysis was conducted incorporating concrete cracking through a rotating crack approach (Selby Vecchio). Arıcı et. al. (2012) compared the final cracking patterns of the two designs (Figure 2.53 and 2.54) in their study. The sandwich model as shown in Figure 2.53 had 3 MPa static tensile strength in the exterior RCC high grade whereas 2 MPa static tensile strength was employed for the core RCC low grade. The

uniform concrete grade on the other hand RCC with a tensile strength of 2 MPa. Analysis results showed that the sandwich dam could experience limited cracking as opposed to the extensive cracking in the uniform grade case. Hence, such a solution was offered as a viable design alternative.

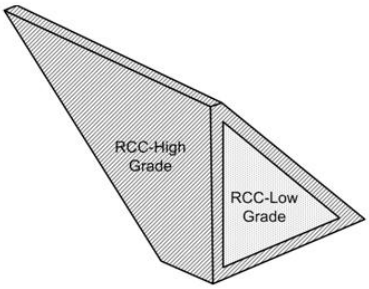

Figure 2.53 Sandwich model sketch

The success of the sandwich model can be observed from the crack patterns on the cross section and bottom view of the dam. Details of this study can be investigated from the Arıcı et. al. study (2011).

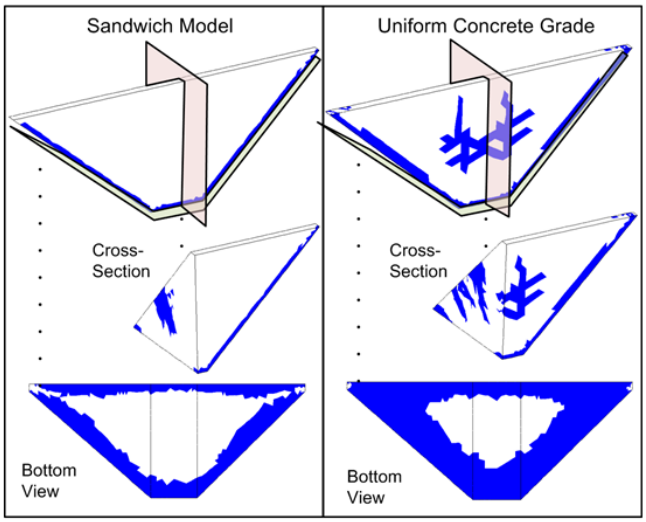

Figure 2.54 Differences of sandwich and classical model on crack pattern

CHAPTER 3

CONCLUSION

3.1 General

In this study, three dimensional earthquake response of concrete gravity dam was investigated by using EACD-3D-08 program. EACD-3D-08 program provides a realistic approach by including the hydrodynamic effects with compressibility of impounded water; moreover the absorptiveness character of the reservoir boundary which results in successful representation of water-dam interaction. In addition, EACD-3D-08 involves flexibility of foundation rock with inertial and damping effects in terms of foundation-dam interaction.

Andıraz Dam, the tallest roller compacted concrete gravity dam designed in Turkey, was analyzed using EACD-3D-08 as a case study. Full dam-water-foundation interaction was considered for the three dimensional dynamic analysis of the dam. Stresses and displacements occurring on the dam body due to ground motion were investigated. A variety of analytical tools were utilized in performing parametric studies to better demonstrate the seismic behavior of the dam. Moreover, in the light of BK Guidelines (2012) the seismic performance criteria using linear analyses were assessed. The conclusion of all the different analyses can be summarized as follows:

- Use of three dimensional solid elements with high order quadratic shape functions is successful in the analyses with optimum number of elements and amount of time for the analyses.

- Three different earthquake scenarios, Operating Basis Earthquake (OBE), Safety Evaluation Earthquake Level 1 and 2 (SEE1, SEE2) were considered in the analyses. It was found that the most critical combinations are x+0.3y+0.3z, x+0.3y-0.3z and x+0.3y for the earthquake load combinations. Results show that upstream direction and vertical direction of ground motion are more important than the cross-stream direction.

- Tensile stress concentration regions are found to be more critical when stress plots were investigated. On the deepest cross-section stress plots, the maximum tensile stresses were observed on the dam body at the downstream side and at the toe of the dam at the upstream side. However, it is observed that maximum tensile stresses occurred in the valley sides. This shows that two dimensional analyses may be insufficient to detect such high stress concentrations.

- According to results of the assessment of seismic performance of linear analyses, Andıraz dam is satisfied with OBE (without any problem) and to a limit extend for SEE1 (almost no problem) ground motions. However, under SEE2 ground motion the results are excessively unsafe, requiring the use of nonlinear analyses.

- Foundation rock and concrete elasticity moduli had a direct effect on maximum tensile stress and maximum displacement of the dam due to the positive effect of foundation-dam interaction as the added radiation damping.

- Compressible impounded water consideration results in slightly higher maximum stress and maximum displacement than the incompressible impounded water. In addition, absorptiveness of reservoir is directly proportional to response of the dam. It was found that, maximum tensile stresses and maximum displacements were decreased with low wave reflection coefficient. However, it was observed that consideration of water compressibility and wave reflection coefficient did not affect the results significantly for the concrete gravity dam.

- Performance criterion of linear analyses provided the assessment of dam behavior by considering the cumulative inelastic durations with the ratio of demand to capacity.

- It can be stated that two dimensional analyses rely on many determination of fundamental resonance of the system only; whereas, three dimensional analyses including the compressibility of the water and also interactions of dam, foundation and reservoir are consistent with the observed real behavior in experiments with accuracy.

- Three dimensional analyses behaved more rigid when compared to two dimensional analyses which resulted in greater frequency values for the first mode. Therefore, three dimensional analyses were exposed to greater spectral acceleration values than the two dimensional analyses.

- Two dimensional analyses underestimate the maximum stresses drastically which highlights the importance of three dimensional analyses. However, in terms of displacement time histories there is not great distinction for two and three dimensional analyses.

- Rigorous treatment of dam-water-foundation model as in EACD-3D-08 program can also be used to estimate the effective damping of the system to further conduct nonlinear analysis. One such example was conducted by Arıcı et. al. (2012) indicating the importance of modeling for proper damping selection.

REFERENCES

Arıcı, Y., Binici, B., & Aldemir, A. (2012, 7 9). Comparison of the expected damage patterns from two and three dimensional nonlinear dynamic analyses of a roller compacted concrete dam. *Structure and Infrasturcture Engineering* , s. 1-11.

Binici, B., & Mosalam, K. M. (2006). Analysis of reinforced concrete columns retrofitted with fiber reinforced polymer lamina. *science direct* , 265-276.

Binici, B., Arıcı, Y., Akman, S. B., & Akman, A. (2012). *Beton barajların deprem analizleri.* Ankara: Beton Barajlar Komitesi.

BK. Baraj tasarımında sismik parametre seçimi rehberi. (2012a). *1. Barajlar Kongresi* (s. No.001). Ankara: DSİ.

BK. Beton barajlar tasarım ilkeleri rehberi. (2012b). *1. Barajlar Kongresi.* Ankara: DSİ.

Chakrabarti, P., & Chopra, A. K. (1972). *Earthquake response of gravity dams including reservoir interaction effects.* California, Berkeley: Earthquake Engineering Research Center.

Chopra, A. K. (2008). Earthquake analysis of arch dams: factors to be considered. *The 14th World Conference on Earthquake Engineering.* Beijing.

Chopra, A. K., & Nuss, L. K. (2009). Seismic safety evaluation and upgrading of arch dams. *23rd Congress on Large Dams.* Brasilia, Brazil.

Clough, R. W., Raphael, J. M., & Mojtahedi, S. (1973). *ADAP-A computer program for static and dynamic analysis of arch dams.* Berkeley, California: EERC 73-14.

Dasgupta, G., & Chopra, A. K. (1977). *Dynamic stiffness matrices for homogeneous viscoelastic halfplanes.* Berkeley, California: Earthquake Engineering Research Center, UCB/EERC-77/26.

Duron, Z. H., & Hall, J. F. (1988). Experimental and finite element studies of the forced vibration response of morrow point dam. *Earthquake Engineering Structural Dynamics* , 1021-1039.

Engineers, U. A. (2003). *Time-history dynamic analysis of concrete hydraulic structures.* Engineering and Design, EM 110-2-6051.

Fenves, G. L., Mojtahedi, S., & Reimer, R. B. (1989). *ADAP-88 A computer program for nonlinear earthquake analysis of concrete arch dams.* Berkeley, California: Earthquake Engineering Research Center, UCB/EERC-89-12.

Fenves, G., & Chopra, A. K. (1984). *EAGD-84 A computer program for earthquake analysis of concrete gravity dams.* Berkeley, California: Earthquake Engineering Research Center.

Fok, K.-L., & Chopra, A. K. (1985). *Earthquake analysis and response of concrete arch dams.* Berkeley, California: Earthquake Engineering Research Center, UCB/EERC-85/07.

Fok, K.-L., Hall, J. F., & Chopra, A. K. (1986). *EACD-3D A computer program for three-dimensional earthquake analysis of concrete dams.* Berkeley, California: Earthquake Engineering Research Center, UCB/EERC-86/09.

Ghanaat, Y., & Clough, R. W. (1989). *EADAP Enhanced arch dam analysis program user's manual.* Berkeley, California: Earthquake Engineering Research Center, UCB/EERC-89/07.

Graves, R., & Derucher, K. (1987). Interface smeared crack model analysis of concrete dams in earthquakes. *Journal of Engineering Mechanics* .

Hall, J. F. (1997). *Efficient nonlinear seismic analysis of arch dams-user's manual of SCADA.* Pasadena, California: California Institute of Technology-Earthquake Engineering Research Laboratory.

Hall, J. F., & Chopra, A. K. (1983, February Vol 109). Dynamic analysis of arch dams including hydrodynamic effects. *Journal of Engineering Mechanics* , s. 149-167.

Hall, J. F., & Chopra, A. K. (1980). *Dynamic response of embankment concrete-gravity and arch dams including hydrodynamic interaction.* Berkeley, California: Earthquake Engineering Research Center, UCB/EERC-80/39.

Holand, I., & Alstedt, E. (1968). *Arch dam analysis by the finite element method.* Trondheim: Technical University of Norway.

ICOLD. (1989). *Selecting seismic parameters for large dams guidelines.* Paris: Committee on Seismic Aspects of Dam Design, Bulletin 72.

Kuo, J. S.-H. (1982). *Fluid-sucture interactions: added mass computations for incompressible fluid.* Berkeley California: Earthquake Engineering Research Center.

McGuire, R. (2001). Deterministic vs probabilistic earthquake hazards and risks. *Soil Dynamics and Earthquake Engineering, 21* , 377-384.

Öziş, Ü., & Alsan, M. (1990, July). Beton baraj inşaatının Türkiye'de gelişmesi. *İMO Teknik Dergi* , s. 147-158.

Öztürk, A., & Yıldız, D. (1998). Silindirle sıkıştırılmış beton baraj (RCC) teknolojisi ve Türkiye'deki uygulamaları. *Türkiye Mühendislik Haberleri* , 39-46.

Proulx, J., & Paultre, P. (1997). Experimental and numerical investigation of dam-reservoir-foundation interaction for a large gravity dam. *Can. J. Civ. Eng.* , 90-105.

Tan, H., & Chopra, A. K. (1997). *EACD-3D-96: A Computer Program for Three-Dimensional Earthquake Analysis of Concrete Dams.* Berkeley, California: Structural Engineering Mechanics and Materials, UCB/SEMM-96/06.

Tan, H., & Chopra, A. K. (1995). *Earthquake Analysis and Response of Concrete Arch Dams.* Berkeley, California: Earthquake Engineering Research Center, UCB/EERC-95/07.

US Army Corps of Engineers. (1995). *Seismic Design Provisions for Roller Compacted Concrete Dams.* Washington, DC: Engineering and Design, EP 110-2-12.

Wang, J. , & Chopra, A. K. (2008). *Analysis and response of concrete arch dams including dam-water-foundation rock interaction to Spatially-Varying Ground Motion.* Berkeley, California: Earthquake Engineering Research Center, EERC 2008-03.

Westergaard, H. M. (1933). Water pressures on dams during earthquakes. *American Society of Civil Engineers* , 419-472.

Wieland, M. (2004). Earthquake Safety of Concrete Dams and Seismic Design Criteria for Major Dam Projects. *ICOLD Committee on Seismic Aspects of Dam Design* .

Yanmaz, P. D. (2010). *Su Enerjisi Araştırmaları Merkezi (SENAM).* Ankara: METU.

Zhang, L., & Chopra, A. K. (1991). *Computation of Spatially Varying Ground Motion and Foundation-Rock Impedance Matrices for Seismic Analysis of Arch Dams.* Berkeley, California: Earthquake Engineering Research Center, UCB/EERC-91/06.

Zienkiewicz, O. C., & Cheung, Y. K. (1967). *The Finite Element in Structural and Continuum Mechanics.* McGraw-Hill.

APPENDIX A

The performance criterion graphs of analyses explained in Section 2.7.3 with combination 9, 11 and 13 for each ground motion type are provided.

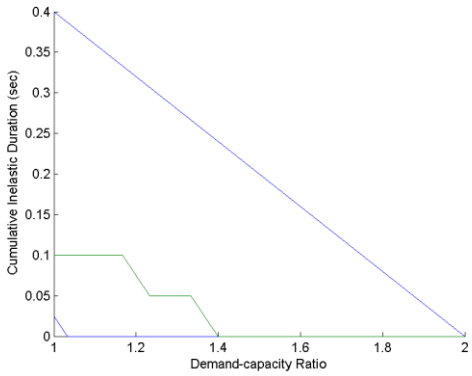

A.1 OBE1 Combination 9

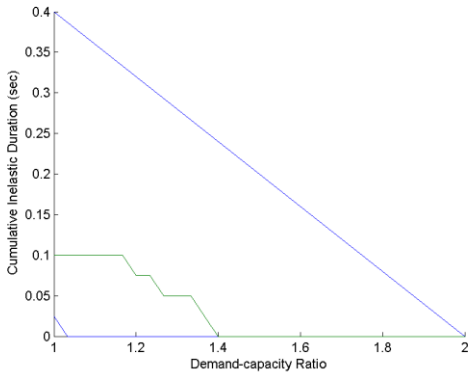

A.2 OBE1 Combination 11

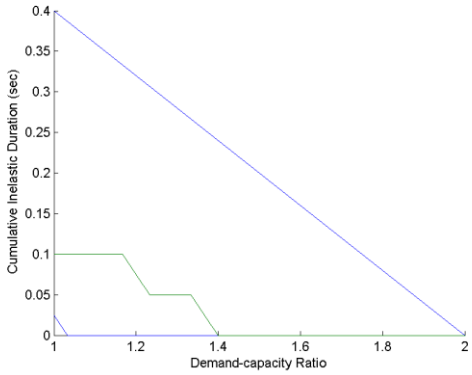

A.3 OBE1 Combination 13

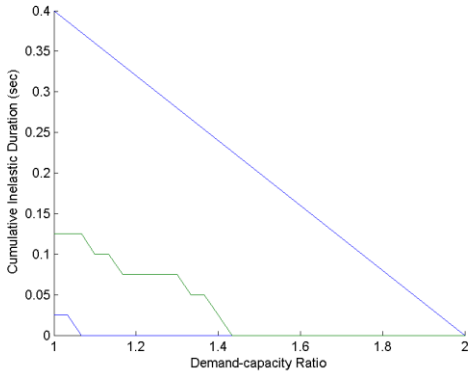

A.4 OBE2 Combination 9

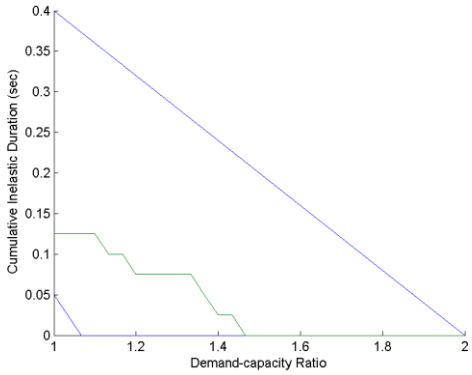

A.5 OBE2 Combination 11

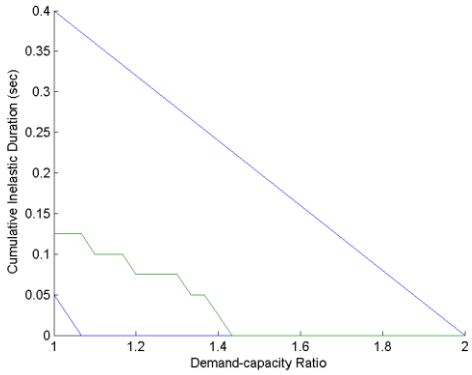

A.6 OBE2 Combination 13

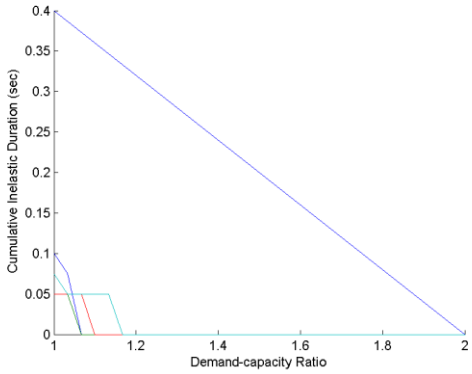

A.7 OBE3 Combination 9

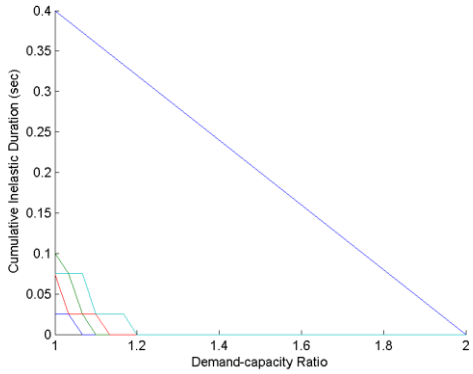

A.8 OBE3 Combination 11

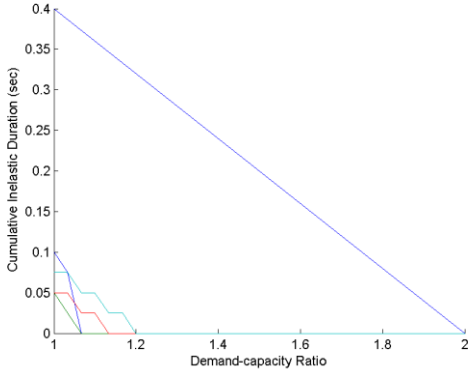

A.9 OBE3 Combination 13

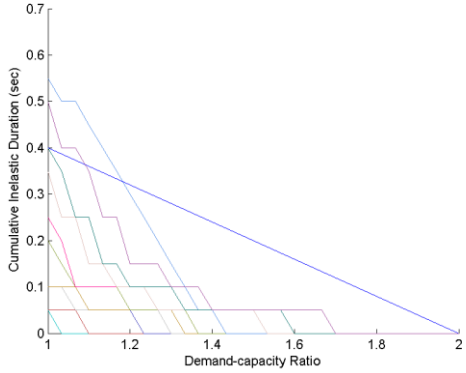

A.10 SEE1-1 Combination 9

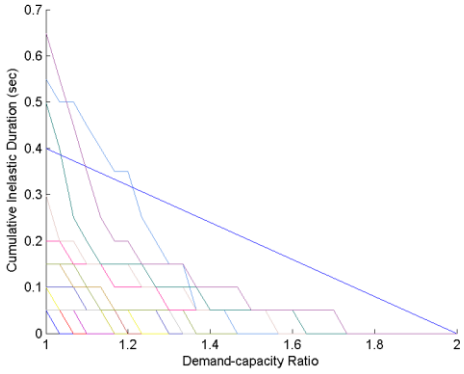

A.11 SEE1-1 Combination 11

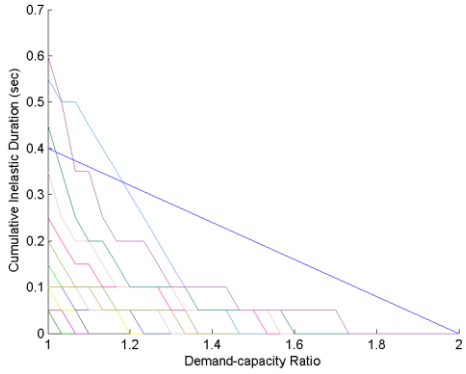

A.12 SEE1-1 Combination 13

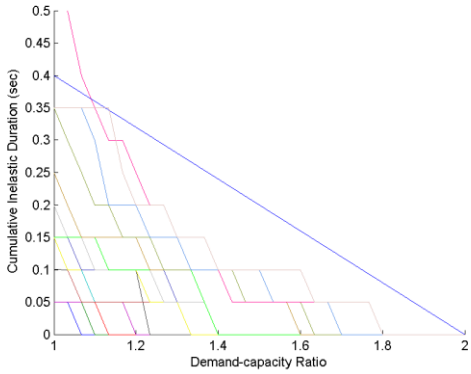

A.13 SEE1-2 Combination 9

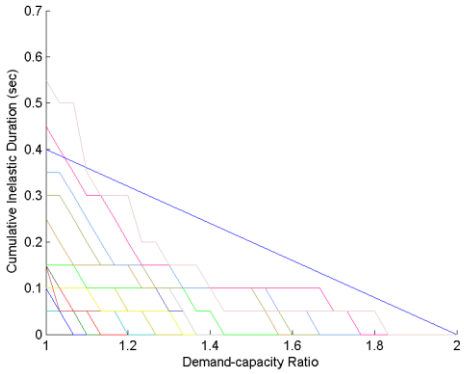

A.14 SEE1-2 Combination 11

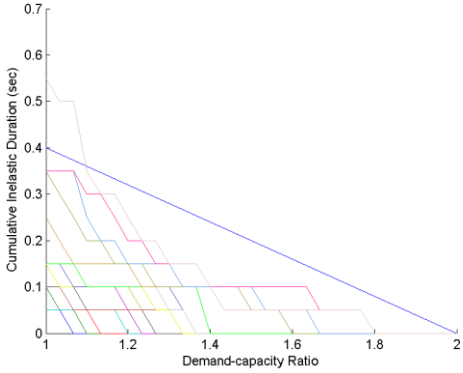

A.15 SEE1-2 Combination 13

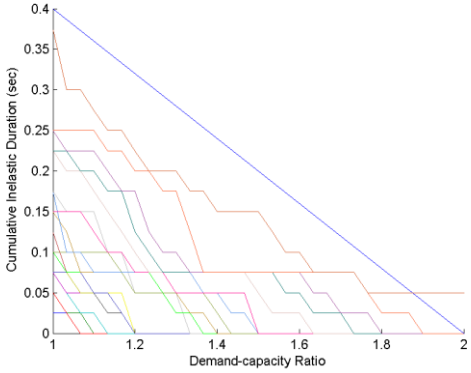

A.16 SEE1-3 Combination 9

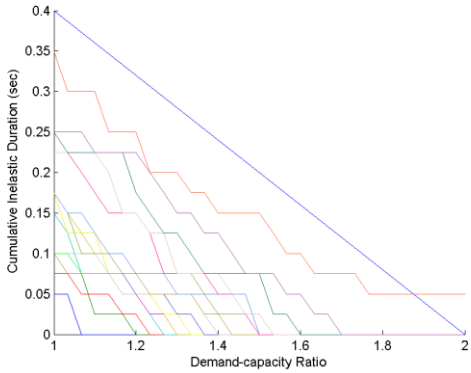

A.17 SEE1-3 Combination 11

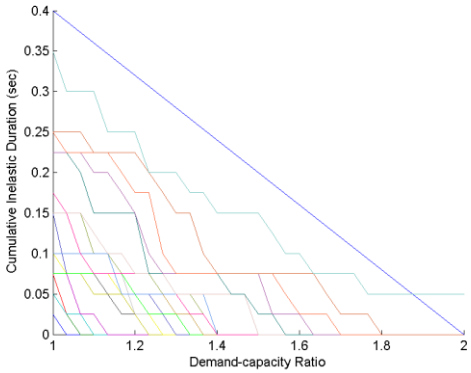

A.18 SEE1-3 Combination 13

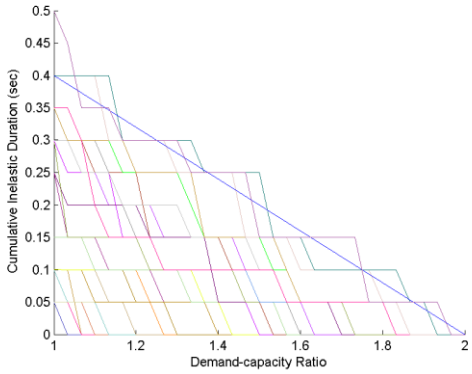

A.19 SEE2-1 Combination 9

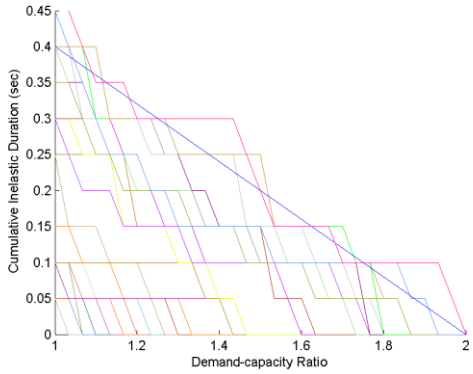

A.20 SEE2-1 Combination 11

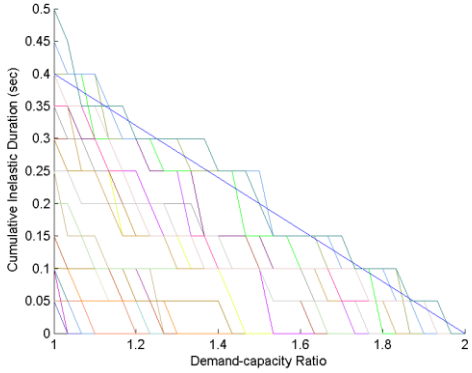

A.21 SEE2-1 Combination 13

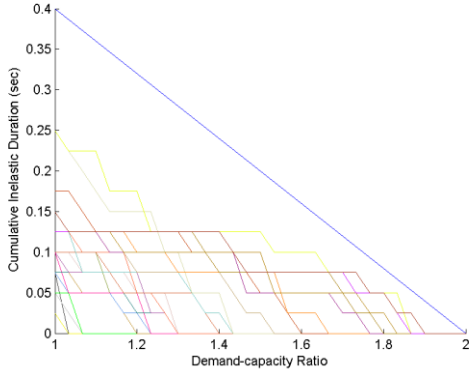

A.22 SEE2-2 Combination 9

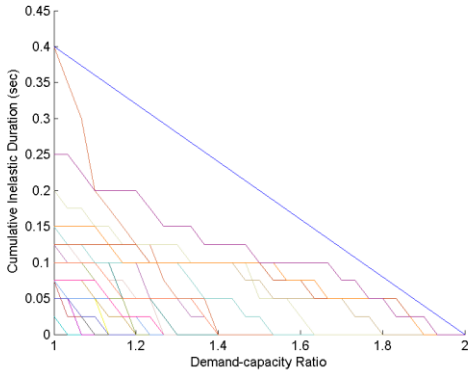

A.23 SEE2-2 Combination 11

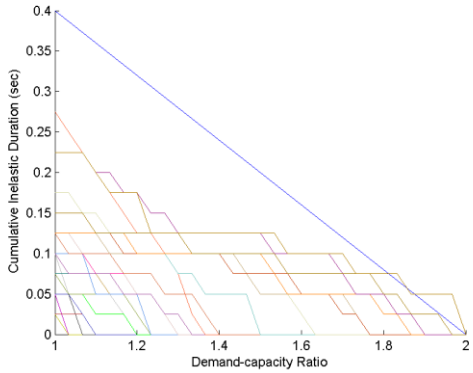

A.24 SEE2-2 Combination 13

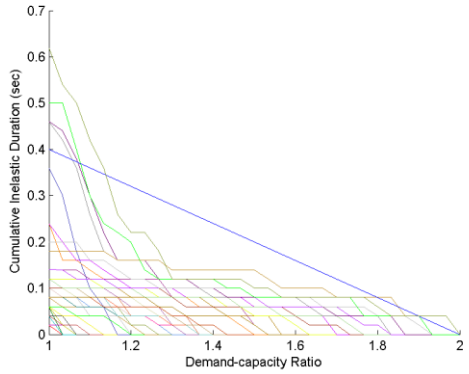

A.25 SEE2-3 Combination 9

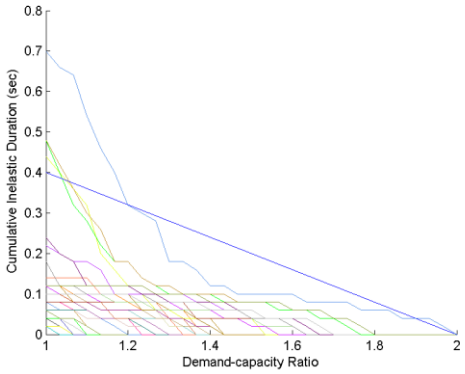

A.26 SEE2-3 Combination 11

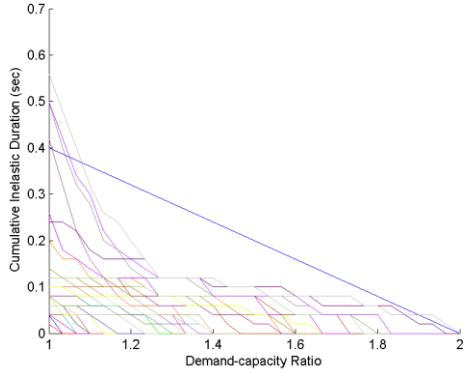

A.27 SEE2-3 Combination13